Faculty of Aerospace Engineering

Envelope Estimation and Protection of Innovative Control Effectors (ICE) Aircraft

A Probabilistic Approach

Mingzhou Yin

June 8, 2018

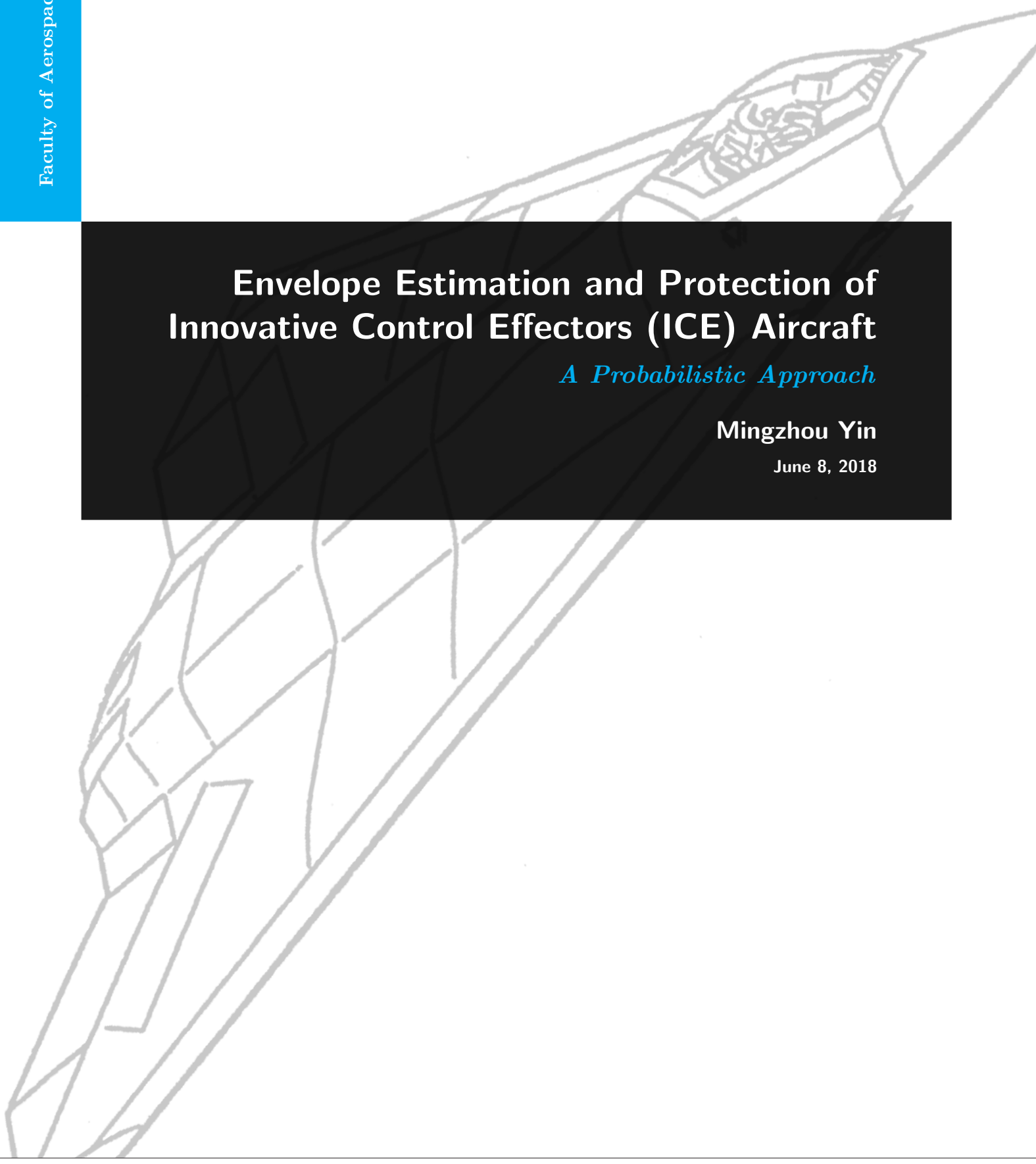

TU Delft Delft University of Technology

Challenge the future

Envelope Estimation and Protection of Innovative Control Effectors (ICE) Aircraft

A Probabilistic Approach

Master of Science Thesis

For obtaining the degree of Master of Science in Aerospace Engineering
at Delft University of Technology

Mingzhou Yin

June 8, 2018

Faculty of Aerospace Engineering · Delft University of Technology

Delft University of Technology

Delft University Of Technology
Department Of
Control and Simulation

The undersigned hereby certify that they have read and recommend to the Faculty of Aerospace Engineering for acceptance a thesis entitled **"Envelope Estimation and Protection of Innovative Control Effectors (ICE) Aircraft"** by **Mingzhou Yin** in partial fulfillment of the requirements for the degree of **Master of Science**.

Dated: June 8, 2018

Supervisors:

dr.ir. Q. P. Chu

dr.ir. C. C. de Visser

Preface

This report is prepared for my master's thesis project that I have been working on since August 2017. The research into a novel methodology in envelope estimation and protection has been a fun and meaningful experience for me and marks a great end to my master phase study in Delft.

This report features three parts: Part I presents an academic paper, which is the main part of the report. The paper discusses all the main methodologies and results of this project in a structured way. Part II is my preliminary thesis report presented in February 2018. This report discusses previous work in this field and the general ideas applied to this project in detail. This part may deviate slightly from the actual implementation in Part I and be rearranged from its original version for clarity. Part III complements the report in the form of appendices with other practicals that are not covered in the first two parts.

The accomplishment of the project will definitely be a milestone in my life. I would like to express my utmost gratitude to my supervisors, Dr. Coen de Visser and Dr. Qiping Chu for offering me the chance to participate in this challenging project and giving me patient and valuable advice and guidance throughout the project. Thanks should also be given to Dr. Michael Niestroy for the nice ICE model. I also want to thank my fellow Dennis van Oorspronk and Ph.D. candidates Ye Zhang and Sihao Sun for their insights and support that help me finish my work.

Mingzhou Yin
Delft, May 2018

Summary

Loss of control is considered as the primary cause of fatal accidents in aviation, which occurs when the aircraft has left the safe flight envelope. To reduce loss-of-control-related accidents, it is important to estimate the safe flight envelope at the current flight condition and integrate it into flight control system design. This task is known as envelope estimation and protection. This project investigates this task on the Innovative Control Effectors aircraft, an over-actuated tailless fighter aircraft with complex aerodynamic coupling between control effectors. It has been observed that this aircraft can easily steer outside the flight envelope and lose control due to its huge control authority.

This thesis proposes a novel and practical framework for safe flight envelope estimation and protection, in order to reduce loss-of-control-related accidents. Despite that multiple envelope estimation methods exist in literature, conventional analytical estimation methods fail to function efficiently for systems with high dimensionality and complex dynamics, which is often the case for high-fidelity aircraft models. In this way, this paper develops a probabilistic envelope estimation method based on Monte Carlo simulation. This method generates a probabilistic estimation of the flight envelope with kernel density estimation by simulating a sample of flight trajectories with extreme control effectiveness, which describes the envelope more practically with fuzzy sets instead of conventional crisp sets. It is shown that this method can significantly reduce the computational load compared with previous optimization-based methods and guarantee feasible and conservative envelope estimation of no less than seven dimensions. This method was applied to the Innovative Control Effectors aircraft developed by Lockheed Martin. The estimation results are demonstrated by comparing different flight conditions and covariance analysis.

The estimated probabilistic flight envelope is used for online envelope protection by a database approach, which estimates the flight envelope offline and carries the results onboard for protection. Both a conventional state-constraint-based and a novel predictive probabilistic flight envelope protection systems were implemented on a multi-loop nonlinear dynamic inversion controller by extending the concept of pseudo control hedging. No systematic framework was available to apply envelope protection to such controller. Real-time simulation results prove that the proposed framework can protect the aircraft within the estimated envelope and save

the aircraft from maneuvers that otherwise would result in loss of control. Possibilities were also explored to employ parametric models in envelope protection to simplify the database.

This work, however, is still limited to offline estimation with open-loop commands. Future work can extend this framework to aircraft damage models and closed-loop commands.

Contents

List of Figures

List of Tables

Acronyms

AMT	all moving wing tips
AoA	angle of attack
CF	command filtering
FEP	flight envelope protection
HJB-PDE	Hamilton-Jacobi-Bellman partial differential equations
ICE	Innovative Control Effectors
INCA	incremental nonlinear control allocation
INDI	incremental nonlinear dynamic inversion
LEF	leading edge flaps
LMTAS	Lockheed Martin Tactical Aircraft Systems
LOC	loss of control
LUT	look-up tables
MATV	multi-axis thrust vectoring
MC	Monte Carlo
NDI	nonlinear dynamic inversion
PCH	pseudo control hedging
PF	pitch flaps
RCAH	rate command attitude hold
SQP	sequential quadratic programming
SSD	spoiler-slot deflectors
TU Delft	Delft University of Technology
TV	thrust vectoring

List of Symbols

A_x, A_y, A_z	=	linear accelerometer measurements, ft/s^2
b	=	wing span, ft
$\bar{c}$	=	mean aerodynamic chord, ft
d	=	number of dimensions
E	=	dynamic flight envelope
$\tilde{E}$	=	probabilistic dynamic flight envelope
F_x, F_y, F_z	=	aerodynamic forces in the body frame, lbf
$\hat{f}(\boldsymbol{x})$	=	kernel density estimator
g	=	gravitational acceleration, ft/s^2
h	=	altitude, ft
h_j	=	bandwidth of the jth variable
I, R	=	invariant and reachable set
J	=	inertia matrix, slug·ft^2
$\tilde{J}$	=	augmented inertia matrix
$\boldsymbol{J}_d$	=	full control effectiveness matrix
$\boldsymbol{J}_d^F, \boldsymbol{J}_d^M$	=	control effectiveness matrix of aerodynamic forces and moments
$\boldsymbol{J}_{env}$	=	gradient of the probabilistic envelope metric
K	=	trim set
$k(\cdot)$	=	kernel function
k_0	=	threshold setting of probabilistic envelope
$l(\boldsymbol{x})$	=	level set function of the trim set
m	=	mass of aircraft, slug
M	=	Mach number
$\boldsymbol{M}_{env}$	=	flight envelope metric
M_x, M_y, M_z	=	aerodynamic moments in the body frame, ft·lbf
N	=	number of samples
n, s	=	number of states and inputs
p, q, r	=	roll, pitch, and yaw rate, rad/s
$\bar{q}$	=	dynamic pressure, psi

$\tilde{R}$	=	fuzzy reachable set
S	=	total wing area, ft^2
S_Φ	=	set of safe flight trajectories
T	=	thrust, lbf
T_f	=	time horizon, s
U	=	set of admissible inputs
u, v, w	=	velocity components in the body frame, ft/s
$V(\cdot)$	=	level set function of the invariant set
V_g	=	ground speed, ft/s
$\boldsymbol{W}$	=	control input sampling weighting
$\boldsymbol{X}$	=	random vector of states
$\boldsymbol{x}$	=	state vector
α, β	=	angle of attack and side-slip angle, rad
$\boldsymbol{\delta}$	=	control input vector
$\boldsymbol{\nu}$	=	virtual control
$\boldsymbol{\nu}_h$	=	hedged virtual control
σ	=	standard deviation
$\boldsymbol{\Phi}$	=	state trajectory
ϕ, θ, ψ	=	roll, pitch, and yaw angle, rad
$\boldsymbol{\chi}$	=	probabilistic envelope compensation term

Part I

Master of Science Thesis Paper

Probabilistic Flight Envelope Estimation and Its Application on Unstable Over-Actuated Aircraft

Mingzhou Yin*
Delft University of Technology, 2629 HS Delft, The Netherlands

This paper proposes a novel and practical framework for safe flight envelope estimation and protection, in order to reduce loss-of-control-related accidents. Conventional analytical envelope estimation methods fail to function efficiently for systems with high dimensionality and complex dynamics, which is often the case for high-fidelity aircraft models. In this way, this paper develops a probabilistic envelope estimation method based on Monte Carlo simulation. This method generates a probabilistic estimation of the flight envelope by simulating flight trajectories with extreme control effectiveness. It is shown that this method can significantly reduce the computational load compared with previous optimization-based methods and guarantee feasible and conservative envelope estimation of no less than seven dimensions. This method was applied to the Innovative Control Effectors aircraft, an over-actuated tailless fighter aircraft with complex aerodynamic coupling between control effectors. The estimated probabilistic flight envelope is used for online envelope protection by a database approach. Both conventional state-constraint-based and novel predictive probabilistic flight envelope protection systems were implemented on a multi-loop nonlinear dynamic inversion controller. Real-time simulation results prove that the proposed framework can protect the aircraft within the estimated envelope and save the aircraft from maneuvers that otherwise would result in loss of control.

Nomenclature

A_x, A_y, A_z	=	linear accelerometer measurements, ft/s^2
b	=	wing span, ft
$\bar{c}$	=	mean aerodynamic chord, ft
d	=	number of dimensions
E	=	dynamic flight envelope
$\tilde{E}$	=	probabilistic dynamic flight envelope
F_x, F_y, F_z	=	aerodynamic forces in the body frame, lbf
$\hat{f}(\boldsymbol{x})$	=	kernel density estimator
g	=	gravitational acceleration, ft/s^2
h	=	altitude, ft
h_j	=	bandwidth of the jth variable
I, R	=	invariant and reachable sets
J	=	inertia matrix, slug·ft^2
$\tilde{J}$	=	augmented inertia matrix
$\boldsymbol{J}_d$	=	full control effectiveness matrix
$\boldsymbol{J}_d^F, \boldsymbol{J}_d^M$	=	control effectiveness matrix of aerodynamic forces and moments
$\boldsymbol{J}_{env}$	=	gradient of the probabilistic envelope metric
K	=	trim set
$k(\cdot)$	=	kernel function
k_0	=	threshold setting of the probabilistic envelope
$l(\boldsymbol{x})$	=	level set function of the trim set
m	=	mass of the aircraft, slug
M	=	Mach number

*MSc Student, Department of Control and Simulation, Faculty of Aerospace Engineering, Kluyverweg 1; mingzhouyin@gmail.com.

$\boldsymbol{M}_{env}$	=	flight envelope metric
M_x, M_y, M_z	=	aerodynamic moments in the body frame, ft·lbf
N	=	number of samples
n, s	=	number of states and inputs
p, q, r	=	roll, pitch, and yaw rate, rad/s
$\bar{q}$	=	dynamic pressure, psi
$\tilde{R}$	=	fuzzy reachable set
S	=	total wing area, ft^2
S_Φ	=	set of safe flight trajectories
T	=	thrust, lbf
T_f	=	time horizon, s
U	=	set of admissible inputs
u, v, w	=	velocity components in the body frame, ft/s
$V(\cdot)$	=	level set function of the invariant set
V_g	=	ground speed, ft/s
$\boldsymbol{W}$	=	control input sampling weights
$\boldsymbol{X}$	=	random vector of states
$\boldsymbol{x}$	=	state vector
α, β	=	angle of attack and side-slip angle, rad
$\boldsymbol{\delta}$	=	control input vector
η	=	speedup factor
$\boldsymbol{\nu}$	=	virtual control
$\boldsymbol{\nu}_h$	=	hedged virtual control
σ	=	standard deviation
$\boldsymbol{\Phi}$	=	state trajectory
ϕ, θ, ψ	=	roll, pitch, and yaw angle, rad
χ	=	probabilistic envelope compensation term

I. Introduction

Safety is the most crucial issue in all sections of aviation, including flight control system (FCS) design. To reduce future accidents, it was observed by various sources [1–3] that loss of control (LOC) in flight is the most common primary cause of fatal accidents. LOC occurs when the aircraft has left the part of the state space where aircraft are safe to operate, which is commonly known as the safe flight envelope [4]. With knowledge of the flight envelope available, LOC can be avoided by adequate envelope protection as shown by case study [5].

Conventionally, flight envelope only deals with slow variables like altitude and airspeed in steady or quasi-steady conditions to achieve upset prevention [6, 7]. However, this type of envelope fails to take the dynamics into account and is usually empirical from flight tests [8, 9]. Therefore, a new type of envelope named the dynamic envelope [10] or the immediate envelope [11], is defined as all the possible states where an airplane can both reach from and be controlled back to a set of initial flight conditions (usually trimmed) within a given time horizon. This definition of the safe flight envelope is used for the remainder of the paper.

Due to its critical position in safety, the flight envelope estimation has been investigated extensively. Results of flight tests or wind tunnel tests were directly applied in [12, 13]. Model-based computation of achievable trim points was conducted in [14]. Bifurcation analysis [15] and vortex lattice algorithms [16] were used in the online estimation of impaired aircraft. Among all the methods, the most rigorous and elaborately studied method is the reachability analysis, which formulates reachability problems with the optimal control framework by studying possible trajectories of the dynamic system [17].

Various methods were developed to solve the reachability problem. For linear systems, convex optimization [18] and geometric methods [19] were applied based on the convexity of the flight envelope. For nonlinear systems, the distance-fields-over-grids method [8] optimizes the state trajectories toward points in a predefined grid. The level set method [20–22] describes the flight envelope with a level set function to be solved by partial differential equations, possibly with the semi-Lagrangian method [23], time-scale separation [24] and stochastic differential equations [25].

However, the common problem with these methods to numerically solve the optimization problem and/or partial differential equations is the high computational load for complex nonlinear systems with high dimensions [21]. The

usual solution is to simply restrict investigation to problems with low dimensions by introducing virtual inputs with time-scale separation [11] or perform domain decomposition [26]. The maximum dimension implemented was four [23, 27].

When the safe flight envelope has been estimated, flight envelope protection (FEP) systems strive to prevent LOC by constraining aircraft within the estimated envelope, preferably in both autopilot and manual control modes [28]. FEP is often implemented to be a human-machine interface as a soft extension to the FCS by open-loop cueing to pilots [29, 30]. This includes stick shakers or pushers [8] and specific display design [31]. Such design focuses on increasing pilots' situation awareness.

In contrast to the above concept, with the emergence of advanced flight control systems, it is more desired to have FEP embedded in the controller itself, such that commands can be automatically justified when the aircraft is close to the boundary of the flight envelope or impaired. This can significantly reduce the workload of pilots. Such concept of FEP is used for the remainder of the paper. The inclusion of FEP has been studied in many types of controllers, including hybrid control [28], model-based predictive control [32], and adaptive neural networks [33]. In fault-tolerant flight control, FEP can be included in the reconfiguring controller [11]. Preliminary implementation of this idea has been observed on modern commercial aircraft such as Boeing 777 and Airbus A380 to avoid stalls or limit load factors. However, to the best of our survey, none of the work was conducted to apply systematic FEP to a multi-loop nonlinear controller.

In this paper, a probabilistic envelope estimation and protection framework is proposed that aims to fill the above gaps observed in previous research, namely high-dimensional envelope estimation for complex systems and FEP with multi-loop nonlinear control. The framework applies a probabilistic method to estimate the reachable sets by sampling promising flight trajectories with Monte Carlo (MC) simulations instead of solving the reachability problem directly. In this way, reasonable estimation results can always be obtained regardless of dimensionality and complexity of the model with suitable sampling sizes. Furthermore, the definition of the estimated envelope is extended with a kernel density estimator to be probabilistic as a fuzzy set.

The estimated envelope is applied to a multi-loop nonlinear dynamic inversion (NDI) controller. The FEP system uses onboard envelope databases derived from the estimated envelope to develop envelope protection laws for LOC avoidance. A novel probabilistic protection law is proposed and compared with the conventional state-constraint-based method. The outer-loop commands are further modified by pseudo control hedging (PCH) to avoid future violation of the envelope.

The general schematic of this framework is illustrated in Fig. 1.

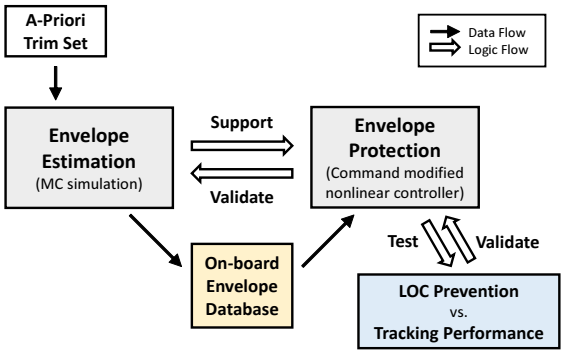

Fig. 1 General schematic of the envelope estimation and protection framework.

This framework is applied to a high-performance fighter aircraft, Lockheed Martin's Innovative Control Effectors (ICE) aircraft [34] to demonstrate its capability. The ICE aircraft is a tailless aircraft with a suite of 13 control effectors in total, including innovative ones such as spoiler-slot deflectors and multi-axis thrust vectoring. With improved lift-to-drag ratio and reduced weight, the ICE aircraft is highly maneuverable. It is noted that the above challenges are more prominent on such aircraft, as 1) tailless aircraft are inherently unstable with less directional control authority, 2) with highly coupled aerodynamics associated with unconventional control effectors, the flight envelope tends to be nonlinear as well, and 3) extreme maneuvers are expected to be made which are closer to the boundary of the flight envelope. It was observed in previous research [35] that the ICE aircraft is prone to LOC when controlled without FEP

systems due to its huge control authority. Therefore, the ICE aircraft is considered a suitable subject to test the proposed framework for both reliability and effectiveness.

The paper is organized as follows. Sec. II introduces the reachability analysis framework for envelope estimation. The methodology to use MC simulation in probabilistic envelope estimation is presented in Sec. III. Sec. IV further discusses the design of the envelope database and associated envelope protection laws. The designed FEP system is integrated into an NDI controller in Sec. V. The implementation of the framework is demonstrated in Sec. VII, with a description of the applied ICE aircraft model given in Sec. VI. The envelope estimation results and controller performance comparisons are shown in Sec. VIII. Sec. IX concludes the paper and proposes future work.

II. The Reachability Analysis Formulation

This section starts by defining the envelope estimation problem within the framework of reachability analysis, followed by introducing the solution proposed by the level set method. Then, the definition is expanded to a probabilistic version.

A. Classical Safe Flight Envelope

It has been shown that the flight envelope estimation problem can be formulated as a reachability problem with the optimal control framework by studying possible trajectories of the dynamic system [17]. Consider an autonomous nonlinear system

$$\dot{\boldsymbol{x}} = \boldsymbol{f}(\boldsymbol{x}, \boldsymbol{\delta}), \tag{1}$$

with $\boldsymbol{x} \in \mathbb{R}^n$, $\boldsymbol{\delta} \in U \subset \mathbb{R}^s$. All the states $\boldsymbol{x}$ that can be reached from a set $K \in \mathbb{R}^n$ with at least one function of admissible inputs $\boldsymbol{\delta}(t) \in U_{[0,T_f]}$ within a time horizon $T_f \geq 0$ form the reachable set $R(T_f, K)$. A similar definition is the invariant set $I(T_f, K)$, which describes all the states $\boldsymbol{x}$ that can remain in a set K with any function of admissible inputs $\boldsymbol{\delta}(t)$ for any time within a time horizon T_f. Mathematically, the above definitions are expressed as

$$R(T_f, K) = \left\{ \boldsymbol{x}(\tau) \in \mathbb{R}^n \,\middle|\, \exists \boldsymbol{\delta}(t) \in U_{[0,T_f]}, \exists \tau \in [0, T_f], \boldsymbol{x}(0) \in K \right\}, \tag{2}$$

$$I(T_f, K) = \left\{ \boldsymbol{x}(0) \in \mathbb{R}^n \,\middle|\, \forall \boldsymbol{\delta}(t) \in U_{[0,T_f]}, \forall \tau \in [0, T_f], \boldsymbol{x}(\tau) \in K \right\}. \tag{3}$$

Furthermore, it was proved that the following principle of duality holds

$$R(T_f, K) = (I(T_f, K^c))^c, \tag{4}$$

which can transform the calculation of reachable sets to invariant sets.

A similar definition can be applied to the same system, but running backward in time,

$$\dot{\boldsymbol{x}} = -\boldsymbol{f}(\boldsymbol{x}, \boldsymbol{\delta}). \tag{5}$$

In this way, the reachable set for the original system is known as the forward reachable set $R_f(T_f, K)$, whereas that for the backward system is known as the backward reachable set $R_b(T_f, K)$.

In the context of flight envelope estimation, K can be selected as the apriori trim set of the aircraft, where the aircraft can stay indefinitely. Then, $R_f(T_f, K)$ defines all the states the aircraft can reach within T_f from steady states, whereas $R_b(T_f, K)$ defines all the states from which the aircraft can be controlled back to steady states within T_f. In this way, the flight envelope to be estimated is defined as the intersection of the above two reachable sets

$$E(T_f, K) = R_f(T_f, K) \cap R_b(T_f, K), \tag{6}$$

according to the definition of the dynamic envelope.

B. The Level Set Method

A famous solution of the invariant set can be found in the level set method, where associated sets are expressed by zero level sets. Define the trim set

$$K = \{ \boldsymbol{x} \in \mathbb{R}^n \,|\, l(\boldsymbol{x}) > 0 \}. \tag{7}$$

Then the definition Eq. 3 can be rewritten in the form of a level set as

$$I(T_f, K) = \left\{ \boldsymbol{x}(0) \in \mathbb{R}^n \middle| V(\boldsymbol{x}, T_f) = \inf_{\boldsymbol{\delta}(\cdot)\in U_{[0,T_f]}} \min_{\tau\in[0,T_f]} l(\boldsymbol{\Phi}(\tau; \boldsymbol{x}(0), \boldsymbol{\delta}(\cdot))) \geq 0 \right\}. \tag{8}$$

It was proved in [17] that the level set function $V(\boldsymbol{x}, T_f)$ can be represented as the viscosity solution to the Hamilton-Jacobi-Bellman partial differential equations (HJB-PDE)

$$\frac{\partial V}{\partial t}(\boldsymbol{x}, t) + \min_{\tau\in[0,t]} \left\{ \inf_{\boldsymbol{\delta}(\cdot)\in U_{[0,t]}} \frac{\partial V}{\partial \boldsymbol{x}}(\boldsymbol{x}, t) \boldsymbol{f}(\boldsymbol{x}, \boldsymbol{\delta}) \right\} = 0, \tag{9}$$

with the boundary conditions $V(\boldsymbol{x}, 0) = l(\boldsymbol{x})$ or $V(\boldsymbol{x}, T_f) = l(\boldsymbol{x})$ for the forward and the backward systems respectively. The HJB-PDE can be further extended to a Hamilton-Jacobi-Isaacs (HJI) problem to include disturbance.

When the aircraft model is affine, i.e., $\boldsymbol{f}(\boldsymbol{x}, \boldsymbol{\delta}) = \boldsymbol{b}(\boldsymbol{x}) + \boldsymbol{A}(\boldsymbol{x})\boldsymbol{\delta}$, which is applicable to most cases, the optimum control selected in Eq. 9 is always one of the extreme admissible values for each control effector. The optimum control of the ith control effector is

$$\delta_i^* = \begin{cases} \delta_{i,\max}, & \dfrac{\partial V}{\partial \boldsymbol{x}}(\boldsymbol{x}, t) \cdot \boldsymbol{A}_{\cdot i}(\boldsymbol{x}) \leq 0 \\ \delta_{i,\min}, & \dfrac{\partial V}{\partial \boldsymbol{x}}(\boldsymbol{x}, t) \cdot \boldsymbol{A}_{\cdot i}(\boldsymbol{x}) > 0 \end{cases}, \tag{10}$$

where $\boldsymbol{A}_{\cdot i}(\boldsymbol{x})$ is the vector of all control effectiveness functions for the ith control surface.

After solving the invariant sets for both the forward and the backward system, the envelope can be estimated by Eq. 4 and 6.

C. Probabilistic Safe Flight Envelope

As discussed above, the classical definition (Eq. 2) defines the flight envelope with a crisp set, i.e., a state is either in the envelope or outside the envelope. However, the situation can be much more sophisticated practically. The actual possibility to adopt an effective maneuver to save the aircraft depends on the range of possible trajectories available. This range leaves room for practical issues such as pilots' reaction time, actuator dynamics of control surfaces, and controller performance, which are not included in the above deterministic definition. Therefore, it is desired to expand the definition to a fuzzy set, whose membership function describes the 'difficulty' to reach from and fly back to steady states for a state. This also enables the possibility to describe other probabilistic or stochastic factors including external disturbances and modeling errors.

Define the set of all safe flight trajectories of time horizon T_f that start and end in the trim set as

$$S_{\boldsymbol{\Phi}}(T_f, K) = \left\{ \boldsymbol{\Phi}(t; \boldsymbol{x}(0), \boldsymbol{\delta}(\cdot)) \middle| \boldsymbol{\Phi}(0) \in K, \boldsymbol{\Phi}(T_f) \in K, t \in [0, T_f] \right\}. \tag{11}$$

It is noted that since aircraft can stay indefinitely in the trim set, safe flight trajectories of $T_{f,0}$ include all safe flight trajectories of $T_f \leq T_{f,0}$. Then the following fuzzy set is defined as the probabilistic flight envelope.

$$\tilde{E}(T_f, K) = \left\{ \left(\boldsymbol{x} \in \mathbb{R}^n, \mu_{\tilde{E}}(\boldsymbol{x}) = \frac{f_X(\boldsymbol{x})}{\max_{\boldsymbol{x}\in\mathbb{R}^n} f_X(\boldsymbol{x})} \right) \right\}, \tag{12}$$

where $f_X(\boldsymbol{x})$ is the probability density function (PDF) of the midpoint state for all safe flight trajectories of time horizon $2T_f$, i.e.,

$$\boldsymbol{X} = \boldsymbol{\Phi}(T_f), \boldsymbol{\Phi} \in S_{\boldsymbol{\Phi}}(2T_f, K). \tag{13}$$

To solve for the membership function $\mu_{\tilde{E}}(\boldsymbol{x})$, the safe flight trajectories can be divided into the forward part and the backward part as

$$S_{\boldsymbol{\Phi},f}(2T_f, K) = \left\{ \boldsymbol{\Phi}(t) \middle| \boldsymbol{\Phi} \in S_{\boldsymbol{\Phi}}(2T_f, K), t \in [0, T_f] \right\}. \tag{14}$$

$$S_{\boldsymbol{\Phi},b}(2T_f, K) = \left\{ \boldsymbol{\Phi}(t) \middle| \boldsymbol{\Phi} \in S_{\boldsymbol{\Phi}}(2T_f, K), t \in [T_f, 2T_f] \right\}. \tag{15}$$

Similarly, define two more PDFs $f_{\boldsymbol{X}_f}(\boldsymbol{x})$ and $f_{\boldsymbol{X}_b}(\boldsymbol{x})$ of random variables

$$\boldsymbol{X}_f = \boldsymbol{\Phi}(T_f), \boldsymbol{\Phi} \in S_{\boldsymbol{\Phi},f}(2T_f, K) \tag{16}$$

and

$$\boldsymbol{X}_b = \boldsymbol{\Phi}(T_f), \boldsymbol{\Phi} \in S_{\boldsymbol{\Phi},b}(2T_f, K). \tag{17}$$

Then, the membership function can be reformulated as

$$\mu_{\tilde{E}}(\boldsymbol{x}) = \frac{f_{\boldsymbol{X}_f}(\boldsymbol{x}) \cdot f_{\boldsymbol{X}_b}(\boldsymbol{x})}{\max_{\boldsymbol{x}\in\mathbb{R}^n} f_{\boldsymbol{X}_f}(\boldsymbol{x}) \cdot f_{\boldsymbol{X}_b}(\boldsymbol{x})}. \tag{18}$$

It should be noted that the following fuzzy sets can be constructed as the fuzzy counterparts of the crisp forward and backward reachable set $R_f(T_f, K)$ and $R_b(T_f, K)$.

$$\tilde{R}_f(T_f, K) = \left\{ \left(\boldsymbol{x} \in \mathbb{R}^n, \mu_{\tilde{R}_f}(\boldsymbol{x}) = \frac{f_{\boldsymbol{X}_f}(\boldsymbol{x})}{\max_{\boldsymbol{x}\in\mathbb{R}^n} f_{\boldsymbol{X}_f}(\boldsymbol{x})} \right) \right\} \tag{19}$$

$$\tilde{R}_b(T_f, K) = \left\{ \left(\boldsymbol{x} \in \mathbb{R}^n, \mu_{\tilde{R}_b}(\boldsymbol{x}) = \frac{f_{\boldsymbol{X}_b}(\boldsymbol{x})}{\max_{\boldsymbol{x}\in\mathbb{R}^n} f_{\boldsymbol{X}_b}(\boldsymbol{x})} \right) \right\} \tag{20}$$

Then the probabilistic flight envelope is the product t-norm of $\tilde{R}_f(T_f, K)$ and $\tilde{R}_b(T_f, K)$ scaled by a factor such that the center of the envelope has a membership value of 1. The difference between the crisp set and the fuzzy set definition of the safe flight envelope is illustrated in Fig. 2 for a univariate case.

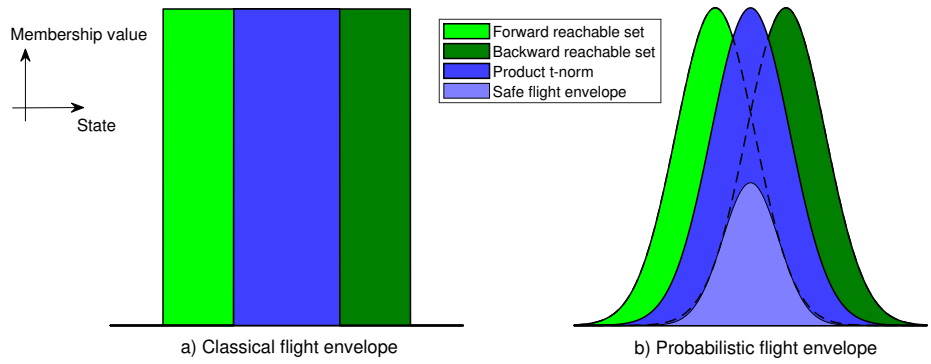

Fig. 2 Comparison of the classical and the probabilistic flight envelope definition for a univariate case.

III. Envelope Estimation by MC Simulation

A computationally-feasible methodology to estimate the probabilistic flight envelope defined by Eq. 12 with high dimensions is discussed in this section. This methodology applies MC simulations to obtain kernel density estimators of PDFs $f_{\boldsymbol{X}_f}(\boldsymbol{x})$ and $f_{\boldsymbol{X}_b}(\boldsymbol{x})$.

MC simulation is a computational algorithm that uses random sampling to obtain a numerical estimation of probability distributions [36]. A general MC simulation routine starts by generating random input variables and conditions. Then, deterministic analysis is performed for a sample of the random variable. This process is repeated for different random input variables and conditions. Finally, the probability distribution is calculated based on the obtained samples. This method has not been applied to envelope estimation yet. The closest application is the workspace determination in robotics [37].

To estimate the envelope, two MC simulation routines are performed to obtain the probability distributions of $\boldsymbol{X}_f$ and $\boldsymbol{X}_b$ respectively. First, a random point in the trim set is selected as the initial state. Then, pseudo-random open-loop control inputs are selected, which should be effective to explore the boundary of the flight envelope. The selection method is discussed in Sec. III.A. With the initial state and control inputs specified, a flight trajectory of time horizon T_f

can be simulated by solving the forward dynamics Eq. 1 or the backward dynamics Eq. 5 under desired flight conditions. The states at time T_f, of which the envelope is to be estimated are stored as one sample. This sampling process is illustrated in Fig. 3. With a large size of samples generated, the probability distributions of $\boldsymbol{X}_f$ and $\boldsymbol{X}_b$ can be estimated by kernel density estimation, details of which are discussed in Sec. III.B. Finally, the membership function of the probabilistic flight envelope is calculated by Eq. 18. A flowchart of the whole process is shown in Fig. 4.

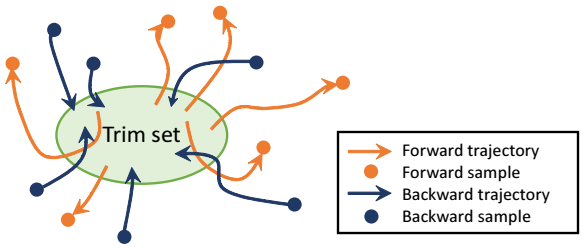

Fig. 3 Illustration of the sampling process in MC simulations.

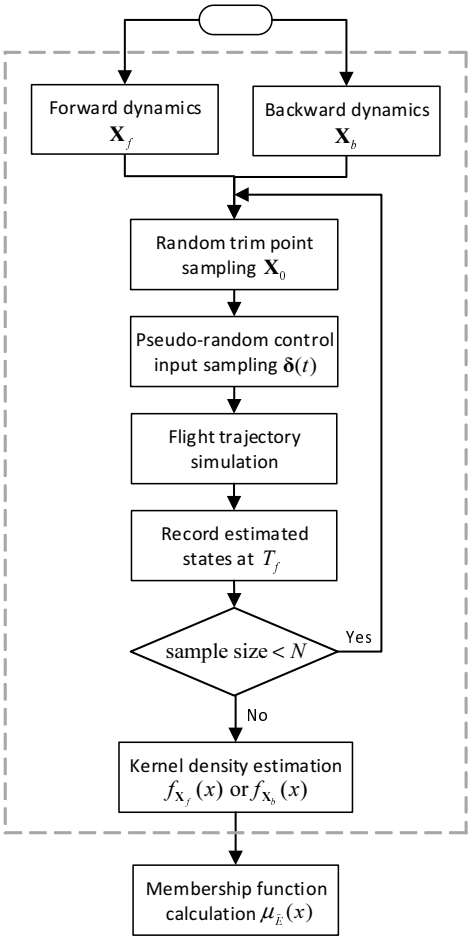

Fig. 4 Flow chart of envelope estimation with MC simulation.

A. Extreme Control Effectiveness Method

The key to a reliable estimation by MC simulation is to avoid severe underestimation. With limited sample sizes, the specific control inputs that steer the aircraft to the boundary of the flight envelope may not be sampled. Thus, the estimated envelope can be too conservative. Therefore, a reliable estimation relies heavily on a good sampling of the random control inputs.

To conquer this problem, the so-called extreme control effectiveness method was proposed for envelope estimation with MC simulation. This method examines the derived equation for the optimal control in the level set method (Eq. 10). For a full degree-of-freedom aircraft model, only the dynamics of rotational and translational velocities are directly dependent on the control surface deflections via aerodynamic forces and moments.

Define the effective states in envelope estimation as

$$\boldsymbol{x}_e = [u\ v\ w\ p\ q\ r]^T. \tag{21}$$

The dynamics of $\boldsymbol{x}_e$ can be expressed in the incremental form as

$$\boldsymbol{f}(\boldsymbol{x}_e, \boldsymbol{\delta}) \approx \dot{\boldsymbol{x}}_{e,0} + \tilde{\boldsymbol{J}}^{-1}\boldsymbol{J}_d\Delta\boldsymbol{\delta}, \tag{22}$$

where $\dot{\boldsymbol{x}}_{e,0}$ is the state derivatives at the current time step, $\Delta\boldsymbol{\delta}$ is the incremental deflections of all active control surfaces and the incremental thrust,

$$\tilde{\boldsymbol{J}}^{-1} = \begin{bmatrix} \mathrm{diag}\left(\frac{1}{m}, \frac{1}{m}, \frac{1}{m}\right) & \boldsymbol{0} \\ \boldsymbol{0} & \boldsymbol{J}^{-1} \end{bmatrix}, \tag{23}$$

$$\boldsymbol{J}_d = \begin{bmatrix} \boldsymbol{J}_d^F \\ \boldsymbol{J}_d^M \end{bmatrix} = \left[\left(\frac{\partial F_x}{\partial \boldsymbol{\delta}}\right)^T \left(\frac{\partial F_y}{\partial \boldsymbol{\delta}}\right)^T \left(\frac{\partial F_z}{\partial \boldsymbol{\delta}}\right)^T \left(\frac{\partial M_x}{\partial \boldsymbol{\delta}}\right)^T \left(\frac{\partial M_y}{\partial \boldsymbol{\delta}}\right)^T \left(\frac{\partial M_z}{\partial \boldsymbol{\delta}}\right)^T \right]^T. \tag{24}$$

Thus, according to Eq. 10, we have

$$\frac{\partial V}{\partial \boldsymbol{x}}(\boldsymbol{x}, t) \cdot \boldsymbol{A}_{\cdot i}(\boldsymbol{x}) = \frac{\partial V}{\partial \boldsymbol{x}_e}(\boldsymbol{x}, t)\tilde{\boldsymbol{J}}^{-1}\boldsymbol{J}_{d,\cdot i}, \tag{25}$$

$$\Delta u_i^* = \begin{cases} \Delta u_{i,\max}, & \dfrac{\partial V}{\partial \boldsymbol{x}_e}(\boldsymbol{x}, t)\tilde{\boldsymbol{J}}^{-1}\boldsymbol{J}_{d,\cdot i} < 0 \\ \Delta u_{i,\min}, & \dfrac{\partial V}{\partial \boldsymbol{x}_e}(\boldsymbol{x}, t)\tilde{\boldsymbol{J}}^{-1}\boldsymbol{J}_{d,\cdot i} > 0 \end{cases}. \tag{26}$$

In Eq. 26, the only unknown term is the gradient of the level set function $\partial V/\partial \boldsymbol{x}_e$. As will be discussed in the following paragraph, this variable determines the optimal exploration direction at the current state. Instead of solving the HJB-PDE for the optimal value, this variable is replaced by a random variable $\boldsymbol{W}$ whose elements are subject to an identical normal distribution with zero mean, such that a random exploration direction is selected. This random variable is sampled at each time step. So, the following strategy of optimal control selection is proposed for the extreme control effectiveness method.

$$\Delta u_i^* = \begin{cases} \Delta u_{i,\max}, & \boldsymbol{W}\tilde{\boldsymbol{J}}^{-1}\boldsymbol{J}_{d,\cdot i} < 0 \\ \Delta u_{i,\min}, & \boldsymbol{W}\tilde{\boldsymbol{J}}^{-1}\boldsymbol{J}_{d,\cdot i} > 0 \end{cases}, W_j \sim N(0, 1), \tag{27}$$

where $j \in \{u, v, w, p, q, r\}$. In this way, the population to sample the control inputs reduces significantly from all admissible control inputs U to limited combinations of extreme control inputs. This reduced population, however, still includes all possible optimal control selections in the level set method. In this way, this method is very efficient by only sampling control inputs that are effective in exploring the boundary of the flight envelope as supported by the level set method.

This method is named extreme control effectiveness method because of its physical implementation. Eq. 27, in essence, aims to optimize a weighted sum of control effectiveness in three translational and three rotational directions. The randomly-sampled partial derivative terms W_j can be regarded as weights to aim for the extreme control effectiveness in that particular direction. So the control input samples generated with this method explore a particular direction of the vector $\boldsymbol{W} = [W_u\ W_v\ W_w\ W_p\ W_q\ W_r]$ in the flight envelope with extreme control effectiveness.

B. Kernel Density Estimation

Density estimation is the process to construct estimators of the probability density functions $f_{\boldsymbol{X}_f}(\boldsymbol{x})$ and $f_{\boldsymbol{X}_b}(\boldsymbol{x})$ based on samples of $\boldsymbol{X}_f$ and $\boldsymbol{X}_b$. The commonly applied density estimation methods include non-parametric ones such as histogram and kernel density estimation [38] and parametric or semi-parametric ones such as orthogonal series estimation [39] and maximum penalized likelihood estimation [40]. Since no prior knowledge is available about the structure of the envelope, a non-parametric method is preferred. In addition, the probabilistic FEP system requires a continuous estimator as will be discussed in Sec. IV.B. Thus, kernel density estimation is applied in this paper.

To estimate the density of a d-dimensional random vector

$$\boldsymbol{X} = (X_1, X_2, ..., X_d)^T \tag{28}$$

by N samples

$$\boldsymbol{y}_i = (y_{i1}, y_{i2}, ..., y_{id})^T, i = 1, 2, ..., N, \tag{29}$$

the multivariate kernel density estimator is given by

$$\hat{f}(\boldsymbol{x}) = \frac{1}{N}\sum_{i=1}^{n} K_H(\boldsymbol{x} - \boldsymbol{y}_i) = \frac{1}{Nh_1h_2...h_d}\sum_{i=1}^{n}\prod_{j=1}^{d} k\left(\frac{x_j - y_{ij}}{h_j}\right), \tag{30}$$

where $k(\cdot)$ is the kernel function for each dimension satisfying

$$\int_{-\infty}^{\infty} k(\zeta)\mathrm{d}\zeta = 1. \tag{31}$$

Usually, a Gaussian kernel function

$$k(\zeta) = \frac{1}{\sqrt{2\pi}} e^{-\frac{1}{2}\zeta^2} \tag{32}$$

is used. The bandwidth h_j is comparable to the bin size in the histogram, which normalizes the kernel by characterizing the range affected by one sample in the estimator. The bandwidth can be selected by the Silverman's rule of thumb [38, 41]

$$h_j = \sigma_j \left[\frac{4}{(d+2)N}\right]^{1/(d+4)}. \tag{33}$$

C. Advantages and Limitations

This method originates from the intention to circumvent the numerical calculation of partial differential equations, which is not feasible for complex aircraft models with high dimensions. In addition, this MC-simulation-based envelope estimation method demonstrates additional advantages over conventional reachability analysis.

First, the conservativeness of the estimated envelope is guaranteed, since sample points are associated with particular flight trajectories and control inputs for reconstruction, whereas for the level set method, only the indirect evolution of the level set function is concerned.

Second, the estimated envelope is probabilistic in the form of fuzzy sets, which gives additional information about the difficulty to reach a certain point within the envelope. This is especially useful in FEP system design. The aggressiveness of FEP can be altered by specifying different α-cuts of the fuzzy set (i.e., different thresholds of the membership function), depending on applications. Furthermore, it can detect the approaching of the envelope boundary in advance by the gradient of the membership function as shown by the predictive probabilistic FEP law proposed in Sec. IV.B.

Finally, this method provides great flexibility to design desired envelope databases. The exact same routine can be applied to any set of states to be protected. Stochastic components such as disturbances can also be directly augmented to simulations since the estimation has already been probabilistic.

On the other hand, it should be noted that this method can not totally circumvent the curse of dimensionality. Despite the fact that a reasonable estimation is always available, the required sample size to achieve the same level of reliability still grows exponentially with the dimensionality. Nevertheless, the base of the exponential complexity for the MC-simulation-based method is usually smaller than that for the level set method. It was shown in Ref. [42] that the required sample size to maintain the same level of the mean integrated squared error (MISE) is

$$N_{\text{req}} = O\left(\text{MISE}^{-\frac{4+d}{4}}\right). \tag{34}$$

For comparison, the level set method has a time complexity of $O\left(N_g^{d+1}\right)$, where N_g is the number of computational grid points in each dimension [43]. So the envelope estimation with MC simulation has a speedup factor of

$$\eta = \left(N_g \cdot \sqrt[4]{\text{MISE}}\right)^d \tag{35}$$

over the level set method. For example, when $N_g = 20$ and $\text{MISE} = 1 \times 10^{-3}$, the speedup factor $\eta \approx 3.56^d$.

In addition, this method is still not efficient enough to be conducted online, a database approach is preferred to estimate the reduced envelopes for different damage cases offline when used in fault-tolerant flight control.

IV. FEP System Design with Probabilistic Envelope

As discussed in Sec. I, the ultimate goal of envelope estimation is to avoid LOC by augmenting the flight control laws to constrain the aircraft within the estimated envelope. This augmented part in the FCS is known as FEP systems. This section continues to discuss the design of FEP systems with the probabilistic envelope defined in Sec. II.C and estimated in Sec. III.

With the classical flight envelope definition, FEP systems are almost always implemented by limiting certain signals in the FCS. This can be achieved by direct state-command limiting, or indirect limiting of control surface deflections or virtual controls with a mapping of the envelope boundaries to avoid dependence on specific controller structures [32]. Such approach is also applicable to the probabilistic envelope by binarizing it with a threshold setting. An approach with dynamic command limiting is discussed in Sec. IV.A. However, such hard constraints not only are impractical as discussed in Sec. II.C, but also make the FCS totally blind before the limits are activated, which affects the ride quality. Therefore, a novel probabilistic FEP is developed in IV.B, which utilizes the additional information provided in the probabilistic envelope to react earlier and render more gentle protective actions. Instead of hard command limiting, this method modifies commands throughout a flight.

In general, online FEP systems with probabilistic envelope estimated offline consist of two parts: 1) an envelope database that generates an envelope metric at the current state in real-time as $\boldsymbol{M}_{\text{env}} = \boldsymbol{M}_{\text{env}}(\boldsymbol{x})$ and 2) FEP laws that modify the references of protected states based on the envelope metric as $\boldsymbol{x}_{\text{fep}} = \boldsymbol{x}_{\text{fep}}(\boldsymbol{x}_{\text{ref}}, \boldsymbol{M}_{\text{env}})$. The detailed formulation of these two parts is discussed in the following sections.

A. State-Constraint-Based FEP

The state-constraint-based FEP starts by converting the probabilistic envelope to a classical envelope with absolute boundaries. A threshold of the membership function is selected. Assuming an uncorrelated normal distribution for $f_{\boldsymbol{X}}(\boldsymbol{x})$, the threshold value at $k_0\sigma$ is

$$\mu_{\tilde{E},0} = e^{-\frac{1}{2}k_0^2}. \tag{36}$$

The k_0 value can be tuned for appropriate aggressiveness of FEP in specific applications.

The envelope metric is then constructed as a matrix of maximum and minimum constraints of protected states as

$$\boldsymbol{M}_{\text{env}}(\boldsymbol{x}) = \left[\boldsymbol{x}_{\min}(\boldsymbol{x})\ \boldsymbol{x}_{\max}(\boldsymbol{x})\right]. \tag{37}$$

These state constraints are defined as follows. When the current state is in the estimated envelope, the constraints are defined as the maximum and minimum values for each state to stay within the envelope with the other states unchanged. When the current state is outside the estimated envelope, the constraints are defined the same as the closest point that is within the envelope. This definition is illustrated in Figure 5 for a bivariate case.

The FEP law for the state-constraint-based method is direct command limiting. The envelope-protected reference is a saturation function of the original reference with the upper and lower limits defined in Eq. 37 as shown in the following equation.

$$\boldsymbol{x}_{\text{fep}} = \max\left[\boldsymbol{x}_{\min}, \min\left(\boldsymbol{x}_{\max}, \boldsymbol{x}_{\text{ref}}\right)\right], \tag{38}$$

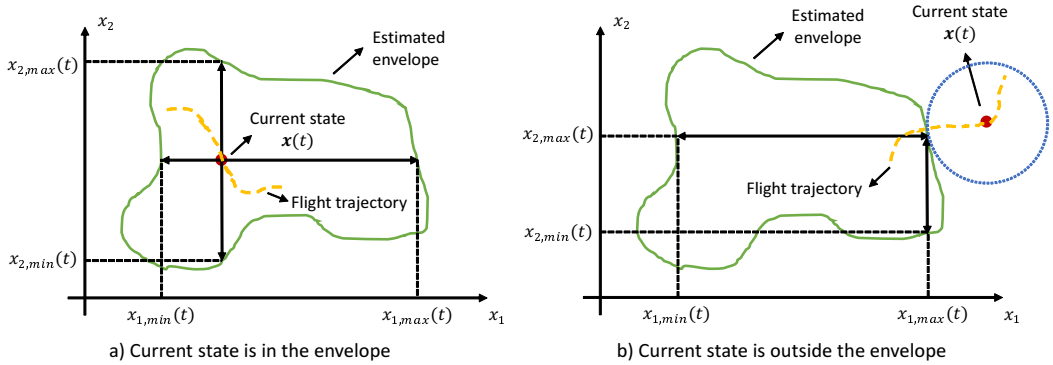

Fig. 5 Definition of dynamic state constraints for a bivariate case.

B. Probabilistic FEP

For probabilistic FEP, the envelope metric stored in the envelope database is constructed as a function of the membership value $\mu_{\tilde{E}}(\boldsymbol{x})$ with

$$M_{\text{env}}(\boldsymbol{x}) = \ln\left(\max\left(\mu_{\tilde{E}}(\boldsymbol{x}), \epsilon\right)\right), \tag{39}$$

where ϵ is a small constant. This metric describes how much the current state needs to be protected. A zero means no protection is needed, whereas a value of $\ln\epsilon$ means maximum protection is needed. In addition to the global evaluation, the amount of protection applied to each protected state is furthermore determined by the gradient of the envelope metric in that direction. A larger gradient means the protection can be more effective by modifying the command in that direction. Thus, the probabilistic FEP law is proposed as

$$\boldsymbol{x}_{\text{fep}} = \boldsymbol{x}_{\text{ref}} + \boldsymbol{\chi}(\boldsymbol{x}), \tag{40}$$

with

$$\boldsymbol{\chi}(\boldsymbol{x}) = \begin{cases} -\left(M_{\text{env}}(\boldsymbol{x}) - M_0\right)\boldsymbol{K}_{\text{fep}}\,\boldsymbol{J}_{\text{env}}^T(\boldsymbol{x}), & M_{\text{env}}(\boldsymbol{x}) > M_0 \\ 0, & M_{\text{env}}(\boldsymbol{x}) \le M_0 \end{cases}, \tag{41}$$

where M_0 is the threshold to activate envelope protection, $\boldsymbol{K}_{\text{fep}}$ is a diagonal gain matrix, $\boldsymbol{J}_{\text{env}} = \partial M_{\text{env}}/\partial \boldsymbol{x}$ is the gradient of the envelope metric.

Comparing both FEP methods, the advantages of the probabilistic FEP are that 1) the aggressiveness of FEP can be altered online by tuning the threshold M_0 and the gain vector $\boldsymbol{K}_{\text{fep}}$ without re-calculating the whole envelope database, 2) the modification to the command is predictive, which starts before reaching the envelope boundary, and 3) the boundedness of the modification term is guaranteed, which completes the boundedness proof of PCH as will be shown in Sec. V. On the other hand, the state-constraint-based FEP guarantees to constrain the command within a fixed region in the state space, so its behavior is more predictable. A comparison of the applied FEP strategies for both methods is illustrated in Fig. 6 for a bivariate case.

V. Multi-Loop NDI Controllers with Command Modification

Both types of FEP systems discussed in the last section interact with the controller by modifying the command. This command modification is trivial for single-loop controllers as the command can be arbitrarily selected. However, the FCS usually utilizes the time-scale separation principle to simplify the controller design and is thus multi-loop. In a multi-loop controller, the inner-loop command is generated by outer loops, which cannot be arbitrarily modified. To solve this issue, the concept of PCH is extended to multi-loop NDI, such that outer loops are 'aware' of and adjusted to inner-loop command modification. This section starts by introducing the general concepts of NDI and incremental NDI, followed by the application of PCH in multi-loop command modification.

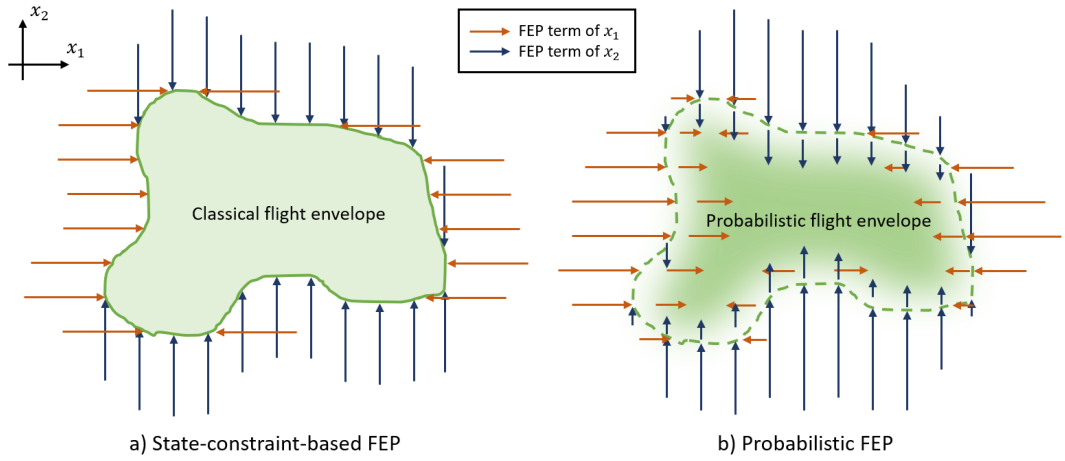

Fig. 6 Comparison of FEP strategies for state-constraint-based and probabilistic methods.

A. The Concept of NDI and Incremental NDI

To tackle problems of complex gain scheduling and low robustness to model inaccuracy and failure observed in conventional linear controllers, NDI was proposed to inherently include nonlinearity in control laws by inverting the flight dynamics. Consider an n-loop affine system

$$\dot{\boldsymbol{x}}_i = \boldsymbol{b}_i(\boldsymbol{x}) + \boldsymbol{A}_i(\boldsymbol{x})\boldsymbol{x}_{i+1}, i = 1, 2, ..., n, \tag{42}$$

where $\boldsymbol{x}_1, \boldsymbol{x}_2, ..., \boldsymbol{x}_n$ are time-scale-separated states, $\boldsymbol{x}_{n+1} = \boldsymbol{\delta}$ is the control inputs. The multi-loop NDI controller of the system consists of two parts for each loop: 1) a linear PID controller that generates the virtual control inputs as

$$\boldsymbol{\nu}_i(\boldsymbol{x}) = \dot{\boldsymbol{x}}_i = \boldsymbol{K}_{\mathrm{p},i}\boldsymbol{e}_i + \boldsymbol{K}_{\mathrm{i},i}\int_0^t \boldsymbol{e}_i \mathrm{d}t + \boldsymbol{K}_{\mathrm{d},i}\frac{\mathrm{d}\boldsymbol{e}_i}{\mathrm{d}t}, \tag{43}$$

where $\boldsymbol{e}_i = \boldsymbol{x}_{i,\mathrm{com}} - \boldsymbol{x}_i$ is the tracking error, and 2) input-output linearization by inverting the dynamics

$$\boldsymbol{x}_{i+1,\mathrm{com}} = \boldsymbol{A}_i^{-1}(\boldsymbol{x})\left(\boldsymbol{\nu}_i(\boldsymbol{x}) - \boldsymbol{b}_i(\boldsymbol{x})\right), \tag{44}$$

that maps the virtual control of the ith loop to the command of the $(i+1)$th loop or the final control inputs.

In order to handle model inaccuracy, incremental NDI was developed in Ref. [44–46] by applying NDI to the incremental form of the dynamic equations, such that only the control effectiveness part of the model is relevant in the controller design. In this way, the robustness is enhanced as the controller is not dependent on accurate internal dynamics. The incremental approach applies first-order Taylor series expansion to the system (Eq. 42) at the current states and inputs as

$$\dot{\boldsymbol{x}}_i \approx \dot{\boldsymbol{x}}_{i,0} + \left.\frac{\partial(\boldsymbol{b}_i + \boldsymbol{A}_i\boldsymbol{x}_{i+1})}{\partial \boldsymbol{x}_i}\right|_{\substack{\boldsymbol{x}_i=\boldsymbol{x}_{i,0}\\ \boldsymbol{x}_{i+1}=\boldsymbol{x}_{i+1,0}}} \left(\boldsymbol{x}_i - \boldsymbol{x}_{i,0}\right) + \boldsymbol{A}_i(\boldsymbol{x}_0)\left(\boldsymbol{x}_{i+1} - \boldsymbol{x}_{i+1,0}\right), i = 1, 2, ..., n. \tag{45}$$

Apply the time-scale separation principle, the second term in Eq. 45 can be neglected. So, the system dynamics and the input-output linearization are approximated to be

$$\dot{\boldsymbol{x}}_i = \dot{\boldsymbol{x}}_{i,0} + \boldsymbol{A}_i(\boldsymbol{x}_0)\Delta\boldsymbol{x}_{i+1}, i = 1, 2, ..., n, \tag{46}$$

$$\boldsymbol{x}_{i+1,\mathrm{com}} = \boldsymbol{A}_i^{-1}(\boldsymbol{x}_0)\left(\boldsymbol{\nu}_i(\boldsymbol{x}) - \dot{\boldsymbol{x}}_{i,0}\right) + \boldsymbol{x}_{i+1,0}, i = 1, 2, ..., n. \tag{47}$$

It should be noted that the incremental approach proposes additional requirements on the control system [44, 47]: 1) the controller should have access to measurements of state derivatives (especially derivatives of angular rates), and 2) the system should have both fast sampling rates and fast control actions. Therefore, a combined approach is usually adopted with the incremental approach for dynamic loops and the ordinary approach for kinematic loops whose equations of motion are universal with no uncertainties.

B. Multi-Loop NDI with PCH

When FEP systems are embedded in the framework of multi-loop NDI, the commands generated by outer loops are no longer directly fed into inner loops, but modified by FEP systems. This will affect both the stability and the tracking performance of outer loops, as NDI assumes stable linear inner-loop dynamics. Therefore, an additional feedback to the outer loop is required to compensate for the discrepancy. In terms of controller structure, a similar framework in multi-loop nonlinear control is observed in command-filtered backstepping [48, 49], which adds command filters between loops, possibly with magnitude and rate constraints, to obtain derivatives of commands required in backstepping. The discrepancy induced by command filters is compensated in outer loops. However, the goal of command-filtered backstepping is still asymptotic stability of the whole system, regardless of saturation in command filters. The compensation strategy thus amplifies future outer-loop commands when inner-loop commands are protected. This will lead to more saturation in inner-loop FEP systems, which is against the safety requirements. In addition, asymptotic stability is not always possible since FEP needs to override tracking of the reference when needed. Therefore, the framework of command filtering is not suitable for the application of FEP.

Then, interest was drawn to another framework, namely PCH. PCH was originally proposed to avoid the effect of input saturation on system identification by adaptive neural network [50, 51]. The concept was later expanded to general flight control systems as a way to avoid and compensate for actuator saturation of control surfaces [52, 53]. It was proved in Ref. [50] that the system will remain bounded with PCH when the modification to the command is bounded. It is noted that the goal of command modification in FEP is also to minimize saturation or activation of FEP systems. When inner-loop commands are protected by FEP systems, future outer-loop commands will be attenuated by PCH to prevent future violation of the flight envelope. Therefore, PCH was selected as the command compensation strategy by generalizing from only the innermost loop for input saturation to multiple loops for both input saturation and FEP.

Consider an affine system as Eq. 42. The block diagram of multi-loop NDI controllers with FEP and PCH is shown in Fig. 7. As shown in Fig. 7, the original command generated by outer-loop NDI is now known as the reference signal $\boldsymbol{x}_{i,\mathrm{ref}}$. This signal is protected by state-constraint-based or probabilistic FEP system with Eq. 38 or 40, and becomes the envelope-protected signal $\boldsymbol{x}_{i,\mathrm{fep}}$. Then, the envelope-protected signal is compensated by PCH to be the final command $\boldsymbol{x}_{i,\mathrm{com}}$ to the inner loop. The following reference model is used for PCH.

$$\dot{\boldsymbol{x}}_{i,\mathrm{com}} = \boldsymbol{K}_{\mathrm{ref},i}(\boldsymbol{x}_{i,\mathrm{fep}} - \boldsymbol{x}_{i,\mathrm{com}}) - \boldsymbol{\nu}_{\mathrm{h},i}, \tag{48}$$

where

$$\boldsymbol{\nu}_{\mathrm{h},i} = \boldsymbol{A}_i(\boldsymbol{x})\left(\boldsymbol{x}_{i+1,\mathrm{ref}} - \boldsymbol{x}_{i+1,\mathrm{fep}}\right) \tag{49}$$

is the hedged virtual control due to inner-loop FEP, $\boldsymbol{K}_{\mathrm{ref},i}$ is the reference model gain.

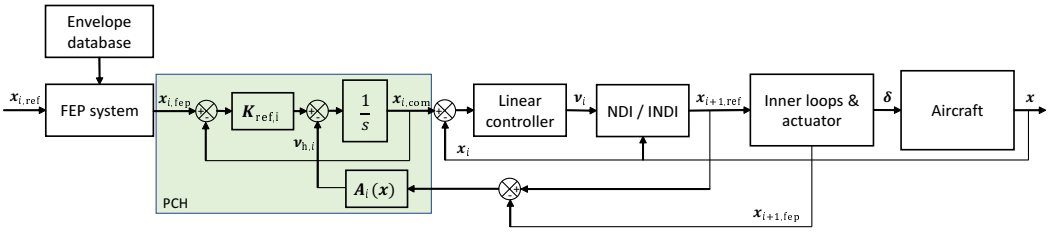

Fig. 7 Block diagram of multi-loop NDI controllers with FEP and PCH.

VI. The ICE Aircraft Model

The proposed probabilistic envelope estimation and protection framework was implemented on a simulation model of Lockheed Martin's ICE aircraft. The ICE project was initiated at the former Wright Laboratory in 1993, aiming to explore novel control surfaces for high-performance fighter aircraft to achieve low radar cross-section, high angle of attack (AoA) effectiveness, low lift-to-drag ratio and reduced hinge moments [54]. Selected designs were later undergone wind tunnel tests for aerodynamic data. This paper focuses on a land-based configuration of the ICE aircraft (ICE 101-TV) with a tailless delta wing with a 65° sweep angle and a single engine. The following sections introduce its control suite and the high-fidelity model used to test the framework.

Table 1 Position and rate limits of the control effectors on the ICE aircraft.

	Positive deflection	Position limit [deg]	Rate limit [deg/s]
Inboard LEF	Leading edge down	$[0, 40]$	$[-40, 40]$
Outboard LEF	Leading edge down	$[-40, 40]$	$[-40, 40]$
AMT	Trailing edge down	$[0, 60]$	$[-150, 150]$
Pitch TV	$\dot{q} > 0$	$[-15, 15]$	$[-150, 150]$
Yaw TV	$\dot{r} > 0$	$[-15, 15]$	$[-150, 150]$
SSD	Trailing edge up	$[0, 60]$	$[-150, 150]$
PF	Trailing edge down	$[-30, 30]$	$[-150, 150]$
Elevons	Trailing edge down	$[-30, 30]$	$[-150, 150]$

A. The ICE Control Suite

The ICE control suite consists of 13 control effectors of six types, namely inboard and outboard leading-edge flaps (LEF), all-moving wing tips (AMT), fluidic multi-axis thrust vectoring (MATV), spoiler-slot deflectors (SSD), pitch flaps (PF), and elevons. The configuration of these control effectors is illustrated in Figure 8.

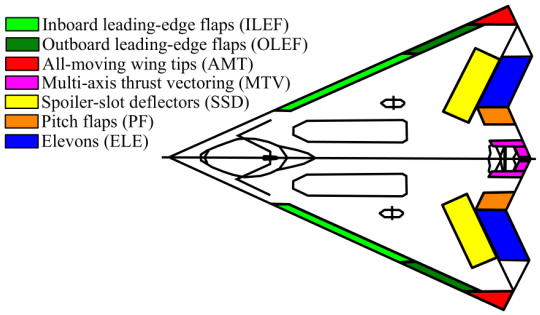

Fig. 8 Control effector configuration of the ICE aircraft [35].

The baseline control of the ICE aircraft is provided by two symmetrically-deflected PFs and two elevons. Elevons can provide both pitching and rolling moments by deflecting symmetrically and asymmetrically respectively. In addition, two inboard and two outboard LEFs can provide lateral-directional control authority at moderate to high AoA. Yaw control authority at very high AoA is rendered by two AMTs. Two specially-designed SSDs can open a slot through the wing for air to flow in when deflected, to provide additional lateral-directional control authority at high AoA and in transonic flight. However, SSDs also induce strong coupling with effectors downstream. These aerodynamic effectors are supplemented by MATV, which alters the direction of the thrust to provide additional forces and moments. This is implemented in both pitch and yaw directions.

Depending on their characteristics, different positions and no-load rate limits are specified for the control effectors, which are summarized in Table 1 [35]. The upper and lower boundaries of the control surface deflections are then

$$\begin{cases} \boldsymbol{\delta}_{\mathrm{u}}(t) = \min\left(\boldsymbol{\delta}_{\max}, \boldsymbol{\delta}_0 + \dot{\boldsymbol{\delta}}_{\max}\Delta t\right) \\ \boldsymbol{\delta}_{\mathrm{l}}(t) = \max\left(\boldsymbol{\delta}_{\min}, \boldsymbol{\delta}_0 - \dot{\boldsymbol{\delta}}_{\min}\Delta t\right) \end{cases}, \tag{50}$$

where $\boldsymbol{\delta}_{\max}, \boldsymbol{\delta}_{\min}$ are the position limits, $\dot{\boldsymbol{\delta}}_{\max}, \dot{\boldsymbol{\delta}}_{\min}$ are the rate limits. These boundaries define the set of admissible inputs U.

B. The High-Fidelity Model of the ICE Aircraft

The ICE aircraft is still in the development phase. However, a high-fidelity aerodynamic model was released based on wind tunnel tests from Lockheed Martin for academic use. The core part of the model describes all the dimensionless

aerodynamic coefficients of forces and moments with respect to states of the aircraft as well as control surface deflections in the aerodynamic model body frame $\mathbb{F}^m$ (back-right-up). These coefficients are expressed by summations of terms which model the contribution of the base airframe, aerodynamic control surfaces, and interactions between control surfaces as

$$C_i = \sum_j C_{ij}\left(\boldsymbol{\delta}, M, \alpha, \beta, p, q, r\right) \tag{51}$$

where $i \in \left\{F_x, F_y, F_z, M_x, M_y, M_z\right\}$. The nonlinear terms C_{ij} are stored in look-up tables (LUT) and interpolated by cubic spline interpolation. Details of the aerodynamic database can be found in Ref. [55]. The contribution of the throttle together with the MATV is described by an additional thrust vectoring model as

$$\begin{cases} F_{x,tv} = T\cos\delta_{\text{ptv}}\sec\delta_{\text{ytv}}, \\ F_{y,tv} = T\cos\delta_{\text{ptv}}\tan\delta_{\text{ytv}}, \\ F_{z,tv} = T\sin\delta_{\text{ptv}}, \\ M_{x,tv} = 0, \\ M_{y,tv} = -Td_n\sin\delta_{\text{ptv}}, \\ M_{z,tv} = -Td_n\cos\delta_{\text{ptv}}\tan\delta_{\text{ytv}}, \end{cases} \tag{52}$$

where δ_{ptv} and δ_{ytv} are deflections of the pitch and yaw thrust vectoring respectively, d_n is the moment arm of the thrust force. The dynamics of the control surface deflections are modeled with second-order dynamics. The engine is modeled with first-order dynamics. Three predefined mass configurations can be used for light-load, nominal, and heavy-load cases. The above databases and models are embedded in a Simulink model that solves the equations of motion in real-time. Simulation results can be displayed to the open-source flight simulator FlightGear for visualization. The simulation model runs at 100Hz.

Previous research elaborated the model with a physical spline identification of the aerodynamic database [56] and an incremental nonlinear control allocation (INCA) scheme which effectively allocates the desired aerodynamic moments to control effectors [35]. The physical spline model identified each of the nonlinear terms C_{ij} with a physical spline of 0th-order continuity. Thus, the control effectiveness matrix

$$\boldsymbol{J}_d = \begin{bmatrix} \sum_{j=1}^{17} \dfrac{\partial C_{F_x,j}(\boldsymbol{\delta}, \boldsymbol{x})}{\partial \boldsymbol{\delta}} \cdot \bar{q}S \\ \sum_{j=1}^{17} \dfrac{\partial C_{F_y,j}(\boldsymbol{\delta}, \boldsymbol{x})}{\partial \boldsymbol{\delta}} \cdot \bar{q}S \\ \sum_{j=1}^{18} \dfrac{\partial C_{F_z,j}(\boldsymbol{\delta}, \boldsymbol{x})}{\partial \boldsymbol{\delta}} \cdot \bar{q}S \\ \sum_{j=1}^{19} \dfrac{\partial C_{M_x,j}(\boldsymbol{\delta}, \boldsymbol{x})}{\partial \boldsymbol{\delta}} \cdot \bar{q}Sb \\ \sum_{j=1}^{18} \dfrac{\partial C_{M_y,j}(\boldsymbol{\delta}, \boldsymbol{x})}{\partial \boldsymbol{\delta}} \cdot \bar{q}S\bar{c} \\ \sum_{j=1}^{19} \dfrac{\partial C_{M_z,j}(\boldsymbol{\delta}, \boldsymbol{x})}{\partial \boldsymbol{\delta}} \cdot \bar{q}Sb \end{bmatrix} \tag{53}$$

can be updated efficiently in real-time by summing up the gradient of each spline model analytically for each aerodynamic control effector. The control effectiveness of MATV is obtained by directly taking partial derivatives of Eq. 52.

Since the control surfaces are highly redundant for the ICE aircraft, the input-output linearization (Eq. 47) of the angular rate loop in the incremental NDI controller is not trivial. The INCA scheme searches for the best combination of incremental control surface deflections that satisfies both the input-output linearization relation and the position and rate limits of the actuators based on the dynamic control effectiveness matrix. This control allocation scheme is also used in the controller design of this paper.

VII. Implementation

The detailed implementation of the probabilistic envelope estimation and protection framework on the ICE aircraft is introduced in this section. This section starts by discussing calculation of the trim set and selection of protected states. Then, the detailed controller structure with FEP is introduced.

A. Trim Set

As the starting point of envelope estimation, the trim set of the ICE aircraft needs to be specified as the apriori safe set K. Trimming aims to find the equilibrium points of the system by formulating a constrained optimization problem that constrains state derivatives to zero.

This paper considers steady-state, straight, and level flights at altitudes between 10000 ft and 30000 ft and Mach numbers between 0.4 and 1.2 as the trim set of the ICE aircraft. Individual trim points are optimized on an altitude-Mach grid within this range. The trim points are then interpolated by cubic splines to form a continuous trim set. Only AMTs, elevons, and pitch thrust vectoring are used to trim the aircraft for efficiency. Note that AMTs and elevons deflect symmetrically in a level flight. Therefore, the following variables are optimized

$$\boldsymbol{x}_{\text{trim}} = [T \ d_{\text{amt}} \ d_{\text{ele}} \ d_{\text{ptv}} \ \alpha]^T, \tag{54}$$

with the following constraints

$$\dot{p} = \dot{q} = \dot{r} = \dot{u} = \dot{v} = \dot{w} = \phi = \theta - \alpha = 0. \tag{55}$$

The objective function is formulated as

$$J = J_1 + k_{\text{trim}} \cdot J_2, \tag{56}$$

where k_{trim} is a weighting factor,

$$J_1 = \left(\frac{T}{T_{\max}}\right)^2, J_2 = d_{\text{amt}}[\text{rad}]^2 + d_{\text{ele}}[\text{rad}]^2 + d_{\text{ptv}}[\text{rad}]^2 \tag{57}$$

are the objectives of minimum thrust and minimum control effort respectively.

This constrained optimization problem is solved by a sequential quadratic programming solver. The trimmed AoA at the nominal mass configuration is shown in Fig. 9. This process is repeated for different mass configurations and the case without thrust vectoring to compare envelope estimation results in Sec. VIII. When thrust vectoring is not activated, PFs are used to trim the aircraft.

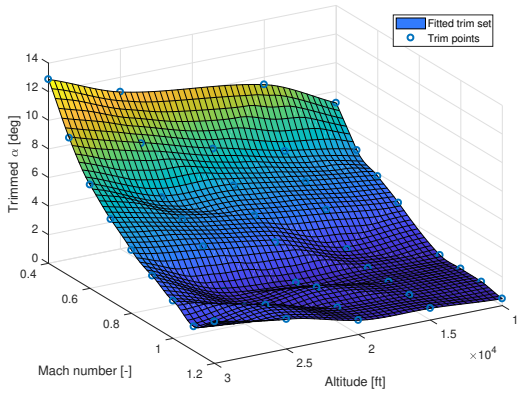

Fig. 9 Trimmed AoA at different altitudes and speeds with nominal mass configuration.

B. State Definition

This paper considers seven states in the FEP of the ICE aircraft, including altitude h, ground speed V_g, aerodynamic angles α, β, and angular rates p, q, r, which can well characterize the agility of the aircraft. It should be noted that roll angle ϕ and pitch angle θ are not included. This is because high-performance fighter aircraft like the ICE aircraft should be able to steer to virtually any attitude. Instead, angular rates are protected to limit specific dangerous maneuvers. In this way, a seven-dimensional envelope database was established.

However, the reachability analysis framework works with open-loop commands only. This limits the time horizon for inherently unstable aircraft like the ICE aircraft, as the flight tends to be unstable with open-loop commands. For the ICE aircraft, random open-loop commands can hardly stabilize the aircraft after 1.5s. This time horizon is smaller than the characteristic time scales of altitude h and ground speed V_g. Thus, the altitude and the speed are not protected in the applied FEP systems, but only used as parameters to obtain the envelope of the other five states.

C. Controller Structure

The controller implemented in this paper is a two-loop controller, which consists of an outer loop of aerodynamic angles ϕ, α, β with ordinary NDI and an inner loop of angular rates p, q, r with incremental NDI. The outer loop is selected to test high AoA maneuvers for which the ICE aircraft is optimized. So, we have

$$\boldsymbol{x}_1 = [\phi\ \alpha\ \beta]^T, \boldsymbol{x}_2 = [p\ q\ r]^T, \boldsymbol{x}_3 = \boldsymbol{\delta}. \tag{58}$$

The dynamics of the outer loop are

$$\begin{aligned}\dot{\boldsymbol{x}}_1 = \frac{\mathrm{d}}{\mathrm{d}t}\begin{bmatrix}\phi\\ \alpha\\ \beta\end{bmatrix} &= \begin{bmatrix} 0 \\ \frac{1}{u^2+w^2}\left(u\tilde{A}_z - w\tilde{A}_x\right) \\ \frac{1}{\sqrt{u^2+w^2}}\left[\frac{-uv}{V_g^2}\tilde{A}_x + (1-\frac{v^2}{V_g^2})\tilde{A}_y - \frac{vw}{V_g^2}\tilde{A}_z\right]\end{bmatrix} + \begin{bmatrix} 1 & \sin\phi\tan\theta & \cos\phi\tan\theta \\ \frac{-uv}{u^2+w^2} & 1 & \frac{-vw}{u^2+w^2} \\ \frac{w}{\sqrt{u^2+w^2}} & 0 & \frac{-u}{\sqrt{u^2+w^2}}\end{bmatrix}\begin{bmatrix}p\\ q\\ r\end{bmatrix} \\ &= \begin{bmatrix}0\\ b_\alpha(\boldsymbol{x})\\ b_\beta(\boldsymbol{x})\end{bmatrix} + \begin{bmatrix}\boldsymbol{a}_\phi(\boldsymbol{x})\\ \boldsymbol{a}_\alpha(\boldsymbol{x})\\ \boldsymbol{a}_\beta(\boldsymbol{x})\end{bmatrix}\boldsymbol{x}_2,\end{aligned} \tag{59}$$

where

$$\tilde{A}_x = A_x - g\sin\theta, \tilde{A}_y = A_y + g\sin\phi\cos\theta, \tilde{A}_z = A_z + g\cos\phi\cos\theta \tag{60}$$

are the linear accelerometer measurements plus gravity components. The NDI control law for the aerodynamic angle loop is

$$\boldsymbol{x}_{2,\mathrm{ref}} = \begin{bmatrix}p_{\mathrm{ref}}\\ q_{\mathrm{ref}}\\ r_{\mathrm{ref}}\end{bmatrix} = \begin{bmatrix}\boldsymbol{a}_\phi(\boldsymbol{x})\\ \boldsymbol{a}_\alpha(\boldsymbol{x})\\ \boldsymbol{a}_\beta(\boldsymbol{x})\end{bmatrix}^{-1}\left(\boldsymbol{\nu}_1 - \begin{bmatrix}0\\ b_\alpha(\boldsymbol{x})\\ b_\beta(\boldsymbol{x})\end{bmatrix}\right). \tag{61}$$

The dynamics of the inner loop in the incremental form are

$$\dot{\boldsymbol{x}}_2 = \frac{\mathrm{d}}{\mathrm{d}t}\begin{bmatrix}p\\ q\\ r\end{bmatrix} = \boldsymbol{J}^{-1}\left(\begin{bmatrix}M_x\\ M_y\\ M_z\end{bmatrix} - \begin{bmatrix}p\\ q\\ r\end{bmatrix}\times\boldsymbol{J}\begin{bmatrix}p\\ q\\ r\end{bmatrix}\right) \approx \begin{bmatrix}\dot{p}_0\\ \dot{q}_0\\ \dot{r}_0\end{bmatrix} + \boldsymbol{I}^{-1}\boldsymbol{J}_d^M(\boldsymbol{x}_0, \boldsymbol{\delta}_0)\Delta\boldsymbol{\delta}, \tag{62}$$

The INDI control law for the angular rate loop is

$$\boldsymbol{x}_{3,\mathrm{ref}} = \boldsymbol{\delta}_{\mathrm{com}} = \left(\boldsymbol{J}_d^M\right)^{-1}\boldsymbol{J}\left(\boldsymbol{\nu}_2 - \begin{bmatrix}\dot{p}_0\\ \dot{q}_0\\ \dot{r}_0\end{bmatrix}\right). \tag{63}$$

It is assumed that the ICE aircraft is equipped with angular acceleration sensors to obtain measurements of angular rate derivatives. The control effectiveness matrix of aerodynamic moments $\boldsymbol{J}_d^M$ is updated at each time step by the onboard aerodynamic database developed in Ref. [56]. Note that $\boldsymbol{J}_d^M$ is non-square for the ICE aircraft due to over-actuation. The procedure to obtain the generalized inversion of the matrix is known as control allocation. In this paper, the INCA scheme developed in Ref. [35] is applied.

The throttle of the aircraft is controlled by a separated auto-throttle loop. The auto-throttle loop applies INDI to the following incremental dynamics of speed

$$\begin{aligned}\dot{V}_g &= \frac{1}{m}\left(\cos\alpha\cos\beta\cdot F_x + \sin\beta\cdot F_y + \sin\alpha\cos\beta\cdot F_z\right) - g\sin\gamma \\ &\approx \dot{V}_{g,0} + \frac{1}{m}\left(\cos\alpha\cos\beta\cdot\frac{\partial F_x}{\partial T} + \sin\beta\cdot\frac{\partial F_y}{\partial T} + \sin\alpha\cos\beta\cdot\frac{\partial F_z}{\partial T}\right)\Delta T \\ &= \dot{V}_{g,0} + a_T(\boldsymbol{x})\Delta T,\end{aligned} \tag{64}$$

The new thrust setting is selected as

$$T_{\text{com}} = T_0 + \frac{k_T(V_{g,\text{ref}} - V_g) - \dot{V}_{g,0}}{a_T(\boldsymbol{x})}, \tag{65}$$

where k_T is the proportional gain. This dynamic inversion is not trivial for the ICE aircraft, since 1) the thrust force can be distributed in all three directions due to MATV, and 2) the ICE aircraft can operate at high AoA and sideslip angles.

To sum up, the complete block diagram of the envelope-protected nonlinear flight control system with aerodynamic angle commands is demonstrated in Fig. 10.

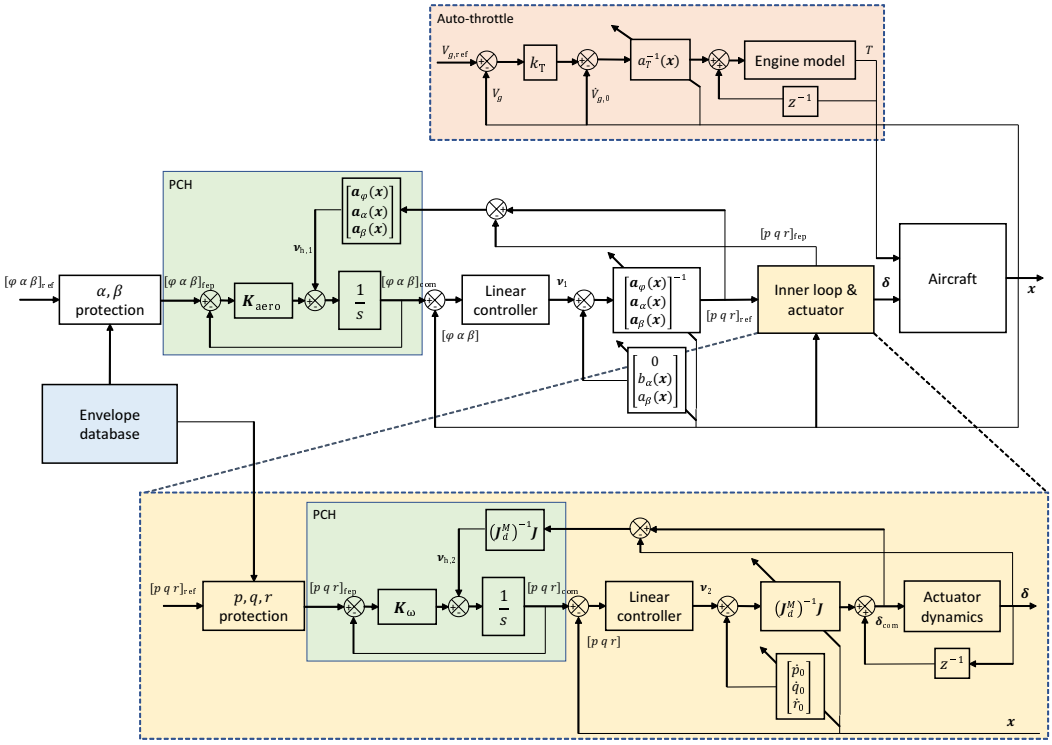

Fig. 10 Block diagram of FCS with FEP on the ICE aircraft.

VIII. Results

This section demonstrates the probabilistic envelope estimation results and performances of the proposed FCS with FEP by a simulation platform built on the high-fidelity model of the ICE aircraft in Matlab and Simulink. The goals are to validate the reliability of the envelope estimation with MC simulations and the effectiveness of the proposed FEP strategies. Unfortunately, the envelope estimation results cannot be validated by directly comparing with other methods such as the level-set method, as other methods are computationally impractical for this model. Therefore, it is validated by comparing the estimated envelopes at different flight conditions to show a reasonable correlation to the size of the envelope. In addition, improved controller performances should be observed when the aircraft is protected within the

estimated envelope. The effectiveness of the FEP strategies is demonstrated by testing maneuvers that result in LOC when no FEP is applied.

The procedures of the probabilistic envelope estimation described in Fig. 4 are demonstrated in Fig. 11. This baseline envelope estimation was conducted with nominal mass configuration, no disturbance, and full control effectors. The time horizon was selected as 1.5 s. These flight conditions were altered for comparison as shown in later results. The sample size of the MC simulation is 10,000. The objective weighting factor in trimming k_{trim} is 1. Two 3-D slices of the estimated envelope are plotted at 20,000 ft and Mach 0.85 to show the longitudinal and lateral envelopes respectively. This routine starts with the raw MC simulation samples in Fig. 11 a), followed by the kernel density estimators of reachable sets in Fig. 11 b). It can be seen that the kernel density estimators can well capture the distribution of the samples. The probabilistic intersections of the reachable sets in Fig. 11 c) form the estimated envelope. Two α-cuts at $k_0 = 1, 2$ are plotted for the fuzzy sets to demonstrate the probabilistic nature of the estimation.

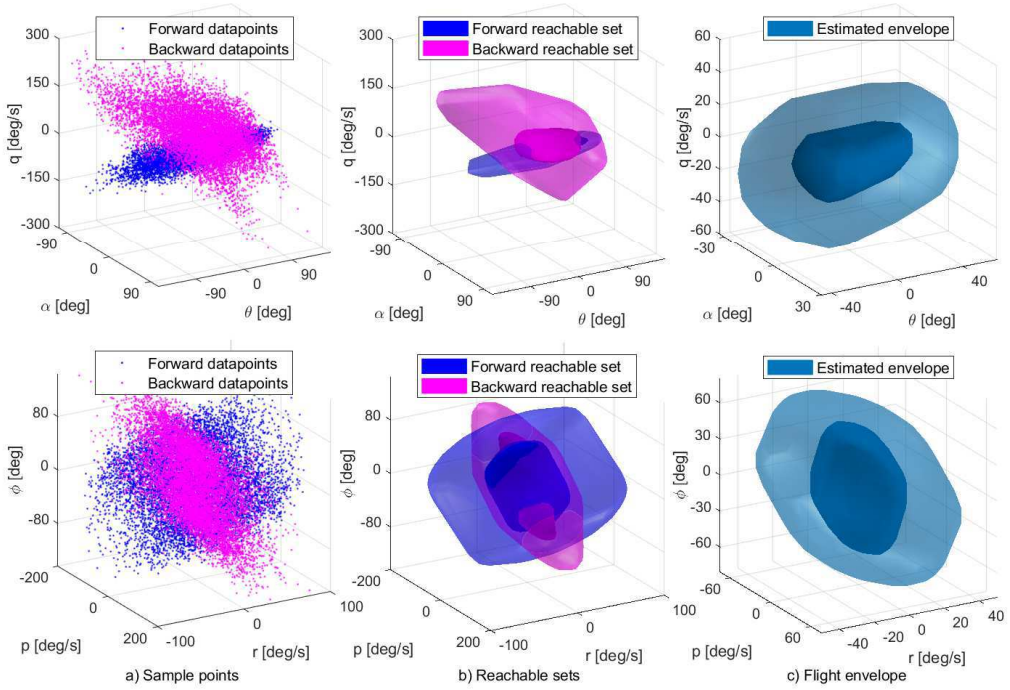

Fig. 11 Demonstration of envelope estimation with MC simulation under the baseline flight condition. Inner volume: the α-cut at 1σ, outer volume: the α-cut at 2σ.

Since it is hard to directly illustrate the whole seven-dimensional envelope, covariance analysis was conducted to show the characteristics of the results as in Fig. 12. The covariance matrices of the five protected states p, q, r, α, β were calculated on a grid of h and V_g and interpolated by fourth-order polynomials. The diagonal elements are square-rooted to be the characteristic sizes of the envelope at 1σ and denoted as

$$\sigma_i = \sqrt{\text{cov}(i,i)}, i \in \{p, q, r, \alpha, \beta\}\,. \tag{66}$$

The off-diagonal elements are normalized to be the correlations between two states and denoted as

$$\rho_{ij} = \frac{\text{cov}(i,j)}{\sigma_i \sigma_j}, i, j \in \{p, q, r, \alpha, \beta\}, i \neq j. \tag{67}$$

It is observed that there is no correlation between longitudinal states q, α and lateral states p, r, β. The other 9 elements are plotted. As shown in Fig. 12, the envelopes of roll and yaw rates enlarge with speed, whereas the envelope of α shrinks with speed. The envelopes of q and β peak at around 850 ft/s.

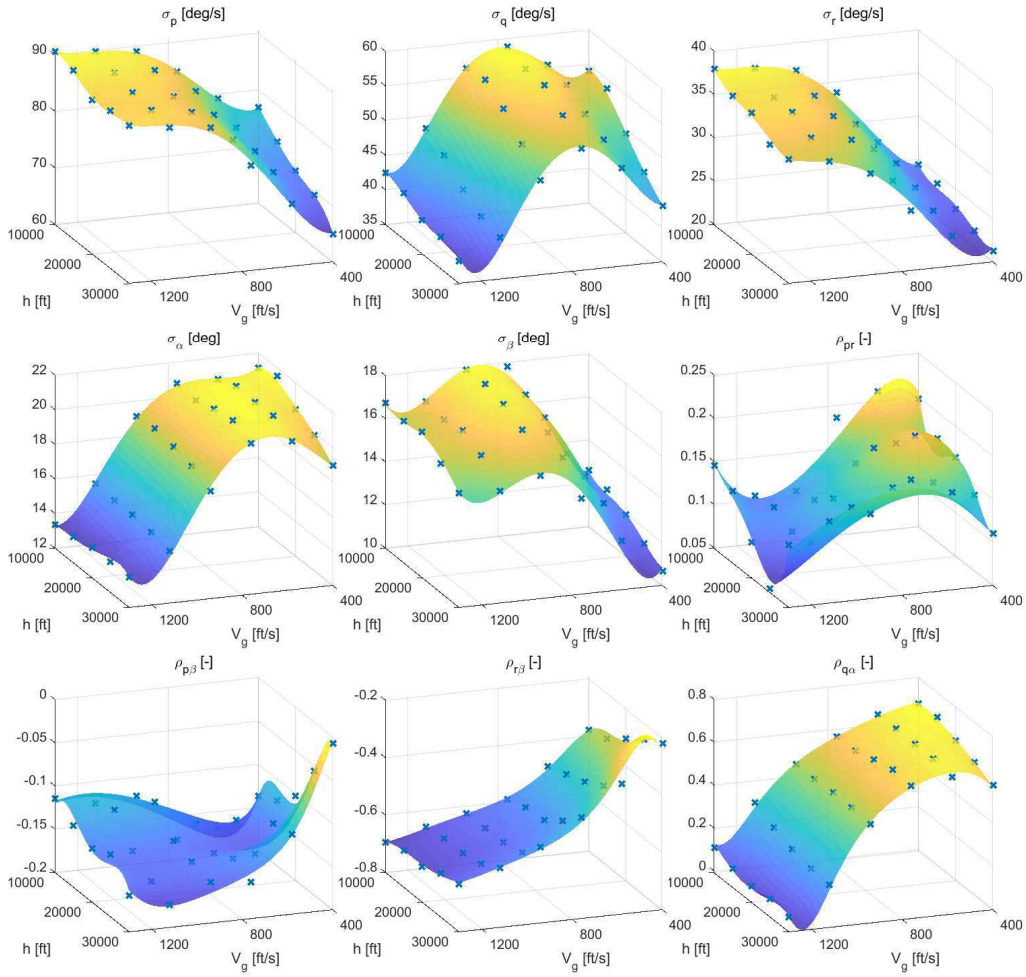

Fig. 12 Covariance analysis of the estimated envelope under the baseline flight condition.

The estimation was validated by comparing various flight conditions. Fig. 13 shows different estimation results under different time horizons, control effectors, disturbances, and mass configurations. 2-D slices of the envelope are plotted both longitudinally and laterally at two different speeds (500 ft/s and 800 ft/s) to compare the envelope size. It is shown that the size of the envelope grows significantly with the time horizon. The inclusion of thrust vectoring especially helps enhance the maneuverability in the yaw direction but has less effect on other states. Severe disturbance can enlarge the estimated envelope, as it may help steer the aircraft in the direction that enlarges the envelope under some cases. As for the mass configuration, a lightweight configuration can also enlarge the envelope. All these correlations agree with predictions.

In the envelope protection scheme, the ranges and resolutions of the states stored in the envelope database are shown in Table 2. The applied linear controller gains for both loops and the auto-throttle are listed in Table 3, as well as the compensation gains of the probabilistic FEP $\boldsymbol{K}_{\text{fep}}$. The reference model gains in PCH $\boldsymbol{K}_{\text{ref},i}$ were selected the same as the proportional gains of the same loop $\boldsymbol{K}_{\text{p},i}$. The threshold k_0 of the state-constraint-based FEP was selected as 3. The threshold to activate the probabilistic envelope protection M_0 is 0. All simulations of the controller start with a trimmed flight at 20,000 ft and Mach 0.85.

The performance of the envelope-protected controller was tested by two sample maneuvers. The first command, known as Maneuver A, is a triangular α signal with a base of 4 s and a height of 90 deg. The selection of triangular signals over pulses or doublets is to demonstrate the difference between the two FEP strategies: state-constraint-based

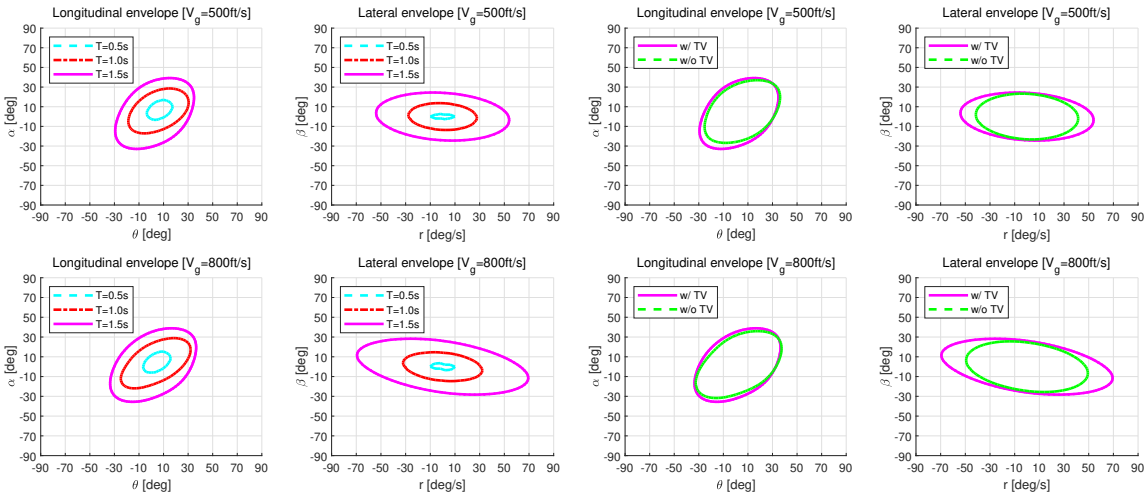

a) Time horizon.

b) Thrust vectoring.

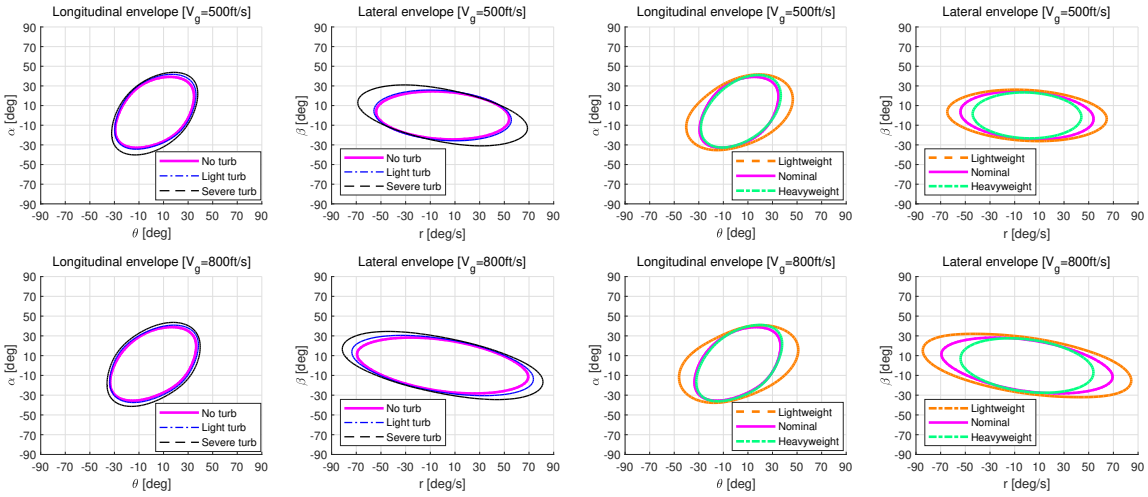

c) Disturbance.

d) Mass configuration.

Fig. 13 Comparison of envelope estimation results under different flight conditions.

FEP only activates above a certain threshold, whereas probabilistic FEP activates throughout the flight. The controller performance is shown in Fig. 14. The second command, known as Maneuver B, is a combined α-β command of two consecutive triangular signals with opposite signs. The triangular signals have a base of 6s and a height of 50 deg. The β signal lags 2s behind the α signal. The controller performance is shown in Fig. 15. The commands are prefiltered by a low-pass filter. For both maneuvers, LOC is observed without FEP.

It can be seen that both FEP strategies are effective in protecting the aircraft against LOC. The state-constraint-based method performs completely the same as a normal controller in the beginning. Then after the state constraints are activated, the command steers to follow the estimated state constraints immediately. In contrast, the probabilistic method actively modifies the command throughout the flight based on the membership value of the current state. Thus, the aircraft response is smoother with better ride quality. A direct comparison of the controller performance in terms of FEP is shown in Fig. 16 by the probabilistic envelope metric. A higher value means the aircraft is safer in the envelope. However, it should be noted that both FEP strategies are flexible in aggressiveness by tuning the threshold value k_0 and the compensation gain $\boldsymbol{K}_{\text{fep}}$ respectively.

Table 2 Grid of the envelope database

	Min	Max	Res
p [deg/s]	-150	150	30
q [deg/s]	-150	150	30
r [deg/s]	-60	60	30
α [deg]	-60	60	5
β [deg]	-45	45	5
V_g [ft/s]	400	1300	180
h [ft]	10,000	30,000	5000

Table 3 Summary of controller gains.

	Inner loop			Outer loop			Auto-throttle
	p	q	r	ϕ	α	β	T
$\boldsymbol{K}_{\text{p}}$	6.50	6.50	5.80	2.00	2.00	1.60	1.00
$\boldsymbol{K}_{\text{i}}$	0.00	0.00	0.00	0.50	0.50	0.30	0.00
$\boldsymbol{K}_{\text{d}}$	0.00	0.00	0.50	0.90	0.90	0.00	0.00
$\boldsymbol{K}_{\text{fep}}$	0.05	0.05	0.05	N/A	0.80	0.80	N/A

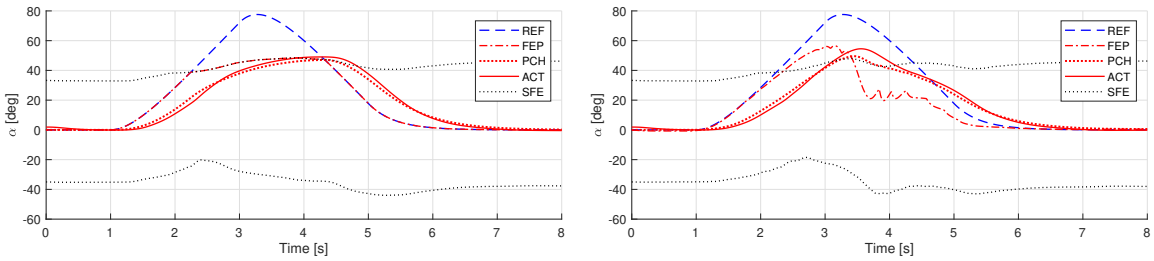

a) State-constraint-based FEP. b) Probabilistic FEP.

Fig. 14 Comparison of FEP performances for Maneuver A. REF: reference, FEP: command after FEP, PCH: command after PCH, ACT: actual response, SFE: estimated envelope boundary.

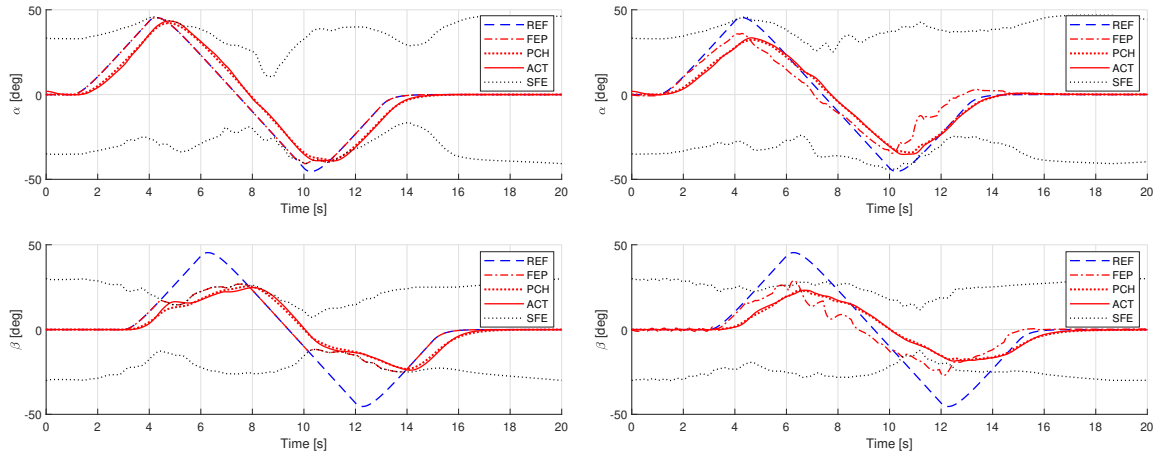

a) State-constraint-based FEP. b) Probabilistic FEP.

Fig. 15 Comparison of FEP performances for Maneuver B. REF: reference, FEP: command after FEP, PCH: command after PCH, ACT: actual response, SFE: estimated envelope boundary.

IX. Conclusion

This paper presents a novel framework to apply high-dimensional envelope estimation and protection to aircraft with complex nonlinear models. The framework extends the definition of the flight envelope to fuzzy sets and uses

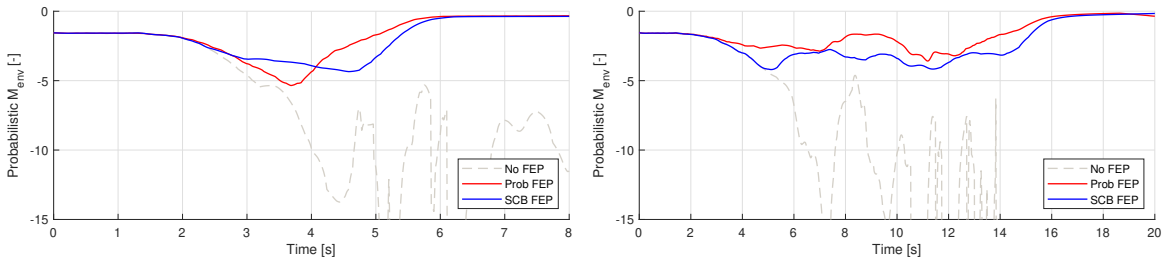

a) Maneuver A. b) Maneuver B.

Fig. 16 Effectiveness of FEP in terms of the probabilistic envelope metric.

MC simulation with extreme control effectiveness sampling to circumvent solving the optimization problem directly. In this way, the probabilistic envelope can be estimated conservatively and efficiently under flexible flight conditions for no less than seven dimensions. Furthermore, the estimated envelope is stored onboard to provide online dynamic FEP to a multi-loop NDI controller with both conventional command limiting and predictive probabilistic modification strategies. Simulation results on a high-performance fighter aircraft show both good validity of the estimation and effective protection capability to avoid LOC.

However, this framework still relies on offline estimation. Future work can be conducted to include aircraft damage models to extend the application to fault tolerant control. It is also preferable to adopt close-loop commands in this framework for envelope estimation of slow variables.

References

[1] Ranter, H., "Airliner accident statistics 2006," Report, Aviation Safety Network, 2007.

[2] "Statistical Summary of Commercial Jet Airplane Accidents: Worldwide Operations 1959–2015," Report, Aviation Safety, Boeing Commercial Airplanes, 2016. URL `http://www.boeing.com/news/techissues/pdf/statsum.pdf`.

[3] "Annual Safety Review," Report, European Aviation Safety Agency, 2011. URL `https://www.easa.europa.eu/system/files/dfu/EASA-Annual-Safety-Review-2011.pdf`.

[4] Kwatny, H. G., Dongmo, J.-E. T., Chang, B.-C., Bajpai, G., Yasar, M., and Belcastro, C., "Nonlinear analysis of aircraft loss of control," *Journal of Guidance, Control, and Dynamics*, Vol. 36, No. 1, 2012, pp. 149–162. doi:10.2514/1.56948.

[5] Smaili, M., and Mulder, J., "Flight data reconstruction and simulation of the 1992 Amsterdam Bijlmermeer airplane accident," *Modeling and Simulation Technologies Conference*, 2000, p. 4586. doi:10.2514/6.2000-4586.

[6] Ruijgrok, G. J. J., *Elements of airplane performance*, VSSG, Delft, the Netherlands, 2009.

[7] Russell, P., and Pardee, J., "Final Report: JSAT Loss of Control: Results and Analysis," Report, Federal Aviation Administration: Commercial Airline Safety Team, 2000. URL `http://www.cast-safety.org/pdf/jsat_loss-control.pdf`.

[8] Helsen, R., Van Kampen, E.-J., de Visser, C. C., and Chu, Q. P., "Distance-Fields-Over-Grids Method for Aircraft Envelope Determination," *Journal of Guidance, Control, and Dynamics*, Vol. 39, No. 7, 2016, pp. 1470–1480. doi:10.2514/1.g000824.

[9] Kwatny, H. G., Donqmo, J.-E. T., Chanq, B.-C., Bajpai, G., Yasar, M., and Belcastro, C. M., "Aircraft accident prevention: Loss-of-control analysis," *AIAA Guidance, Navigation, and Control Conference*, 2009, pp. 10.2514/6.2009–6256.

[10] van Oort, E. R., "Adaptive Backstepping Control and Safety Analysis for Modern Fighter Aircraft," Thesis, 2011.

[11] Tang, L., Roemer, M., Ge, J., Crassidis, A., Prasad, J. V. R., and Belcastro, C., "Methodologies for adaptive flight envelope estimation and protection," *AIAA Guidance, Navigation, and Control Conference*, 2009, p. 6260. doi:10.2514/6.2009-6260.

[12] Boškovic, J. D., Redding, J., and Knoebel, N., "An Adaptive Fault Management (AFM) system for resilient flight control," *AIAA Guidance, Navigation, and Control Conference*, 2009. doi:10.2514/6.2009-6263.

[13] Roemer, M., Tang, L., Bharadwaj, S., and Belcastro, C., "An integrated aircraft health assessment and fault contingency management system for aircraft," *AIAA Guidance, Navigation and Control Conference and Exhibit*, 2008, p. 6505. doi:10.2514/6.2008-6505.

[14] Goman, M. G., Khramtsovsky, A. V., and Kolesnikov, E. N., "Evaluation of aircraft performance and maneuverability by computation of attainable equilibrium sets," *Journal of guidance, control, and dynamics*, Vol. 31, No. 2, 2008, p. 329. doi:10.2514/1.29336.

[15] Kwatny, H. G., and Allen, R. C., "Safe set maneuverability of impaired aircraft," *AIAA Atmospheric Flight Mechanics Conference*, 2012. doi:10.2514/6.2012-4405.

[16] Menon, P., Kim, J., Sengupta, P., Vaddi, V., Yang, B.-J., and Kwan, J., "Onboard estimation of impaired aircraft performance envelope," *AIAA Guidance, Navigation, and Control Conference*, 2011. doi:10.2514/6.2011-6688.

[17] Lygeros, J., "On reachability and minimum cost optimal control," *Automatica*, Vol. 40, No. 6, 2004, pp. 917–927. doi:10.1016/j.automatica.2004.01.012.

[18] Goman, M. G., and Demenkov, M. N., "Computation of controllability regions for unstable aircraft dynamics," *Journal of Guidance Control and Dynamics*, Vol. 27, No. 4, 2004, pp. 647–656. doi:10.2514/1.4038.

[19] Girard, A., "Reachability of uncertain linear systems using zonotopes," *Hybrid Systems: Computation and Control*, Vol. 5, Springer, 2005, pp. 291–305. doi:10.1007/978-3-540-31954-2_19.

[20] Nabi, H. N., Lombaerts, T., Zhang, Y., van Kampen, E., Chu, Q. P., and de Visser, C. C., "Effects of Structural Failure on the Safe Flight Envelope of Aircraft," *Journal of Guidance, Control, and Dynamics*, 2018, pp. 1–19. doi:10.2514/1.g003184.

[21] Lombaerts, T., Schuet, S., Wheeler, K., Acosta, D. M., and Kaneshige, J., "Safe maneuvering envelope estimation based on a physical approach," *AIAA Guidance, Navigation, and Control (GNC) Conference*, 2013, pp. 1–20. doi:10.2514/6.2013-4618.

[22] Zhang, Y., de Visser, C. C., and Chu, Q. P., "Online Safe Flight Envelope Prediction for Damaged Aircraft: A Database-Driven Approach," *AIAA Modeling and Simulation Technologies Conference*, 2016, p. 1189. doi:10.2514/6.2016-1189.

[23] van Oort, E. R., Chu, Q. P., and Mulder, J. A., *Maneuver envelope determination through reachability analysis*, Springer, Berlin, Heidelberg, 2011, pp. 91–102. doi:10.1007/978-3-642-19817-5_8.

[24] Kitsios, I., and Lygeros, J., "Launch pad abort flight envelope computation for a personnel launch vehicle using reachability," *AIAA Guidance, Navigation, and Control Conference and Exhibit*, 2005. doi:10.2514/6.2005-6150.

[25] van den Brandt, R., "Safe Flight Envelope Uncertainty Quantification using Probabilistic Reachability Analysis," Thesis, 2017.

[26] Tomlin, C., Mitchell, I., Bayen, A., and Oishi, M., "Computational techniques for the verification of hybrid systems," *Proceedings of the IEEE*, Vol. 91, No. 7, 2003, pp. 986–1001. doi:10.1109/jproc.2003.814621.

[27] Seube, N., Moitie, R., and Leitmann, G., "Viability analysis of an aircraft flight domain for take-off in a windshear," *Mathematical and computer modelling*, Vol. 36, No. 6, 2002, pp. 633–641. doi:10.1016/s0895-7177(02)00164-4.

[28] Tomlin, C., Lygeros, J., and Sastry, S., "Aerodynamic envelope protection using hybrid control," *1998 American Control Conference*, Vol. 3, IEEE, 1998, pp. 1793–1796. doi:10.1109/acc.1998.707322.

[29] Gingras, D. R., Barnhart, B., Ranaudo, R., Ratvasky, T. P., and Morelli, E., "Envelope protection for in-flight ice contamination," *47th AIAA Aerospace Sciences Meeting*, 2009. doi:10.2514/6.2009-1458.

[30] Hossain, K. N., Sharma, V., Bragg, M. B., and Voulgaris, P. G., "Envelope protection and control adaptation in icing encounters," *41st Aerospace Sciences Meeting and Exhibit*, Vol. 25, 2003. doi:10.2514/6.2003-25.

[31] Lombaerts, T., Schuet, S., Acosta, D., Kaneshige, J., Shish, K., and Martin, L., "Piloted simulator evaluation of maneuvering envelope information for flight crew awareness," *AIAA Guidance, Navigation, and Control Conference*, 2015. doi:10.2514/6.2015-1546.

[32] Falkena, W., Borst, C., Chu, Q. P., and Mulder, J. A., "Investigation of practical flight envelope protection systems for small aircraft," *Journal of Guidance Control and Dynamics*, Vol. 34, No. 4, 2010, p. 976. doi:10.2514/6.2010-7701.

[33] Yavrucuk, I., Unnikrishnan, S., and Prasad, J., "Envelope protection for autonomous unmanned aerial vehicles," *Journal of Guidance, Control, and Dynamics*, Vol. 32, No. 1, 2009, pp. 248–261. doi:10.2514/1.35265.

[34] Bowlus, J., Multhopp, D., and Banda, S. S., "Challenges and opportunities in tailless aircraft stability and control," *Guidance, Navigation, and Control Conference*, 1997, pp. 1713–1718. doi:10.2514/6.1997-3830.

[35] Matamoros, I., and de Visser, C. C., "Incremental Nonlinear Control Allocation for a Tailless Aircraft with Innovative Control Effectors," *2018 AIAA Guidance, Navigation, and Control Conference*, 2018. doi:10.2514/6.2018-1116.

[36] Mahadevan, S., *Monte carlo simulation*, CRC Press, New York, 1997, book section 4, pp. 123–146.

[37] Guan, Y., Yokoi, K., and Zhang, X., "Numerical methods for reachable space generation of humanoid robots," *The International Journal of Robotics Research*, Vol. 27, No. 8, 2008, pp. 935–950. doi:10.1177/0278364908095142.

[38] Heidenreich, N.-B., Schindler, A., and Sperlich, S., "Bandwidth selection in kernel density estimation: A review," *SSRN Electronic Journal*, 2010. doi:10.2139/ssrn.1726428.

[39] Efromovich, S., "Orthogonal series density estimation," *Wiley Interdisciplinary Reviews: Computational Statistics*, Vol. 2, No. 4, 2010, pp. 467–476. doi:10.1002/wics.97.

[40] Eggermont, P. P. B., and LaRiccia, V. N., *Maximum penalized likelihood estimation*, Springer Series in Statistics, Vol. 2, Springer, New York, NY, 2009. doi:10.1007/b12285.

[41] Silverman, B. W., *Density estimation for statistics and data analysis*, Vol. 26, Routledge, New York, 1986. doi:10.1201/9781315140919.

[42] Terrell, G. R., and Scott, D. W., "Variable Kernel Density Estimation," *The Annals of Statistics*, Vol. 20, No. 3, 1992, pp. 1236–1265. doi:10.1214/aos/1176348768.

[43] Stapel, J., de Visser, C. C., Kampen, E.-J. V., and Chu, Q. P., "Efficient Methods for Flight Envelope Estimation through Reachability Analysis," *AIAA Guidance, Navigation, and Control Conference*, American Institute of Aeronautics and Astronautics, 2016. doi:10.2514/6.2016-0083.

[44] Sieberling, S., Chu, Q. P., and Mulder, J. A., "Robust flight control using incremental nonlinear dynamic inversion and angular acceleration prediction," *Journal of guidance, control, and dynamics*, Vol. 33, No. 6, 2010, pp. 1732–1742. doi:10.2514/1.49978.

[45] Simplício, P., Pavel, M. D., van Kampen, E., and Chu, Q. P., "An acceleration measurements-based approach for helicopter nonlinear flight control using Incremental Nonlinear Dynamic Inversion," *Control Engineering Practice*, Vol. 21, No. 8, 2013, pp. 1065–1077. doi:10.1016/j.conengprac.2013.03.009.

[46] Acquatella, P. B., Falkena, W., van Kampen, E.-J., and Chu, Q. P., "Robust nonlinear spacecraft attitude control using incremental nonlinear dynamic inversion," *AIAA Guidance, Navigation, and Control Conference*, 2012, pp. 1–20. doi:10.2514/6.2012-4623.

[47] Acquatella, P. B., van Kampen, E., and Chu, Q. P., "Incremental backstepping for robust nonlinear flight control," *EuroGNC 2013, 2nd CEAS Specialist Conference on Guidance, Navigation and Control*, 2013.

[48] Farrell, J. A., Polycarpou, M., Sharma, M., and Dong, W., "Command filtered backstepping," *2008 American Control Conference*, Vol. 54, 2008, pp. 1391–1395. doi:10.1109/acc.2008.4586773.

[49] Dong, W., Farrell, J. A., Polycarpou, M. M., Djapic, V., and Sharma, M., "Command filtered adaptive backstepping," *IEEE Transactions on Control Systems Technology*, Vol. 20, No. 3, 2012, pp. 566–580. doi:10.1109/TCST.2011.2121907.

[50] Johnson, E. N., and Calise, A. J., "Pseudo-control hedging: A new method for adaptive control," *Advances in navigation guidance and control technology workshop*, 2000.

[51] Johnson, E. N., and Calise, A. J., "Neural network adaptive control of systems with input saturation," *2001 American Control Conference*, Vol. 5, IEEE, 2001, pp. 3527–3532. doi:10.1109/acc.2001.946179.

[52] Lombaerts, T., Looye, G., Chu, Q., and Mulder, J. A., "Pseudo control hedging and its application for safe flight envelope protection," *AIAA Guidance, Navigation, and Control Conference*, 2010. doi:10.2514/6.2010-8280.

[53] Holzapfel, F., "Nichtlineare adaptive Regelung eines unbemannten Fluggerätes," Thesis, 2004.

[54] Dorsett, K. M., and Mehl, D. R., "Innovative control effectors (ICE)," Report, Lockheed Martin Tactical Aircraft Systems, 1996. URL `http://www.dtic.mil/dtic/tr/fulltext/u2/b212813.pdf`.

[55] Niestroy, M. A., Dorsett, K. M., and Markstein, K., "A Tailless Fighter Aircraft Model for Control-Related Research and Development," *AIAA Modeling and Simulation Technologies Conference*, 2017, p. 1757. doi:10.2514/6.2017-1757.

[56] van der Peijl, I. V., "Physical Splines for Aerodynamic Modelling of Innovative Control Effectors," Thesis, 2017.

Part II

Preliminary Thesis Report

Chapter 1

Introduction

Safety is the most crucial issue in all sections of aviation including flight control system design. It was observed by various sources (Ranter, 2007; Boeing Commercial Airplanes, 2016; European Aviation Safety Agency, 2011) that loss of control (LOC) in flight is the most common primary cause of fatal accidents. LOC occurs when the aircraft has left the part of the state space where aircraft are safe to operate, which is commonly known as the safe flight envelope (Kwatny et al., 2012). Unfortunately, the determination of the safe flight envelope is not trivial even when the dynamics of the system are assumed completely known. Highly nonlinear systems including advanced flight control systems usually rely on reachability analysis to obtain the safe flight envelope. However, such envelope prediction techniques suffer from the curse of dimensionality. The maximum dimension implemented is four (Oort, Chu, & Mulder, 2011; Seube, Moitie, & Leitmann, 2002).

When the safe flight envelope is known, flight envelope protection (FEP) systems aim to keep aircraft within the envelope, ranging from control augmentation systems that help pilots identify the proximity of envelope boundaries through stick shakers or displays, to compensators that directly modify pilots' inputs in manual control, to constraints embedded in automatic flight control system (Yavrucuk, Unnikrishnan, & Prasad, 2009). With the emergence of nonlinear and adaptive flight control, automatic envelope protection is more desired to modify commands online when aircraft is close to the boundary of flight envelope or suffered damage to achieve carefree maneuvering. Preliminary implementation of such concept has been observed on modern commercial aircraft such as Boeing 777 and Airbus A380 to avoid stalls or limit load factors.

On the other hand, in military applications, tailless aircraft emerge with the need of low signature characteristics and reduced structural weight. In this way, the above challenges are more prominent in the context of high-performance tailless aircraft with unconventional control effectors, as

- tailless aircraft are inherently unstable with less directional control authority,
- with highly nonlinear dynamics and unconventional control effectors, the flight envelope tends to be highly nonlinear as well,

- extreme maneuvers are expected to be made which are closer to the boundary of the flight envelope.

Flight control systems of such aircraft often involve model-based nonlinear control including nonlinear dynamic inversion and backstepping with control allocation scheme.

One example of high-performance tailless aircraft is the Innovative Control Effectors (ICE) aircraft designed by Lockheed Martin (Bowlus, Multhopp, & Banda, 1997). The ICE aircraft is a tailless aircraft with a suite of 13 control effectors in total, including spoiler-slot deflectors and thrust vectoring. With improved lift-to-drag ratio and reduced weight, the ICE aircraft is highly maneuverable. It was observed in previous research (Matamoros & Visser, 2018) that the ICE aircraft tends to steer outside the envelope without an FEP system.

1-1 Research Objectives

To tackle the above challenges, in terms of envelope prediction, this project will explore a stochastic method to obtain a reliable and safe estimation of the flight envelope by Monte Carlo (MC) simulation. Though being offline, this method is promising in solving envelopes with high dimensions and complex dynamics within limited computation time and power, while avoiding overestimation. In terms of envelope protection, an envelope-protected multi-loop nonlinear controller will be developed with the functionality to automatically modify commands to protect the envelope. The designed controller will be integrated with an onboard envelope database obtained by the offline envelope estimation.

In this way, the goal of this project is to develop a computationally efficient algorithm for high-dimensional envelope estimation and to design a nonlinear controller that constrains aircraft within the estimated envelope while tracking desired commands. This envelope prediction and protection algorithm will be tested by simulation with a high-fidelity model of the ICE aircraft. Thus, the research objective is to

1. develop an envelope estimation method that can be efficiently solved for high dimensions by MC simulation, and then
2. develop an envelope protection method to automatically restrict maneuvers that will drive aircraft out of the estimated flight envelope by a nonlinear controller with command modification methods similar to command filtering (CF) and pseudo control hedging (PCH).

The validity of above methods is to be verified on the ICE aircraft by simulation. It should be noted that the envelope estimation can be conducted offline and carried onboard by database approach due to a practical limitation of onboard computational power. Thus, it may not be effective when the aircraft is impaired or malfunctioning unless the case is already studied and stored in the database.

The above objectives can be further divided to be achieved in sequence as follows.

1. To develop an MC simulation routine that can estimate envelopes of selected states.

2. To develop a baseline multi-loop nonlinear controller that can handle state constraints to provide envelope protection.
3. To establish an onboard model that can translate stored envelopes to state constraints.
4. To tune the controller parameters such that the envelope is protected while the controller maintains satisfactory tracking performances.

This project will be innovative to apply multiple techniques into the framework of envelope prediction and protection including stochastic MC simulations to estimate the safe flight envelope and multi-loop nonlinear controller with envelope prediction by a database approach. With these techniques, this project will be the first to explore the envelope of the ICE aircraft, despite that LOC is already often observed in previous research.

1-2 Research Questions

To reach the aforementioned project objectives, the following research questions are formulated.

1. How can the full safe flight envelope be estimated with limited computational power?
    - What states and state combinations are useful in envelope protection?
    - How is the apriori trim set determined which served as the starting point of envelope estimation?
    - How should the open-loop control inputs be sampled with?
    - How is the validity and accuracy of the envelope estimation?
        - Is it under-estimated or over-estimated?
        - How is it compared with reachability-analysis-based methods such as the level set method?
        - How is it affected by the fidelity of the simulation model?
2. How can the estimated envelope be applied as state constraints in a multi-loop nonlinear controller?
    - How should the offline envelope estimation results be stored onboard?
    - What command modification method is the most appropriate?
        - What are their modification strategies when approaching the boundary of the envelope?
        - How is their robustness under model inaccuracy?
3. Is the proposed envelope prediction and protection method effective in reducing LOC-related accidents compared to the baseline incremental nonlinear control allocation (INCA) method?
    - What representative LOC modes should be investigated?

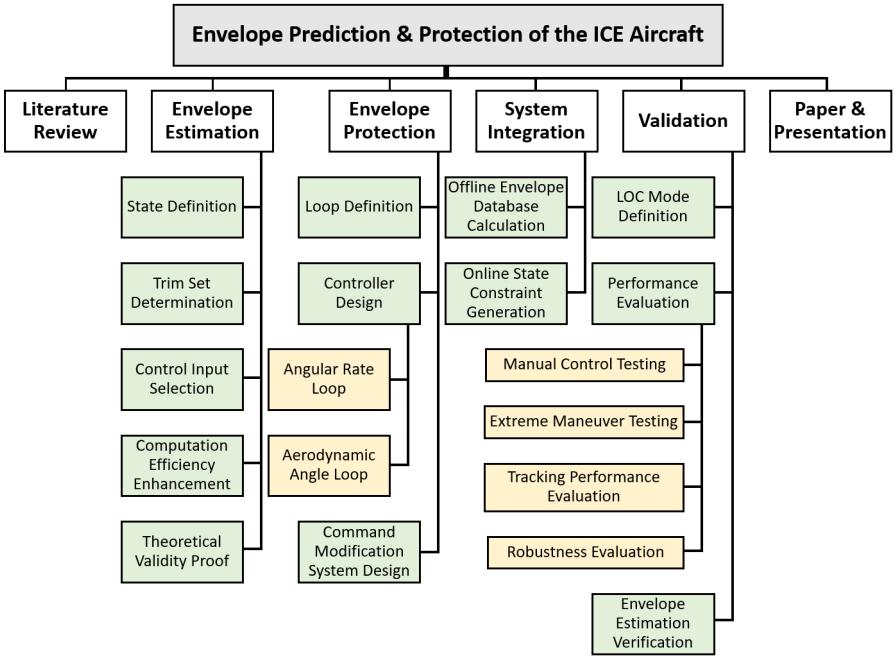

Figure 1-1: The work breakdown structure of the project.

- To what extent can the violation of flight envelope be avoided?
- How is tracking performance affected by the introduction of envelope prediction?

Based on the above discussion of research objectives and questions, the work is broken down as shown in Figure 1-1.

The rest of the preliminary report organizes as follows. Chapter 2 surveys the state of art in-flight envelope prediction and protection as well as control system design of the ICE aircraft. The design of the ICE aircraft and corresponding Simulink model are also discussed. Chapter 3 targets at the gap in current research and presents methodology applied in this research. Chapter 4 demonstrates and discusses current results. Chapter 5 concludes the report and proposes plans for the next phase of research.

Chapter 2

Literature Survey

This chapter aims to investigate available methods for envelope prediction and protection, in order to select suitable methods to be applied to the ICE aircraft in this project. Since the project deals with three distinctive topics, namely envelope prediction, envelope protection, and the ICE aircraft, the literature review surveys the state-of-the-art for the three topics respectively as follows.

2-1 Envelope Prediction

As discussed in Chapter 1, the key to reducing LOC accidents by control system design is to obtain a reliable estimation of the flight envelope. Various applications rely on this information. In fault-tolerant flight control, the flight envelope of impaired aircraft is needed in the reconfiguring controller (Tang et al., 2009). It is also useful in display design to increase situation awareness of pilots (Lombaerts et al., 2015). More directly, it is used to support FEP systems to reduce the workload or achieve automatic control as in this project (Yavrucuk et al., 2009; Falkena, Borst, Chu, & Mulder, 2010).

Intuitively, the flight envelope describes the set of all possible flight conditions where an airplane is constrained to operate (Helsen, Van Kampen, Visser, & Chu, 2016). However, the conventional envelope only deals with slow variables like altitude and airspeed in steady or quasi-steady conditions to achieve upset prevention (Ruijgrok, 2009). To identify LOC, five envelopes were defined in (Russell & Pardee, 2000), all of which are two-dimensional. However, this type of envelope fails to take the dynamics into account and is usually empirical from flight tests (Helsen et al., 2016; Kwatny et al., 2009). Therefore, a new type of envelope is defined as all the possible states where an airplane can reach from and be controlled back to a set of initial flight conditions within a given time horizon, which is also known as the dynamic envelope (Oort, 2011) or the immediate envelope (Tang et al., 2009). The set of initial flight conditions is usually selected as the trim set, where all the state derivatives can be regulated to zero. This is also the type of flight envelope that will be discussed in this research. Definition 2-1 and 2-2 are used for the remaining part of the report.

Definition 2-1 (Trim set) A state space where aircraft can stay indefinitely.

Definition 2-2 (Dynamic flight envelope) A state space where aircraft can reach from and fly back to the trim set within a finite time horizon.

Due to its critical position in safety, the flight envelope prediction has been investigated by various methods. Results of flight tests or wind tunnel tests were directly applied in (Bokovic, Redding, & Knoebel, 2009; Roemer, Tang, Bharadwaj, & Belcastro, 2008). Model-based computation of achievable trim points was conducted in (Goman, Khramtsovsky, & Kolesnikov, 2008). Bifurcation analysis (Kwatny & Allen, 2012) and a vortex lattice algorithm combined with an extended Kalman filter (Menon et al., 2011) were used in the online estimation of impaired aircraft. Among all the methods, the most rigorous and extensively studied method is the reachability analysis, which will be explained in detail in the following section.

2-1-1 Reachability Analysis

It has been proved that the flight envelope estimation problem can be formulated as a reachability problem with the optimal control framework by studying possible trajectories of the dynamic system (Lygeros, 2004). This formulation is extensively applied in envelope prediction (Lombaerts, Schuet, Wheeler, Acosta, & Kaneshige, 2013; Nabi et al., 2018). Consider an autonomous nonlinear system

$$\dot{\boldsymbol{x}} = \boldsymbol{f}(\boldsymbol{x}, \boldsymbol{\delta}), \tag{2-1}$$

with $\boldsymbol{x} \in \mathbb{R}^n$, $\boldsymbol{\delta} \in U \subset \mathbb{R}^s$, where U is the set of admissible inputs. All the states $\boldsymbol{x}$ that can be reached from a set K with at least one admissible input $\boldsymbol{\delta} \in U$ within a time horizon T_f form the reachable set $R(T_f, K)$. A similar definition is the invariant set $I(T_f, K)$, which describes all the states $\boldsymbol{x}$ that can be remained in a set K with any admissible input $\boldsymbol{\delta} \in U$ for any time in a time horizon T_f. Mathematically, the above definitions are expressed as

$$R(T_f, K) = \{\boldsymbol{x}(\tau) \in \mathbb{R}^n | \exists \boldsymbol{\delta}(t) \in U_{[0,T_f]}, \exists \tau \in [0, T_f], \boldsymbol{x}(0) \in K\}, \tag{2-2}$$

$$I(T_f, K) = \{\boldsymbol{x}(0) \in \mathbb{R}^n | \forall \boldsymbol{\delta}(t) \in U_{[0,T_f]}, \forall \tau \in [0, T_f], \boldsymbol{x}(\tau) \in K\}. \tag{2-3}$$

Furthermore, it was proved that the following principle of duality holds

$$R(T_f, K) = (I(T_f, K^c))^c, \tag{2-4}$$

where A^c denotes the complement of A.

Similar definition can be applied to the same system but runs backward in time,

$$\dot{\boldsymbol{x}} = -\boldsymbol{f}(\boldsymbol{x}, \boldsymbol{\delta}). \tag{2-5}$$

In this way, the reachable set for the original system $R^f(T_f, K)$ is known as the forward reachable set, where as that for the backward system $R^b(T_f, K)$ is known as backward reachable set.

If K is selected as the apriori trim set of the aircraft, $R^f(T_f, K)$ defines all the states the aircraft can reach within T_f from steady state; $R^b(T_f, K)$ defines all the states the aircraft can

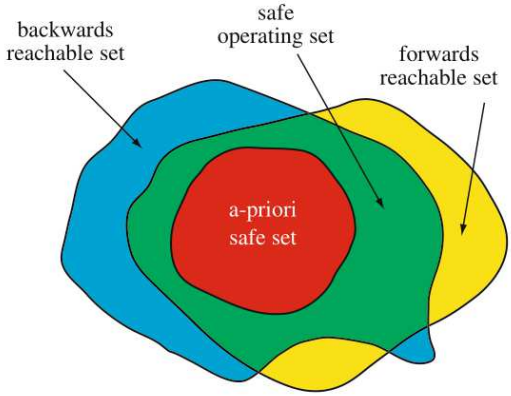

Figure 2-1: Schematic of reachability analysis in envelope prediction.
(Oort et al., 2011)

be controlled back to steady state within T_f. In this way, the flight envelope to be estimated is the intersection of the above two reachable sets

$$E_{dyn}(T_f, K) = R^f(T_f, K) \cap R^b(T_f, K), \tag{2-6}$$

according to the definition of dynamic envelope. Figure 2-1 summarizes the relation between reachable set and envelope prediction.

Various methods are available to solve the reachable set. For linear systems, convex optimization (Goman & Demenkov, 2004) and geometric methods which describe the set with geometric primitives (Girard, 2005) were developed based on the convexity of the reachable set. For nonlinear systems, widely studied methods include the distance-fields-over-grids method (Helsen et al., 2016) and the level set method (Nabi et al., 2018; Lombaerts et al., 2013; Zhang, Visser, & Chu, 2016), possibly with the semi-Lagrangian method (Oort et al., 2011) or time-scale separation (Kitsios & Lygeros, 2005). The distance-fields-over-grids method uses a predefined grid of the state space as the target states and optimizes the control inputs at each time step such that the distance between the final and the target state is minimized. For the system Eq. 2-1, the optimal-control problem aims to minimize

$$J = \frac{1}{2}||\boldsymbol{x}(T_f) - \boldsymbol{g}_p||^2, \tag{2-7}$$

where $\boldsymbol{g}_p$ is one grid point. Thus, the convex hull of all optimized final states forms an estimation of the reachable set.

The level set method formulates the level set of invariant sets $V(\boldsymbol{x}, t)$ from the level set of the trim set $l(\boldsymbol{x})$ by an optimization problem and solve it by a partial differential equation

$$\frac{\partial V}{\partial t}(\boldsymbol{x}, t) + \min_{\tau \in [0, T_f]} \left\{ \inf_{\boldsymbol{\delta} \in U} \frac{\partial V}{\partial \boldsymbol{x}}(\boldsymbol{x}, t) \boldsymbol{f}(\boldsymbol{x}, \boldsymbol{\delta}) \right\} = 0, \tag{2-8}$$

which is known as Hamilton-Jacobi-Bellman partial differential equations (HJB-PDE). The invariant set can be converted to the reachable set by Eq. 2-4. A MATLAB toolbox is available to solve the HJB-PDE for the level set method (Mitchell, 2008).

However, the common problem with these methods to numerically solve the optimal control problem and/or the partial differential equations is the high computational load for nonlinear systems with higher dimensions (Lombaerts et al., 2013). The maximum dimension implemented is four (Oort et al., 2011; Seube et al., 2002). The common solution is simply restricting investigation to problems with low dimensions, usually by introducing virtual inputs to simplify the system dynamics (Tang et al., 2009). The maximum dimension implemented is four (Oort et al., 2011; Seube et al., 2002).

2-1-2 Monte Carlo Simulation

Given the above problem, an idea was proposed to repeatedly sample the control inputs that may be selected in the optimal control framework of the level set method randomly, instead of solving the HJB-PDE for the exact optimal control inputs. This concept, in general, is known as MC simulations. Unfortunately, there is no research to apply MC simulations in flight envelope estimation yet. The closest application is workspace determination in robotics (Guan, Yokoi, & Zhang, 2008), where a robotic system was randomly simulated to obtain its physical limits geometrically. However, only simple geometry and kinematics were considered in this research.

A general MC simulation follows the following procedure (Mahadevan, 1997):

1. generate random input variables based on their probability distributions,
2. perform deterministic analysis and record the results,
3. repeat Step 1 and 2 for a number of times, and
4. calculate the probability of occurrence based on the results.

In this project, the sampling of initial states and control inputs plays the most important role, as it determines if the results of the simulations are valid when compared with the framework of the reachability analysis.

Another side product of this method is that a probabilistic envelope can be generated to show how likely a state is within the envelope instead of an absolute boundary obtained by the level set method. To convert the point cloud obtained by MC simulation to a probability distribution of the reachable set, i.e., Step 4 in the MC simulation procedure, density estimation is needed (Silverman, 1986). The commonly used density estimation methods include histogram, kernel density estimation (Heidenreich, Schindler, & Sperlich, 2010), orthogonal series estimation (Efromovich, 2010), and maximum penalized likelihood estimation (Eggermont & LaRiccia, 2009).

Histogram divides bins in each dimension of data and counts the number of sample points in each bin. Then, the probability density for all points in the same bin is defined as the number of sample points over the bin size. The main problem with histogram is that it is not continuous at the boundary of each bin. Kernel density estimation improves histogram by replacing fixed bins with a continuous kernel function. Consider a multi-variate case, to estimate a d-dimensional random vector

$$\boldsymbol{X} = (X_1, X_2, ..., X_d)^T \tag{2-9}$$

by n samples

$$\boldsymbol{y}_i = (y_{i1}, y_{i2}, ..., y_{id})^T, i = 1, 2, ..., n, \tag{2-10}$$

the multivariate kernel density estimator is given by

$$\hat{f}(\boldsymbol{x}) = \frac{1}{n}\sum_{i=1}^{n} K_H(\boldsymbol{x} - \boldsymbol{y}_i) = \frac{1}{nh_1h_2...h_d}\sum_{i=1}^{n}\prod_{j=1}^{d} k(\frac{x_j - y_{ij}}{h_j}), \tag{2-11}$$

where h_j is the bandwidth of the jth variable, $k(\cdot)$ is the kernel function for each dimension satisfying

$$\int_{-\infty}^{\infty} k(x)\mathrm{d}x = 1. \tag{2-12}$$

Usually, a Gaussian function is used. The bandwidth is comparable to the bin size in histogram, which determines the range of data that is involved in the estimator. The bandwidth can be selected by the Silverman's rule of thumb (Silverman, 1986; Heidenreich et al., 2010)

$$h_j = \sigma_j \left[\frac{4}{(d+2)n}\right]^{1/(d+4)}, \tag{2-13}$$

where σ_j is the standard deviation of the jth variable.

Orthogonal series estimation decomposes the probability density function into orthogonal series (usually trigonometric) and estimates weights of orthogonal terms. Maximum penalized likelihood estimation solves for the probability density function that maximizes the likelihood to obtain the same sample, while penalized for the 'roughness' of the function.

2-1-3 Trimming

Trimming is the process of finding the equilibrium points of the system (Kampen, Chu, Mulder, & Emden, 2007). Although this is not the central task of this research, in estimating the flight envelope by reachability analysis, an apriori safe set is needed, which is usually selected as the trim set. This is because the aircraft can stay indefinitely inside the trim set, which is inherently safe. This will be the starting point of reachability analysis. Trimming is usually implemented by formulating an optimization problem that constrains state derivatives to zero. The cost function can be selected as thrust or control deflections. The trim set can be solved by ordinary nonlinear solvers such as the interior-point method and sequential quadratic programming (SQP) (Nocedal & Wright, 2006), interval analysis (Kampen et al., 2007), and bifurcation (Ananthkrishnan & Sinha, 2001).

2-2 Envelope Protection

With the estimated flight envelope available, the objective of envelope protection is to ensure the states of the aircraft remain within the bounds specified by the envelope, preferably in both autopilot modes and manual control (Tomlin, Lygeros, & Sastry, 1998). This can be done by open-loop cueing to pilots (Gingras, Barnhart, Ranaudo, Ratvasky, & Morelli, 2009;

Hossain, Sharma, Bragg, & Voulgaris, 2003), or integrated into the flight control system. The latter method is to be investigated in this project. The objective of the FEP system is to override pilot's command when the aircraft is about to cross the pre-defined safe flight envelope. This has been implemented in many types of controllers, including hybrid control (Tomlin et al., 1998), model-based predictive control (Falkena et al., 2010), and adaptive neural networks (Yavrucuk et al., 2009). Among them, one of the most convenient ways is to impose envelope protection in model-based nonlinear control such as nonlinear dynamic inversion or backstepping by command modification (Slotine & Li, 1991). This section first introduces the framework of advanced flight control systems, followed by available command modification methods.

2-2-1 Advanced Flight Control System

An airplane is a highly nonlinear system. However, conventional flight control systems only use classical linear control theory and cope with nonlinearity by dividing the workspace into separate operating regimes with gain scheduling (Enns, Bugajski, Hendrick, & Stein, 1994). This is clearly not suitable for FEP systems as no universal control law is available for command modification. This type of controller also suffers complex gain scheduling, low robustness to model inaccuracy and fails to include failure detection and fault tolerant control. Therefore, advanced flight control systems were developed to include nonlinearity in control laws by inverting the flight dynamics. Two famous methods are nonlinear dynamic inversion (NDI) and backstepping. To enhance robustness to model inaccuracy, controllers can be made adaptive or incremental. The former updates the aircraft model based on measured aircraft response; the latter only includes the control effectiveness part of the model to reduce the effect of model inaccuracy. The incremental approach will be applied to this project.

Nonlinear Dynamic Inversion & Backstepping

Consider an affine nonlinear system

$$\dot{\boldsymbol{x}} = \boldsymbol{f}(\boldsymbol{x}) + \boldsymbol{g}(\boldsymbol{x})\boldsymbol{\delta}, \tag{2-14}$$

the NDI controller consists of two parts: 1) a linear controller that generates the virtual control input $\boldsymbol{\nu}(\boldsymbol{x}) = \dot{\boldsymbol{x}}$, which is usually a PID controller, and 2) input-output linearization

$$\boldsymbol{\delta} = \boldsymbol{g}^{-1}(\boldsymbol{x})(\boldsymbol{\nu}(\boldsymbol{x}) - \boldsymbol{f}(\boldsymbol{x})), \tag{2-15}$$

that maps the virtual control to the actual input.

In the application of flight control, the controller is usually designed in multiple loops, making use of the principle of time-scale separation. For multi-loop systems, NDI controllers assume the reference to the inner loop controller is the same as the real aircraft response. Thus, different loops can be totally separated. However, no analytical stability proof is available for this assumption. This theoretical flaw is solved by backstepping, which adds a cross term between loops that compensates the difference between the reference state and the actual aircraft response. The tracking error of this method was proved to be asymptotically stable (Sonneveldt, Chu, & Mulder, 2007).

Consider an n-loop affine system

$$\dot{\boldsymbol{x}}_i = \boldsymbol{f}_i(\boldsymbol{x}_i) + \boldsymbol{g}_i(\boldsymbol{x}_i)\boldsymbol{x}_{i+1}, i = 1, 2, ..., n, \tag{2-16}$$

where $\boldsymbol{x}_1, \boldsymbol{x}_2, ..., \boldsymbol{x}_n$ are states, $\boldsymbol{\delta} = \boldsymbol{x}_{n+1}$ is the control input. The backstepping method proposes the following cascaded equations to obtain the control input.

$$\boldsymbol{\alpha}_1 = \frac{1}{\boldsymbol{g}_1}(-\boldsymbol{K}_1\boldsymbol{z}_1 - \boldsymbol{f}_1 + \dot{\boldsymbol{y}}_r) \tag{2-17}$$

$$\boldsymbol{\alpha}_i = \frac{1}{\boldsymbol{g}_i}(-\boldsymbol{g}_{i-1}\boldsymbol{z}_{i-1} - \boldsymbol{K}_i\boldsymbol{z}_i - \boldsymbol{f}_i + \dot{\boldsymbol{\alpha}}_{i-1}), i = 2, 3, ..., n, \tag{2-18}$$

where $\boldsymbol{K}_i$ are linear control gains, $\boldsymbol{\alpha}_n$ is the control input, $\boldsymbol{z}_i$ are tracking errors to $\boldsymbol{x}_i$ with

$$\boldsymbol{z}_1 = \boldsymbol{x}_1 - \boldsymbol{y}_r, \boldsymbol{z}_i = \boldsymbol{x}_i - \boldsymbol{\alpha}_{i-1}. \tag{2-19}$$

The Incremental Approach

In order to handle model inaccuracy, an incremental form of backstepping was developed at Delft University of Technology (TU Delft) (Acquatella, Kampen, & Chu, 2013; Lu, Van Kampen, & Chu, 2015) by modifying a backstepping controller such that only the control effectiveness part of the model is relevant in the controller design. The internal dynamics part of the system is approximated by state derivatives. In this way, the controller is less dependent on accurate dynamics, and the robustness of the controller is enhanced. Consider a nonlinear system as in Eq. 2-1, the incremental approach linearizes the system at the current time step in realtime as

$$\dot{\boldsymbol{x}} \approx \dot{\boldsymbol{x}}_0 + \left.\frac{\partial(\boldsymbol{f} + \boldsymbol{g}\boldsymbol{\delta})}{\partial \boldsymbol{x}}\right|_{\substack{\boldsymbol{x}=\boldsymbol{x}_0 \\ \boldsymbol{\delta}=\boldsymbol{\delta}_0}} (\boldsymbol{x} - \boldsymbol{x}_0) + \boldsymbol{g}(\boldsymbol{x}_0)\left(\boldsymbol{\delta} - \boldsymbol{\delta}_0\right), \tag{2-20}$$

where $\boldsymbol{x}_0$ and $\boldsymbol{\delta}_0$ are the states and inputs at the current time step respectively. Applying the time-scale separation principle, the second term in Eq. 2-20 can be neglected since the variation of states is much slower than that of control inputs. Similar method can also be applied in nonlinear dynamic inversion (Sieberling, Chu, & Mulder, 2010; Simplcio, Pavel, Kampen, & Chu, 2013; Acquatella, Falkena, Kampen, & Chu, 2012).

It should be noted that the incremental approach proposes additional requirements on the control system as follows (Acquatella et al., 2013; Sieberling et al., 2010).

- The controller should have access to measurements of state derivatives (especially derivatives of angular rates). This can be obtained directly by angular acceleration sensors, or by differentiating and filtering the gyro measurements from the inertial measurement unit.
- To legitimize the time-scale separation, the system should have both a fast sampling rate and fast control action.

Therefore, it is suggested to apply the incremental approach for dynamic loops, and the ordinary approach for kinematic loops since their equations of motion are universal with no uncertainties.

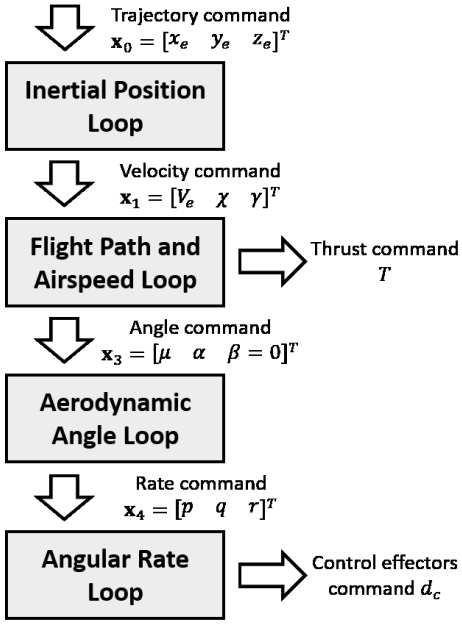

Figure 2-2: Schematic of full trajectory nonlinear flight control system.

Structure of the flight control system

There are different control modes for flight control systems depending on their applications. In manual control, the rate command attitude hold (RCAH) mode is often implemented (Falkena et al., 2010), where pilots give commands of attitude derivatives $\dot{\phi}_{ref}, \dot{\theta}_{ref}$ from the stick. This command is intuitive to pilots and reduces workload. The controller integrates the input and uses it as the reference together with a zero side-slip angle β command. In autopilot modes, higher levels of control are implemented including aerodynamic angles μ, α, β, the velocity vector V_g, χ, γ (or u, v, w), and the position x_e, y_e, z_e. The schematic of a full trajectory control system is illustrated in Figure 2-2.

The equations of motion for the above control modes are summarized in Eqs. 2-21 to 2-28 (Sonneveldt, Van Oort, Chu, & Mulder, 2009; Lombaerts, Looye, Chu, & Mulder, 2010).

Position

$$\frac{\mathrm{d}}{\mathrm{d}t}\begin{bmatrix} x_e \\ y_e \\ z_e \end{bmatrix} = \begin{bmatrix} V_g \cos\chi\cos\gamma \\ V_g \sin\chi\cos\gamma \\ -V_g \sin\gamma \end{bmatrix} \tag{2-21}$$

Velocity vector

$$\frac{\mathrm{d}}{\mathrm{d}t}\begin{bmatrix} V_g \\ \chi \\ \gamma \end{bmatrix} = \begin{bmatrix} \frac{1}{m} & 0 & 0 \\ 0 & \frac{1}{mV_g\cos\gamma} & 0 \\ 0 & 0 & -\frac{1}{mV_g} \end{bmatrix} \left(T_{vb}\begin{bmatrix} F_x \\ F_y \\ F_z \end{bmatrix} + T_{ve}\begin{bmatrix} 0 \\ 0 \\ mg \end{bmatrix} \right), \tag{2-22}$$

where F_x, F_y, F_z are aerodynamic and propulsion forces in the body frame,

$$T_{vb} = \begin{bmatrix} \cos\alpha\cos\beta & \sin\beta & \sin\alpha\cos\beta \\ -\cos\alpha\sin\beta\cos\mu + \sin\alpha\sin\mu & \cos\beta\cos\mu & -\sin\alpha\sin\beta\cos\mu - \cos\alpha\sin\mu \\ -\cos\alpha\sin\beta\sin\mu - \sin\alpha\cos\mu & \cos\beta\sin\mu & -\sin\alpha\sin\beta\sin\mu + \cos\alpha\cos\mu \end{bmatrix} \tag{2-23}$$

is the transformation matrix from the body frame to the velocity frame,

$$T_{ve} = \begin{bmatrix} \cos\chi\cos\gamma & \sin\chi\cos\gamma & -\sin\gamma \\ -\sin\chi & \cos\chi & 0 \\ \cos\chi\sin\gamma & \sin\chi\sin\gamma & \cos\gamma \end{bmatrix} \tag{2-24}$$

is the transformation matrix from the earth frame to the velocity frame.

In the body frame, we have

$$\frac{\mathrm{d}}{\mathrm{d}t}\begin{bmatrix} u \\ v \\ w \end{bmatrix} = \begin{bmatrix} -qw + rv - g\sin\theta + \frac{F_x}{m} \\ -ru + pw + g\cos\theta\sin\phi + \frac{F_y}{m} \\ -pv + qu + g\cos\theta\cos\phi + \frac{F_z}{m} \end{bmatrix} \tag{2-25}$$

Aerodynamic angles

$$\begin{aligned} \frac{\mathrm{d}}{\mathrm{d}t}\begin{bmatrix} \alpha \\ \beta \end{bmatrix} &= \begin{bmatrix} \frac{-uv}{u^2+w^2} & 1 & \frac{-vw}{u^2+w^2} \\ \frac{w}{\sqrt{u^2+w^2}} & 0 & \frac{-u}{\sqrt{u^2+w^2}} \end{bmatrix}\begin{bmatrix} p \\ q \\ r \end{bmatrix} \\ &+ \begin{bmatrix} \frac{1}{u^2+w^2}\left[u(A_z + g\cos\phi\cos\theta) - w(A_x - g\sin\theta)\right] \\ \frac{1}{\sqrt{u^2+w^2}}\left[\frac{-uv}{V_g^2}(A_x - g\sin\theta) + (1 - \frac{v^2}{V_g^2})(A_y + g\sin\phi\cos\theta) - \frac{vw}{V_g^2}(A_z + g\cos\phi\cos\theta)\right] \end{bmatrix}, \end{aligned} \tag{2-26}$$

where A_x, A_y, A_z are linear accelerometer measurements.

Euler angles

$$\frac{\mathrm{d}}{\mathrm{d}t}\begin{bmatrix} \phi \\ \theta \\ \psi \end{bmatrix} = \begin{bmatrix} 1 & \sin\phi\tan\theta & \cos\phi\tan\theta \\ 0 & \cos\phi & -\sin\phi \\ 0 & \sin\phi\sec\theta & \cos\phi\sec\theta \end{bmatrix}\begin{bmatrix} p \\ q \\ r \end{bmatrix} \tag{2-27}$$

Angular rates

$$\frac{\mathrm{d}}{\mathrm{d}t}\begin{bmatrix} p \\ q \\ r \end{bmatrix} = \boldsymbol{I}^{-1}\left(\begin{bmatrix} M_x \\ M_y \\ M_z \end{bmatrix} - \begin{bmatrix} p \\ q \\ r \end{bmatrix} \times \boldsymbol{I}\begin{bmatrix} p \\ q \\ r \end{bmatrix}\right), \tag{2-28}$$

where M_x, M_y, M_z are aerodynamic moments in the body frame,

$$\boldsymbol{I} = \begin{bmatrix} I_{xx} & -I_{xy} & -I_{xz} \\ -I_{yx} & I_{yy} & -I_{yz} \\ -I_{zx} & -I_{zy} & I_{zz} \end{bmatrix} \tag{2-29}$$

is the inertia matrix.

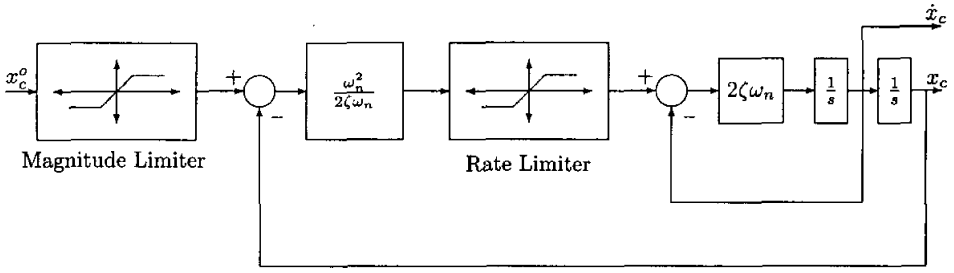

Figure 2-3: Second-order command filter with magnitude and rate constraints. (Farrell, Polycarpou, & Sharma, 2004)

2-2-2 Command Modification

With the FEP system, the command to the controller will be modified to satisfy the state constraints specified by the envelope database. A second-order filter is often used which can handle magnitude and rate constraints. The block diagram is shown in Figure 2-3.

However, in a multi-loop controller, the modification of intermediate state commands or control inputs will affect the stability and tracking performance of outer-loop commands. Thus, outer loops need to be compensated based on the difference between the original and modified inner-loop commands. Two commonly-used methods on this are CF with tracking error compensation (Farrell, Polycarpou, Sharma, & Dong, 2008; Dong, Farrell, Polycarpou, Djapic, & Sharma, 2012) and PCH (Johnson & Calise, 2000, 2001). CF originated from the need to find an alternative way to obtain derivatives of commands which is required in the backstepping controller design, as it is usually extremely tedious to derive them analytically in a multi-loop system. When the filter is augmented with magnitude and rate constraints, this method can also constrain the states and control inputs. PCH was originally proposed to avoid the effect of input saturation on system identification by adaptive neural network. The concept was later expanded to general flight control systems as a way to avoid and compensate for actuator saturation of control surfaces (Lombaerts et al., 2010; Holzapfel, 2004).

Currently, the applications of the above two methods are limited. CF is used in multi-loop backstepping; PCH is used in the inner loop of adaptive nonlinear dynamic inversion for input saturation only. Here, the background controller structures are omitted. Eqs. 2-32 to 2-35 characterizes their approaches to command modification in particular.

Consider a system

$$\dot{\boldsymbol{x}} = \boldsymbol{f}(\boldsymbol{x}, \boldsymbol{\delta}_{act}), \tag{2-30}$$

with actuator dynamics

$$\dot{\boldsymbol{\delta}}_{act} = \boldsymbol{f}(\boldsymbol{\delta}_{act}, \boldsymbol{\delta}_c). \tag{2-31}$$

where $\boldsymbol{\delta}_c$ is the input command from the controller. The state command $\boldsymbol{x}_{ref}$ will be modified by

Command filtering

$$\boldsymbol{x}_c = H(s)(\boldsymbol{x}_{ref} - \boldsymbol{\chi}) \tag{2-32}$$

$$\dot{\boldsymbol{\chi}} = -\boldsymbol{K}\boldsymbol{\chi} + [\boldsymbol{f}(\boldsymbol{x}, \boldsymbol{\delta}_{act}) - \boldsymbol{f}(\boldsymbol{x}, \boldsymbol{\delta}_c)] \tag{2-33}$$

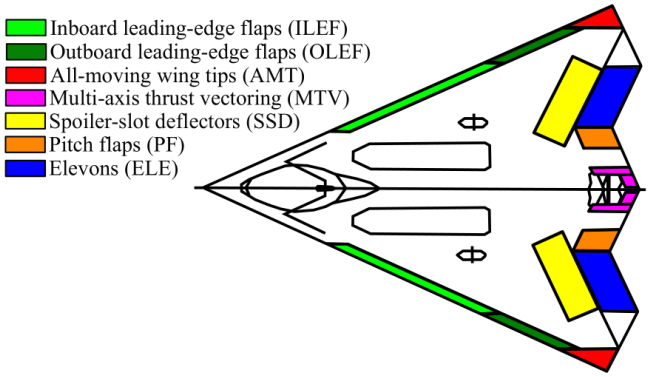

Figure 2-4: Control effector configuration of the ICE aircraft. (Matamoros & Visser, 2018)

Pseudo control hedging

$$\dot{\boldsymbol{x}}_c = \boldsymbol{K}_{ref}(\boldsymbol{x}_{ref} - \boldsymbol{x}_c) - \boldsymbol{\nu}_h \tag{2-34}$$

$$\boldsymbol{\nu}_h = \boldsymbol{f}(\boldsymbol{x}, \boldsymbol{\delta}_c) - \boldsymbol{f}(\boldsymbol{x}, \boldsymbol{\delta}_{act}) \tag{2-35}$$

where $\boldsymbol{x}_c$ is the modified state command, $H(s)$ is the dynamics of the command filter, usually selected as a second-order filter, $\boldsymbol{K}$ is the same as the linear controller gain, $\boldsymbol{K}_{ref}$ is a separate reference model gain.

2-3 The Innovative Control Effectors Aircraft

The ICE project was initiated at the former Wright Laboratory in 1993, aiming to explore novel control surfaces for high-performance fighter aircraft to achieve low radar cross section characteristics, high angle of attack effectiveness, low lift-to-drag ratio and reduced hinge moment (Dorsett & Mehl, 1996). Selected designs were later undergone wind tunnel tests at Lockheed Martin Tactical Aircraft Systems (LMTAS). Two distinctive baseline configurations were developed for land and carrier applications respectively. The land-based configuration has a tailless delta wing with a 65° sweep angle. The carrier-based configuration has a canard-delta planform with a 42° leading edge sweep angle. Both configurations use a single engine. The thesis focuses on a land-based configuration of the ICE aircraft `ICE 101-TV`.

2-3-1 The ICE Control Suite

After investigation and flight tests, six types of control effectors are included in the current design applied in this research, namely leading edge flaps (LEF), all moving wing tips (AMT), multi-axis thrust vectoring (MATV), spoiler-slot deflectors (SSD), pitch flaps (PF), and elevons, which will be discussed as follows. The configuration of those control effectors are illustrated in Figure 2-4.

Leading edge flaps Four LEF are used on the ICE aircraft, including two inboard ones and two outboard ones. With asymmetric differential deflections, LEF can provide lateral-directional control authority at moderate to high angle of attack (AoA). They are effective in roll coordination and stability augmentation at high AoA and low speed (Dorsett & Mehl, 1996).

All moving wing tips AMT can rotate completely around the Y_b axis, to provide yaw control authority as well as coupled rolling moments. They are used for yaw control at very high AoA (Dorsett, 1997). The direction of AMT deflections is constrained to trailing edge down for radar cross section reduction.

Multi-axis thrust vectoring MATV can alter the direction of thrust from the engine to provide additional moments. On the ICE aircraft, thrust vectoring (TV) is implemented for both pitch and yaw directions. This gives the ICE aircraft addition control authority to fulfill agility requirements at high AOA.

Spoiler-slot deflectors SSD is a kind of spoilers that open a slot through the wing for air to flow in when deflected. They are superior to conventional spoilers in providing lateral-directional control authority at high AoA and in transonic flight. However, SSD have strong interference with other control effectors downstream. When they are activated, the control effectiveness of elevons will be reduced.

Pitch flaps PF provide baseline pitch authority and contribute to longitudinal trim. Although two PF are used, they are designed to move symmetrically only, and thus considered as one control effector in controller design.

Elevons Elevons serve as both elevators and ailerons for conventional aircraft. The two elevons can provide both pitching and rolling moments by deflecting symmetrically and asymmetrically respectively.

To sum up, the total number of independent control effectors is thirteen, which is highly redundant. Depending on their characteristics, different position and rate limits are specified for the control effectors, which are summarized in Table 2-1 (Matamoros & Visser, 2018). The dynamics of LEF deflections are described by

$$H_1(s) = \frac{1800}{(s+18)(s+100)}. \tag{2-36}$$

The dynamics of other control surface deflections are described by

$$H_2(s) = \frac{4000}{(s+40)(s+100)}. \tag{2-37}$$

2-3-2 The High-Fidelity Aerodynamic Model of the ICE Aircraft

The ICE aircraft is still in the development phase, so there is no physical prototype available to test the algorithm developed in this research. However, there is a high-fidelity aerodynamic database of the ICE aircraft based on wind tunnel tests from Lockheed Martin for academic

Table 2-1: Position and rate limits of the control effectors on the ICE aircraft.

	Positive deflection	Position limit [deg]	Rate limit [deg/s]
Inboard LEF	Leading edge down	$[0, 40]$	$[-40, 40]$
Outboard LEF	Leading edge down	$[-40, 40]$	$[-40, 40]$
AMT	Trailing edge down	$[0, 60]$	$[-150, 150]$
Pitch TV	$\dot{q} > 0$	$[-15, 15]$	$[-150, 150]$
Yaw TV	$\dot{r} > 0$	$[-15, 15]$	$[-150, 150]$
SSD	Trailing edge up	$[0, 60]$	$[-150, 150]$
PF	Trailing edge down	$[-30, 30]$	$[-150, 150]$
Elevons	Trailing edge down	$[-30, 30]$	$[-150, 150]$

use. In this research, this database will be used in aircraft modeling, envelope prediction, as well as controller design.

The core part of the model consists of a set of look-up tables (LUT), which describes all the aerodynamic coefficients for forces and moments with respect to states of the aircraft as well as control surface deflections other than TV. In detail, the aerodynamic coefficients are defined in the aerodynamic model body frame $\mathbb{F}^m$ (back-right-up) with

$$C_X = \frac{X}{\bar{q}S}, C_Y = \frac{Y}{\bar{q}S}, C_Z = \frac{Z}{\bar{q}S}, \tag{2-38}$$

$$C_L = \frac{L}{\bar{q}Sb}, C_M = \frac{M}{\bar{q}S\bar{c}}, C_N = \frac{N}{\bar{q}Sb}, \tag{2-39}$$

where $[X\ Y\ Z]^T$ is the vector of aerodynamic forces, $[L\ M\ N]^T$ is the vector of aerodynamic moments, ρ is the air density, V is the true airspeed, S is the total wing area, b is the wing span, and $\bar{c}$ is the mean aerodynamic chord. These coefficients are expressed by a summation of terms contributed by the base airframe, different control surfaces, and interactions between control surfaces. Each term is evaluated by a single LUT, with a total of 108 LUT. Mach number M, angle of attack α, sideslip angle β, and control surface deflections $\boldsymbol{\delta} \in \mathbb{R}^{13}$ are directly involved in the LUT. Body angular rates p, q, r and the true airspeed V are indirectly involved in linear terms.

The contribution of TV and the throttle is described by the following TV model.

$$\begin{cases} F_{X,tv} = T\cos(d_{ptv})\sec(d_{ytv}), \\ F_{Y,tv} = T\cos(d_{ptv})\tan(d_{ytv}), \\ F_{Z,tv} = T\sin(d_{ptv}), \\ M_{X,tv} = 0, \\ M_{Y,tv} = -Td_n\sin(d_{ptv}), \\ M_{Z,tv} = -Td_n\cos(d_{ptv})\tan(d_{ytv}), \end{cases} \tag{2-40}$$

where d_n is the moment arm of the thrust force.

This aerodynamic database is embedded in a Simulink model that solves the equations of motion for aircraft in realtime by evaluating the LUT. Cubic spline interpolation is used

to interpolate LUT. Thus, the model can simulate the response of the aircraft under three different mass configuration by giving open-loop control surface deflections and thrust settings. The model can output 26 common states of aircraft, which are assumed to be available for controller design in this research.

This model provided by Lockheed Martin was elaborated at TU Delft. A physical spline model was developed in (Peijl, 2017), which converted all the LUT into physical splines to enhance continuity and computational efficiency. This spline model will be used as the onboard aerodynamic model for the flight control system design. The control effectiveness matrix can be obtained by calculating the Jacobian of the aerodynamic coefficients, which is not possible with the original LUT. Since the control surfaces are highly redundant for the ICE aircraft, an INCA scheme was implemented in (Matamoros & Visser, 2018), which can allocate all the control surface deflections to obtain desired aerodynamic moments. The simulation results can be displayed to the FlightGear interface [1] for visualization.

It should be noted that the ranges of the available data for aerodynamic coefficients are limited. Thus some parts of the flight envelope can stretch into parts where there are no experimental data available. In practice, the data tables are extrapolated by clipping or linear extrapolation.

2-3-3 Previous Research on the ICE Aircraft

Most of the previous research on the control system of the ICE aircraft focused on baseline control system design and the control allocation problem of the ICE aircraft. The system was linearized at different conditions and controlled by a linear controller in (J. F. Buffington, 1999; Nieto-Wire & Sobel, 2011). Sliding mode control was applied in (Shtessel, Buffington, & Banda, 2002; Peng, Wei-wei, & Zhi-qiang, 2009). Linear control allocation was implemented in (J. M. Buffington, 1997) and extended with the weighted pseudo-inverse method in (Davidson, Lallman, & Bundick, 2001a, 2001b).

At TU Delft, the aerodynamic characteristics of the control effectors were modeled with physical splines based on the available flight test data (Peijl, 2017). The physical spline model is stored onboard to generate Jacobians of aerodynamic forces and moments with respect to states and control surface deflections in realtime. This spline model is used to design an INCA controller for angular rate control with NDI (Matamoros & Visser, 2018). As the ICE aircraft is significantly over-actuated, the input-output linearization in Eq. 2-15 is not trivial. The INCA method searches for the best combination of incremental control surface deflections that satisfies the position and rate limits of the actuators and

$$\frac{\partial \boldsymbol{\Phi}(\boldsymbol{x}, \boldsymbol{\delta})}{\partial \boldsymbol{\delta}} \Delta \boldsymbol{\delta} = \boldsymbol{d}_c, \tag{2-41}$$

where $\frac{\partial \boldsymbol{\Phi}(\boldsymbol{x}, \boldsymbol{\delta})}{\partial \boldsymbol{\delta}}$ is the control effectiveness matrix obtained from the onboard spline model, $\boldsymbol{d}_c$ is the desired incremental aerodynamic moment from the NDI controller. Linear solvers

[1] FlightGear is an open-source flight simulator. It can be used to demonstrate the controller performance intuitively.

are used including redistributed weighted pseudo-inverse and active-set-based quadratic programming. This control allocation scheme will also be used in this research. However, no research is related to the flight envelope or the LOC problem for the ICE aircraft.

To sum up, solid algorithms are available for envelope estimation but too computationally intensive to directly apply to the ICE aircraft. Envelope protection can be implemented with additional filters at different places in the flight control system but has not been applied to IBS controllers. Furthermore, no research has been conducted about the flight envelope for the ICE aircraft. In this way, this research aims to bridge the above research gaps, as discussed in the following chapters.

Chapter 3

Preliminary Methodology

This chapter discusses the methodology of the project. On a high level, the two sub-tasks in this project, namely envelope prediction and envelope protection, are relatively separated on their own. On the other hand, the results of envelope prediction are used as the database to implement envelope protection. Therefore, it was planned to first independently develop algorithms for envelope prediction and protection, and then process the envelope estimation results to fit the requirements of envelope protection in the form of state constraints. In this way, the performance of envelope protection can, in turn, validates the envelope estimation algorithm. A schematic of this general methodology is illustrated in Figure 3-1. The following sections discuss the detailed methodology of the two parts of the project.

3-1 Envelope Estimation with MC Simulations

As discussed in Section 2-1, the available deterministic methods for envelope estimation within the framework of reachability analysis suffer from high computational complexity. This problem is even more crucial in this project, as the dynamics of the ICE aircraft are so complex that no analytical system equations are available. The response of the aircraft can only be obtained by Simulink simulation which requires an evaluation of 108 data tables or physical spline models at each time step. In this way, the MC simulation approach is proposed in this project as a more flexible and robust approach to envelope estimation.

According to Definition 2-2, the general idea of envelope estimation with MC simulations is to generate two point clouds that consist of sample points in the state space that an airplane can reach from and fly back to the trim set respectively, by simulation with random control inputs. The intersection of the two point clouds forms the estimated envelope. In this project, the following steps were conducted to obtain a probabilistic flight envelope estimation: 1) define relevant states to be estimated, 2) obtain apriori trim sets, 3) conduct MC simulations, 4) generate probabilistic flight envelopes, which are discussed in the following sections respectively.

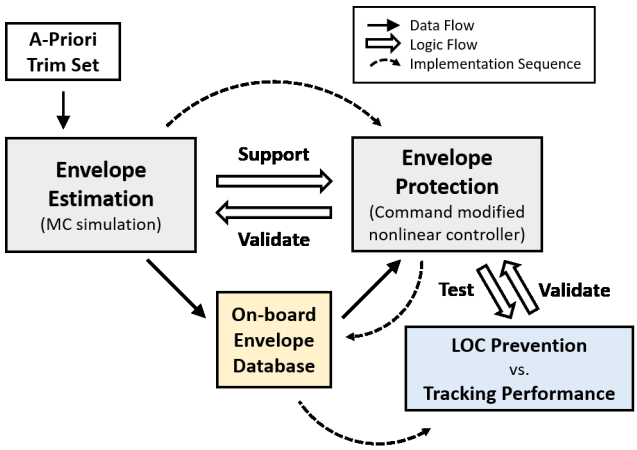

Figure 3-1: The schematic of the overall methodology.

3-1-1 State Definition

The first thing to be determined in envelope estimation is what are the relevant variables. In this project, the estimated envelope is applied in FEP systems as constraints of reference signals of controlled states. Thus, the estimated states should be preferably selected from the states that can be directly involved in flight control systems, which are summarized in Table 3-1. Among these fourteen states, the absolute values of horizontal position x, y and yaw angle ψ have no meaning in envelope estimation since they can take any value. In addition, since high-performance fighter aircraft like ICE aircraft can safely roll and pitch in any direction, roll angle ϕ and pitch angle θ should not be restricted. Finally, heading angle χ and flight path angle γ determine the course of the aircraft but are not directly related to the aerodynamic characteristics of the aircraft. So, they are less important in envelope estimation.

Therefore, the flight envelope of the remaining seven states is expected to be estimated in this project, namely vertical position z (or altitude $h = -z$), ground speed V_g, angle of attack α, sideslip angle β, and angular rates p, q, r. It should be noted that in practice, only envelopes within a limited time horizon can be estimated due to limited computational power. This time horizon was selected as around 1 s in much previous research (Helsen et al., 2016; Nabi et al., 2018). For slow variables like altitude and ground speed, this is significantly smaller than their characteristic time scales, i.e., the aircraft can not reach the envelope boundary within the time horizon. As a result, the estimated envelope of these two states are not suitable to be used directly in protection, but can serve as parameters in protection of other states.

3-1-2 Trim Set Estimation

To find the starting points of MC simulations, the apriori trim set is obtained by formulating and solving a constrained optimization problem. This project considers steady-state and level trim points. A grid of pitch angle θ is selected, and optimal corresponding angle of attack

Table 3-1: Relevant aircraft states in flight control systems.

Category	Name	Symbol	Unit
Position	-	x	m
	-	y	m
	-	z	m
Velocity vector	Ground speed	V_g	m/s
	Heading angle	χ	rad
	Flight path angle	γ	rad
Aerodynamic angle	Angle of attack	α	rad
	Sideslip angle	β	rad
Euler angle	Roll angle	ϕ	rad
	Pitch angle	θ	rad
	Yaw angle	ψ	rad
Angular rate	Roll rate	p	rad/s
	Pitch rate	q	rad/s
	Yaw rate	r	rad/s

α is solved.[1] Two different control surface configurations are applied to trim the aircraft as follows.

- **With TV**: Left and right AMT, left and right elevons, and pitch TV;
- **Without TV**: Left and right AMT, left and right elevons, and PF.

It is noted that since only level flights are considered, both the two AMT and the two elevons are locked to move symmetrically only. The above variables together with the thrust form the vector to be optimized as

$$\boldsymbol{x} = [T \ d_{amt} \ d_{ele} \ d_{ptv} \ \alpha]^T \tag{3-1}$$

or

$$\boldsymbol{x} = [T \ d_{amt} \ d_{ele} \ d_{pf} \ \alpha]^T. \tag{3-2}$$

The following constraints are proposed for level and steady-state trim points.

$$\dot{p} = \dot{q} = \dot{r} = \dot{u} = \dot{v} = \dot{w} = \phi = 0. \tag{3-3}$$

The aircraft responses are obtained by running the high-fidelity aerodynamic model of the ICE aircraft for one time step. Two objectives are relevant for this problem, namely minimum thrust

$$J_1 = \left(\frac{T}{T_{max}}\right)^2, \tag{3-4}$$

[1] In the final implementation, only straight trim points are considered. Instead, interest was drawn to include trim points at different speeds and altitudes.

where T_{max} is the full thrust, and minimum control effort

$$J_2 = d_{amt}[\text{rad}]^2 + d_{ele}[\text{rad}]^2 + d_{ptv}[\text{rad}]^2 + d_{pf}[\text{rad}]^2. \tag{3-5}$$

So, the objective function is formulated as

$$J = J_1 + k_{trim} \cdot J_2, \tag{3-6}$$

where k is a weighting factor. This constrained optimization problem is solved by an SQP solver. The trim points at different θ are interpolated by smoothing splines to form the trim set.

3-1-3 Monte Carlo Simulation

An accurate estimation of the flight envelope by MC simulation relies heavily on a good sampling of the forward and the backward reachable sets. By the nature of this approach, the reachable sets are not overestimated, as each sample of the sets is attached to a known initial state and a known trajectory. However, a poor sampling of random control inputs can lead to significant underestimation of the reachable set, as the specific control inputs that drive the aircraft to the boundaries of the flight envelope may not be selected. Furthermore, it is not practically possible to apply conventional deterministic approaches to high-dimensional envelope estimation with a complex aircraft model like this project for comparison.

To conquer this problem, the so-called extreme control effectiveness method was proposed for envelope estimation with MC simulation. This method examines the derived equation for the optimal control in the level set method, which is the most widely-used and mature technique in envelope estimation (see Section 2-1-1). In the level set method (Nabi et al., 2018), the optimal control to find the boundary of the flight envelope is selected as

$$\boldsymbol{\delta}^* = \arg\min_{\boldsymbol{\delta}\in U} H = \arg\min_{\boldsymbol{\delta}\in U} \frac{\partial V}{\partial \boldsymbol{x}_e}(\boldsymbol{x}_e, t) \cdot \boldsymbol{f}(\boldsymbol{x}_e, \boldsymbol{\delta}), \tag{3-7}$$

where H is the Hamiltonian to be minimized, V is the level set for the invariant set, $\boldsymbol{x}_e$ are the state variables that are explicitly dependent on the control inputs, $\boldsymbol{f}(\boldsymbol{x}_e, \boldsymbol{\delta})$ are the system dynamics. For the ICE aircraft, the control surfaces deflections have an explicit influence on both aerodynamic forces and moments, so $\boldsymbol{x}_e$ is selected as $[u\ v\ w\ p\ q\ r]^T$. Rewrite dynamics of $\boldsymbol{x}_e$ (Eqs. 2-25 and 2-28) in the incremental form, we have

$$\boldsymbol{f}(\boldsymbol{x}_e, \boldsymbol{\delta}) \approx \dot{\boldsymbol{x}}_{e,0} + \tilde{\boldsymbol{J}}^{-1}\boldsymbol{J}_d\Delta\boldsymbol{\delta}, \tag{3-8}$$

where

$$\tilde{\boldsymbol{J}}^{-1} = \begin{bmatrix} \text{diag}(\frac{1}{m}, \frac{1}{m}, \frac{1}{m}) & \mathbf{0} \\ \mathbf{0} & \boldsymbol{J}^{-1} \end{bmatrix}, \tag{3-9}$$

$\dot{\boldsymbol{x}}_{e,0}$ is the state derivatives at current time step, m is the mass, $\boldsymbol{J}$ is the initial matrix, $\Delta\boldsymbol{\delta}$ is

the incremental deflections of all active control surfaces and the incremental thrust,

$$\boldsymbol{J}_d = \begin{bmatrix} \frac{\partial F_x}{\partial \boldsymbol{\delta}} \\ \frac{\partial F_y}{\partial \boldsymbol{\delta}} \\ \frac{\partial F_z}{\partial \boldsymbol{\delta}} \\ \frac{\partial M_x}{\partial \boldsymbol{\delta}} \\ \frac{\partial M_y}{\partial \boldsymbol{\delta}} \\ \frac{\partial M_z}{\partial \boldsymbol{\delta}} \end{bmatrix} \tag{3-10}$$

is the full Jacobians of forces and moments. The Jacobians for control surfaces other than TV are obtained by the spline model developed in (Peijl, 2017); the Jacobians for TV and the thrust are obtained by taking partial derivatives of the TV model (Eq. 2-40) analytically.

Thus,

$$\Delta u_i^* = \begin{cases} \Delta u_{i,max}, & \frac{\partial V}{\partial \boldsymbol{x}_e}(\boldsymbol{x},t)\tilde{\boldsymbol{J}}^{-1}\boldsymbol{J}_{d,\cdot i} < 0 \\ \Delta u_{i,min}, & \frac{\partial V}{\partial \boldsymbol{x}_e}(\boldsymbol{x},t)\tilde{\boldsymbol{J}}^{-1}\boldsymbol{J}_{d,\cdot i} > 0 \end{cases} \tag{3-11}$$

In Eq. 3-11, the only unknown term is the partial derivative of the level set function $\frac{\partial V}{\partial \boldsymbol{x}_e}$. Instead of solving the HJB-PDE as in the level set method, the term is randomly sampled at each time step in this approach, assuming an identical normal distribution for each element. In this way, the simulations only sample in all possible optimal control selections in the level set method. This method is named as extreme control effectiveness method because Eq. 3-11 aims to minimize a weighted control effectiveness in three translational and three rotational directions. The randomly-sampled partial derivative term can be regarded as a weighting vector which describes how important it is for the aircraft to obtain extreme control effectiveness in each direction. So, only sets of extreme control inputs can be selected in MC simulations such that the aircraft is controlled towards the boundaries of the flight envelope.

Other issues considered in the MC simulations are listed as follows.

Initial states The initial states used in the simulations are randomly selected from the trim set for each sample.

Time horizon The selection of time horizon T_f will significantly affect the size of the estimated envelope. It should be noted that since the ICE aircraft is inherently unstable, it is difficult to stabilize the aircraft for a long time horizon with open-loop control inputs.

Disturbance The approach gives freedom to apply any kind of disturbance or gust into simulations due to its probabilistic nature.

Backwards system For an autonomous system, the following two formulations are equivalent.

$$\dot{x}(t) = f(x(t), u), x(T_f) = x_f \tag{3-12}$$

$$\dot{x}(T_f - t) = -f(x(T_f - t), u), x(0) = x_f \tag{3-13}$$

So, to run the aircraft model backward in time, the signs of all dynamics equations are inverted.

3-1-4 Probability Density Estimation

By running MC simulations for the original and the backward systems, two large samples of the forward and the backward reachable sets $\boldsymbol{y}_{f,i}$, $\boldsymbol{y}_{b,i}$ are obtained. By definition, the desired dynamic flight envelope is the intersection of the above two sets. To calculate the intersection from the two samples of reachable sets, Definition 3-1 and 3-2 were proposed.[2]

> **Definition 3-1 (Safe flight trajectory)** A trajectory in the state space for a finite duration of T_f that starts and ends in the trim set.
>
> **Definition 3-2 (Probabilistic dynamic flight envelope)** The multivariate probability density function of the states of aircraft at time $T_f/2$ for all safe flight trajectories of duration T_f.

Definition 3-2 does not define an absolute boundary of the envelope, but uses a probability density value to indicate how likely a point in the state space is within the envelope. In this way, flexibility is maintained to choose from a more conservative envelope to a more exaggerated envelope for different applications. It should be noted that since the aircraft can stay indefinitely in the trim set, safe flight trajectories of duration $T_{f,0}$ actually cover all safe flight trajectories of duration $T_f \leq T_{f,0}$. In this way, Definition 3-2 is comparable to Definition 2-2. Similarly, the probabilistic form of Eq. 2-6 was proposed as

$$g_{env}(\boldsymbol{x}) = \frac{g_f(\boldsymbol{x}) g_b(\boldsymbol{x})}{\iiint_V g_f(\cdot) g_b(\cdot) \mathrm{d}\mathbb{V}}, \tag{3-14}$$

where g_{env} is the probabilistic dynamic flight envelope, g_f, g_b are the probability density functions of the forward and backward reachable sets respectively, $\mathbb{V}$ defines the whole state space of the aircraft.

The probability density functions of the forward and backward reachable sets $g_f(\boldsymbol{x})$, $g_b(\boldsymbol{x})$ are estimated from the samples by probability density estimation methods discussed in Section 2-1-2. Since no information is available about the shape of the envelope, the non-parametric method, kernel density estimation is more appropriate for this project. This is achieved by applying Eqs. 2-11 and 2-13 to the samples $\boldsymbol{y}_{f,i}$, $\boldsymbol{y}_{b,i}$, with a Gaussian kernel function

$$k(x) = \frac{1}{\sqrt{2\pi}} e^{-\frac{1}{2}x^2}. \tag{3-15}$$

To convert the probabilistic dynamic flight envelope to a normal dynamic flight envelope with absolute boundaries, a threshold of the probability density can be selected. Assuming an uncorrelated normal distribution of the probabilistic dynamic flight envelope, the threshold value at $k\sigma$ is

$$p_0(k) = e^{-\frac{1}{2}k^2} \cdot \max\, g_{env}(\boldsymbol{x}), \tag{3-16}$$

where d is the dimension of the state space. In this way, the k value can be tuned to find the suitable size of the envelope for specific applications.

[2] The definition of probabilistic envelope is further formalized in the paper as fuzzy sets.

Compared with conventional reachability analysis, the MC simulation approach proposed here is much more flexible and feasible, as 1) the states to be estimated can be freely selected, 2) the aggressiveness of estimation can be controlled by a threshold value, and 3) other flight conditions like disturbances can be included. On the other hand, it should be noted that this method can not truly overcome the curse of dimensionality, as the sampling points needed for density estimation to achieve the same level of reliability still grow exponentially with the dimensionality. However, this method can always provide reasonable results with current computational capacity.

3-2 Envelope Protection with Nonlinear Controller

Based on the estimated flight envelope, the envelope protection part aims to always constrain the aircraft within the specified flight envelope. The FEP system proposed in this project acts upon an ordinary nonlinear flight control system. The general idea is that when the pilot's command is not violating the flight envelope, the aircraft is controlled by a normal incremental nonlinear dynamic inversion (INDI) controller. When the pilot is giving a command that drives the aircraft outside the envelope, the FEP system detects the trend and activates to modify the pilot's command.[3]

To achieve this, an envelope database needs to be established which updates constraints of states in realtime from the estimated envelope. At each time step, the state command of each loop is monitored by comparing with the state constraints specified in the envelope database. If the command violates the state constraints, a saturation filter is applied to the command. On the other hand, when commands of inner loops are modified, the tracking performance and even stability of the outer loops will also be affected. In addition, the violation of inner-loop envelope is fundamentally caused by inadequate outer-loop commands. Thus, an additional feedback term to outer loops is needed to compensate for the difference between the original and envelope-protected commands of inner loops.

To sum up, two additional components are needed in the envelope-protected nonlinear controller: a filter to constrain the command within the state constraints specified in the envelope database, and a command modification term to compensate for the discrepancy in inner-loop commands due to FEP. The schematic of the controller is illustrated in Figure 3-2.[4]

The following sections elaborate the schematic in Figure 3-2 by explaining the overall controller structure, the design of the envelope database and the approach to command modification.

3-2-1 Controller Structure

The controller implemented in this project is a two-loop controller, which consists of an outer loop of aerodynamic angles ϕ, α, β and an inner loop of angular rates p, q, r. The outer loop is controlled by an NDI controller since this loop is governed by kinematic equations with no

[3]This section only considers the state-constraint-based FEP but not probabilistic FEP.
[4]In the final implementation, the inner-loop compensation comes after the FEP system.

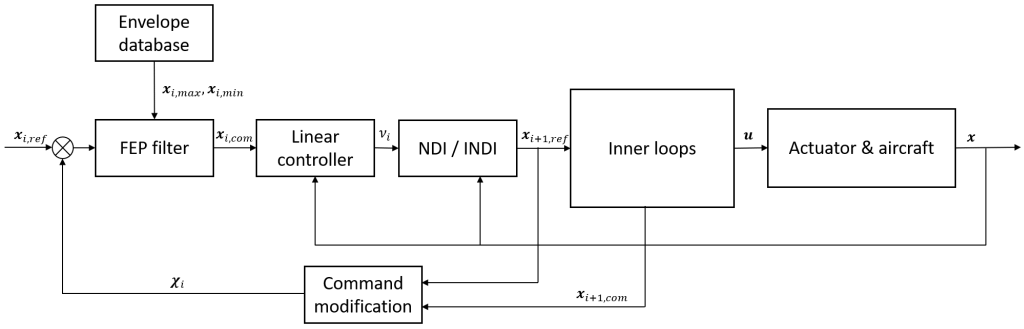

Figure 3-2: Schematic of the envelope-protected nonlinear control system.

uncertainty. The dynamics of ϕ, α, β are shown in Eqs. 2-26 and 2-27, and denoted as

$$\frac{\mathrm{d}}{\mathrm{d}t}\begin{bmatrix}\phi\\ \alpha\\ \beta\end{bmatrix} = \begin{bmatrix}0\\ b_\alpha(\boldsymbol{x})\\ b_\beta(\boldsymbol{x})\end{bmatrix} + \begin{bmatrix}a_\phi(\boldsymbol{x})\\ a_\alpha(\boldsymbol{x})\\ a_\beta(\boldsymbol{x})\end{bmatrix}\begin{bmatrix}p\\ q\\ r\end{bmatrix}. \tag{3-17}$$

So the NDI control law for this loop is

$$\begin{bmatrix}p_c\\ q_c\\ r_c\end{bmatrix} = \begin{bmatrix}a_\phi(\boldsymbol{x})\\ a_\alpha(\boldsymbol{x})\\ a_\beta(\boldsymbol{x})\end{bmatrix}^{-1}\left(\begin{bmatrix}\nu_\phi(\boldsymbol{x})\\ \nu_\alpha(\boldsymbol{x})\\ \nu_\beta(\boldsymbol{x})\end{bmatrix} - \begin{bmatrix}0\\ b_\alpha(\boldsymbol{x})\\ b_\beta(\boldsymbol{x})\end{bmatrix}\right), \tag{3-18}$$

where $[\nu_\phi(\boldsymbol{x}), \nu_\alpha(\boldsymbol{x}), \nu_\beta(\boldsymbol{x})]^T$ are the virtual controls from the linear controller, $[p_c, q_c, r_c]^T$ are the command to the inner loop.

The inner loop is controlled by an INDI controller with INCA developed in (Matamoros & Visser, 2018). The dynamics of p, q, r in the incremental form are

$$\begin{bmatrix}\dot{p}\\ \dot{q}\\ \dot{r}\end{bmatrix} = \begin{bmatrix}\dot{p}_0\\ \dot{q}_0\\ \dot{r}_0\end{bmatrix} + \boldsymbol{J}^{-1}\boldsymbol{J}_d(\boldsymbol{x}_0, \boldsymbol{\delta}_0)\Delta\boldsymbol{\delta}, \tag{3-19}$$

where I is the inertia matrix as in Eq. 2-29, $\boldsymbol{\delta}$ is the control surface deflections, $\boldsymbol{J}_d(\boldsymbol{x}_0, \boldsymbol{\delta}_0)$ is the control effectiveness matrix of control surfaces deflections on aerodynamic moments.

So the INDI control law for this loop is

$$\Delta\boldsymbol{\delta}_c = \boldsymbol{J}_d^{-1}(\boldsymbol{x}_0, \boldsymbol{\delta}_0)\boldsymbol{J}\left(\begin{bmatrix}\nu_p(\boldsymbol{x})\\ \nu_q(\boldsymbol{x})\\ \nu_r(\boldsymbol{x})\end{bmatrix} - \begin{bmatrix}\dot{p}_0\\ \dot{q}_0\\ \dot{r}_0\end{bmatrix}\right), \tag{3-20}$$

where $[\nu_p(\boldsymbol{x}), \nu_q(\boldsymbol{x}), \nu_r(\boldsymbol{x})]^T$ are the virtual controls from the linear controller.

Note that it is assumed that the ICE aircraft is equipped with angular acceleration sensors to obtain measurements of angular rate derivatives.

The throttle setting of the aircraft is controlled by a separated auto-throttle loop. This auto-throttle loop applies INDI to the following dynamics of airspeed

$$\dot{V}_g = \frac{1}{m}(\cos\alpha\cos\beta\cdot F_x + \sin\beta\cdot F_y + \sin\alpha\cos\beta\cdot F_z) - g\sin\gamma. \tag{3-21}$$

Rewrite in the incremental form with respect to the thrust T,

$$\begin{aligned}\dot{V}_g &= \dot{V}_{g,0} + \frac{1}{m}\left(\cos\alpha\cos\beta\cdot\frac{\partial F_x}{\partial T} + \sin\beta\cdot\frac{\partial F_y}{\partial T} + \sin\alpha\cos\beta\cdot\frac{\partial F_z}{\partial T}\right)\mathrm{d}T \\ &= \dot{V}_{g,0} + g_T(\boldsymbol{x})\mathrm{d}T,\end{aligned} \tag{3-22}$$

where $\dot{V}_{g,0}$ is the current derivative of airspeed, $g_T(\boldsymbol{x})$ denotes the control effectiveness of the thrust on the airspeed. Thus, the new thrust is selected as

$$T_c = T_0 + \frac{k_T(V_{g,des} - V_g) - \dot{V}_{g,0}}{g_T(\boldsymbol{x})}, \tag{3-23}$$

where T_0 is the current thrust, k_T is a proportional gain factor.

It should be noted that this dynamic inversion is not trivial for the ICE aircraft, since 1) the thrust force can be distributed in all three directions due to MATV as shown in the TV model (Eq. 2-40), and 2) the ICE aircraft can operate at high angles of attack and sideslip angles.

3-2-2 The Envelope Database

The envelope database aims to convert the probabilistic flight envelope estimated in Section 3-1 into magnitude constraints of aircraft states such that they can be directly applied to the nonlinear controller.

Based on the current controller design, five states, namely angle of attack α, sideslip angle β, and angular rates p, q, r are protected. The roll angle ϕ is not protected to maintain the agility of the ICE aircraft. Since the estimated envelopes are nonlinear, the constraints of each state are dependent on the current values of the five states as well as two slow variables altitude h and ground speed V_g. Therefore, a total of 10 multivariate functions are stored in the envelope database, namely

$$\begin{cases} f_{11} = p_{max}(p,q,r,\alpha,\beta;h,V_g), f_{12} = p_{min}(p,q,r,\alpha,\beta;h,V_g), \\ f_{21} = q_{max}(p,q,r,\alpha,\beta;h,V_g), f_{22} = q_{min}(p,q,r,\alpha,\beta;h,V_g), \\ f_{31} = r_{max}(p,q,r,\alpha,\beta;h,V_g), f_{32} = r_{min}(p,q,r,\alpha,\beta;h,V_g), \\ f_{41} = \alpha_{max}(p,q,r,\alpha,\beta;h,V_g), f_{42} = \alpha_{min}(p,q,r,\alpha,\beta;h,V_g), \\ f_{51} = \beta_{max}(p,q,r,\alpha,\beta;h,V_g), f_{52} = \beta_{min}(p,q,r,\alpha,\beta;h,V_g). \end{cases} \tag{3-24}$$

The 10 functions of state constraints are stored in the form of 7-D LUTs. First, a threshold of the probability density value is selected for the probabilistic flight envelope, to determine the boundary of the flight envelope. Then, a 7-D grid is established as data points of the database. For each point within the grid, the maximum and minimum values for each state to stay within the envelope are evaluated while keeping the other states unchanged. These maximum and minimum values are stored as the maximum and minimum constraints for this state at the current data point. This idea is illustrated in Figure 3-3 for a simplified 2-D case. When the current state is outside the estimated envelope, the constraints are defined the same as the closest point that is within the envelope.

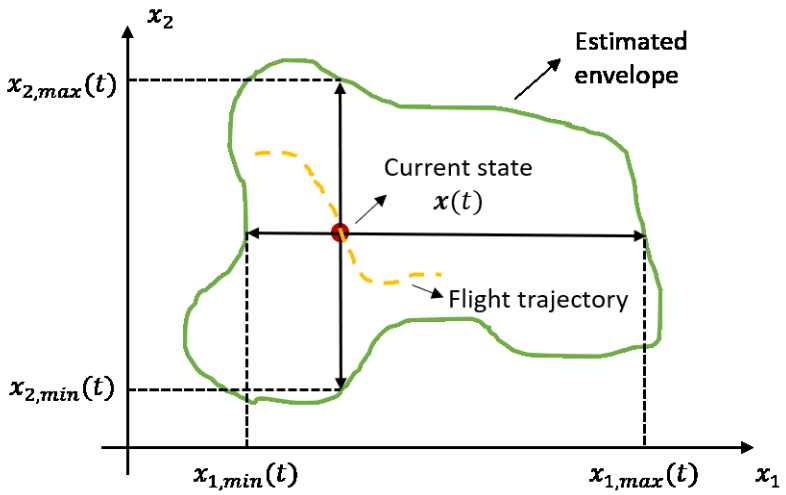

Figure 3-3: Example of realtime state constraints generation in 2-D.

When integrated into the control system, the current states of the aircraft $(p, q, r, \alpha, \beta, h, V_g)$ are the inputs to the database. By evaluating the 10 LUTs, the envelope database can output the maximum and minimum constraints of the five variables (p, q, r, α, β) to the envelope protection filter in realtime.

3-2-3 The Command Modification Approach

As discussed in Section 2-2-2, two approaches, namely CF and PCH are available to include state or input constraints in nonlinear controllers. To demonstrate their strategies in command modification, the dynamic models of the two approaches (Eqs. 2-32 to 2-35) are combined as the following.

Command filtering

$$\boldsymbol{x}_c = H(s)\boldsymbol{x}_{ref} - H(s)\frac{1}{s+\boldsymbol{K}}[\boldsymbol{f}(\boldsymbol{x},\boldsymbol{\delta}_{act}) - \boldsymbol{f}(\boldsymbol{x},\boldsymbol{\delta}_c)] \tag{3-25}$$

Pseudo control hedging

$$\boldsymbol{x}_c = \frac{\boldsymbol{K}_{ref}}{s+\boldsymbol{K}_{ref}}\boldsymbol{x}_{ref} + \frac{1}{s+\boldsymbol{K}_{ref}}[\boldsymbol{f}(\boldsymbol{x},\boldsymbol{\delta}_{act}) - \boldsymbol{f}(\boldsymbol{x},\boldsymbol{\delta}_c)] \tag{3-26}$$

It can be seen that the two methods actually share a similar structure in command modification, except that they have different filter terms and more importantly, they have different signs for the second term of deviation update. In other words, they apply the opposite command modification strategy to inner-loop envelope protection (or actuator dynamics). CF imposes an even larger command when the previous command is not fully achieved, whereas PCH reduces the command. This difference in strategy results from their application. CF always strives for the best possible tracking performance, whereas PCH aims to avoid actuator saturation only. In the application of envelope protection, the objective is similar to PCH,

which is to avoid 'saturating' the flight envelope. However, PCH is only defined for the innermost loop but not for outer loops.[5] Thus, the command modification strategy applied in this project is based on the structure of CF which is applicable to multi-loop systems but applies a similar strategy to PCH, which reduces further commands when inner-loop commands violate the flight envelope. This is achieved by reversing the sign of the deviation update term. So the following equations are applied to modify the command in this project.

$$\boldsymbol{x}_{i,c} = H(s)(\boldsymbol{x}_{i,ref} - \boldsymbol{\chi}_i) \tag{3-27}$$

$$\dot{\boldsymbol{\chi}}_i = -\boldsymbol{K}\boldsymbol{\chi}_i - [\boldsymbol{f}(\boldsymbol{x}_i, \boldsymbol{x}_{i+1,c}) - \boldsymbol{f}(\boldsymbol{x}_i, \boldsymbol{x}_{i+1,ref})] \tag{3-28}$$

[5] An extended version of PCH in multi-loop is used instead of the modified command filter in the final implementation.

Chapter 4

Preliminary Results

This chapter demonstrates preliminary results obtained with the methodology discussed in Chapter 3. The first example shows results of envelope estimation for three longitudinal states θ, α, q. First, the trim set generated by fitting nonlinear-optimized trim points is illustrated in Figure 4-1. Then, Figure 4-2 plots raw sampling points generated directly from MC simulations with the proposed extreme control effectiveness method. These sampling points were translated into probability density function of forward and backward reachable sets by kernel density estimation, three different percentiles of which are shown in Figure 4-3. It can be observed that the estimated reachable sets can capture the shape of the distribution of the sampling points and cover most of the sampling points within the set. Finally, the probabilistic flight envelope was obtained by calculating the probabilistic intersection of the above two sets as shown in Figure 4-4 and 4-5.

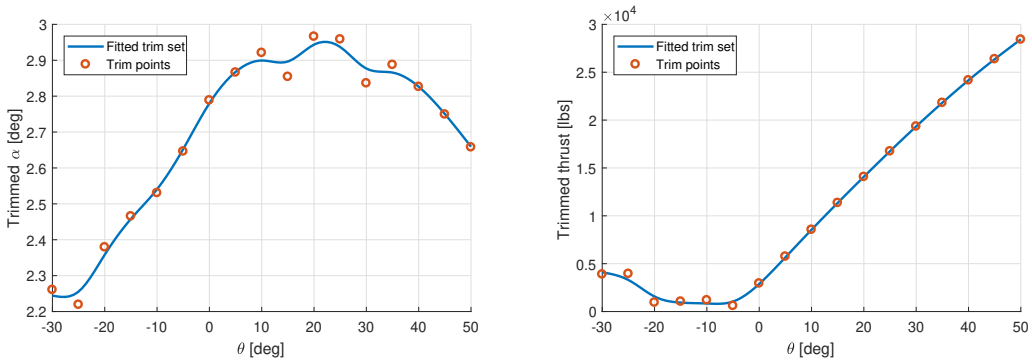

Figure 4-1: Fitted trim set of α (left) and the thrust (right) with respect to θ.

Another example estimates the flight envelope of four lateral states ϕ, β, p, r to demonstrate the flexibility of this MC-simulation-based envelope estimation method in the selection of states. The estimated reachable sets and the final flight envelope are shown in Figure 4-6 and 4-7 respectively. Parameters used in envelope estimation of the above two examples are summarized in Table 4-1.

Table 4-1: Summary of parameters in examples of envelope estimation.

Parameter	Symbol	Value	Unit
Flight condition			
Altitude	h	20,000	ft
Ground speed	V_g	880	ft/s
Mach number	M	0.85	-
Mass configuration	-	Nominal	-
Selected control effectors	-	All 13	-
Disturbance	-	None	-
Trim set			
Resolution of θ grid	-	5	deg
Objective weighting factor	k_{trim}	1	-
Nonlinear solver	-	SQP	-
Solver tolerance	ϵ	1×10^{-4}	-
MC simulation			
Time horizon	T_f	1	s
Sampling size	N	10,000	-
Step size of simulation	$\mathrm{d}t$	0.01	s
Rate of control system	f_{ctr}	100	Hz
Kernel density estimation			
Grid points for each dimension	n_{grid}	100	-
Kernel function	-	Gaussian function	-
Plotted percentiles	-	0.199, 0.739, 0.971	-

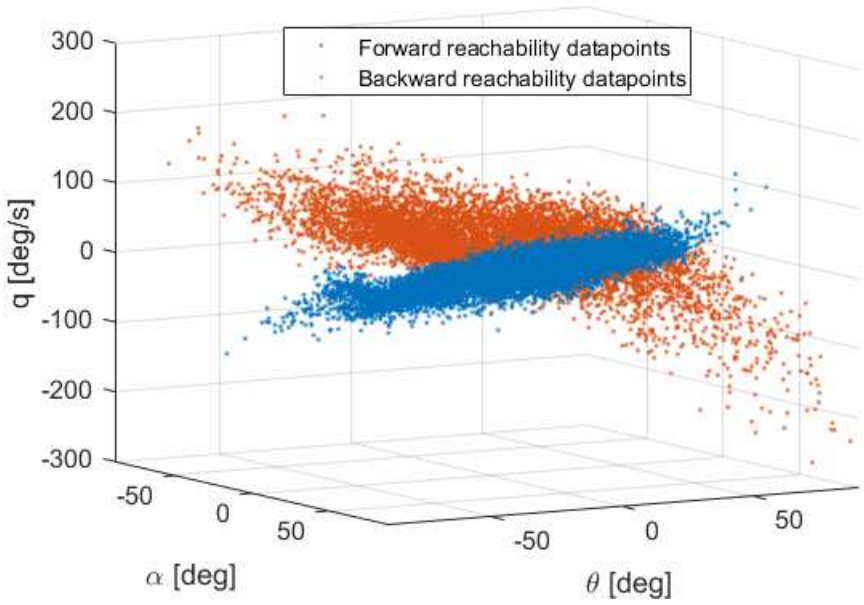

Figure 4-2: Sampling points of MC simulations in longitudinal envelope estimation.

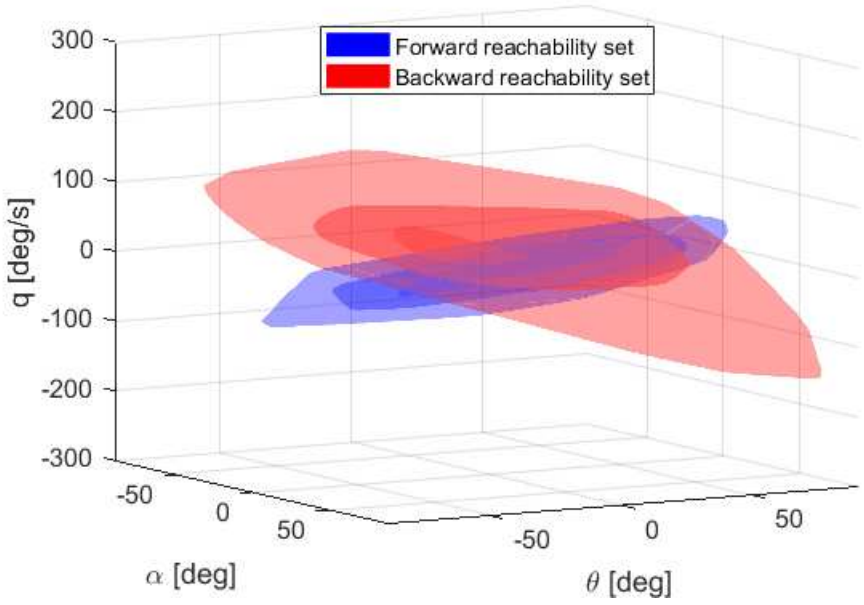

Figure 4-3: Estimated probabilistic forward and backward reachable sets in the longitudinal direction.

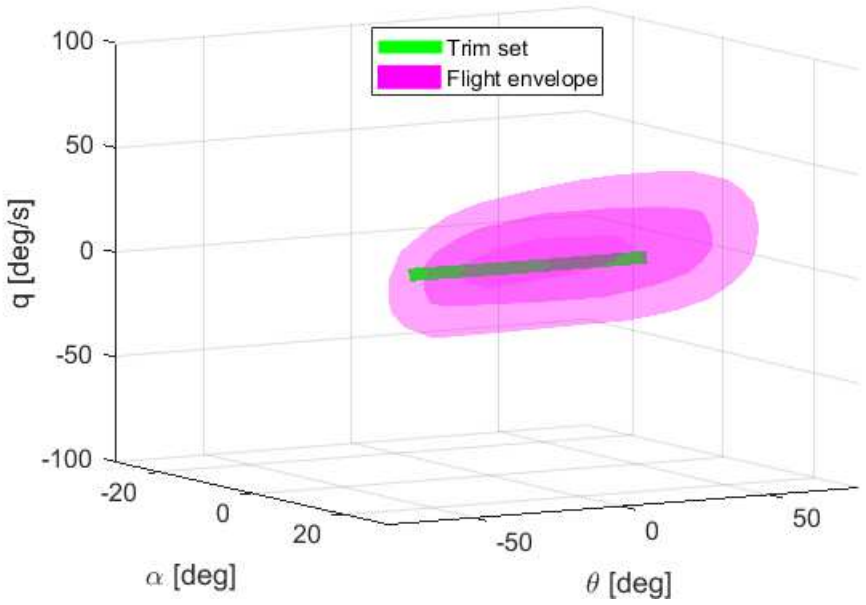

Figure 4-4: Estimated probabilistic safe flight envelope in the longitudinal direction.

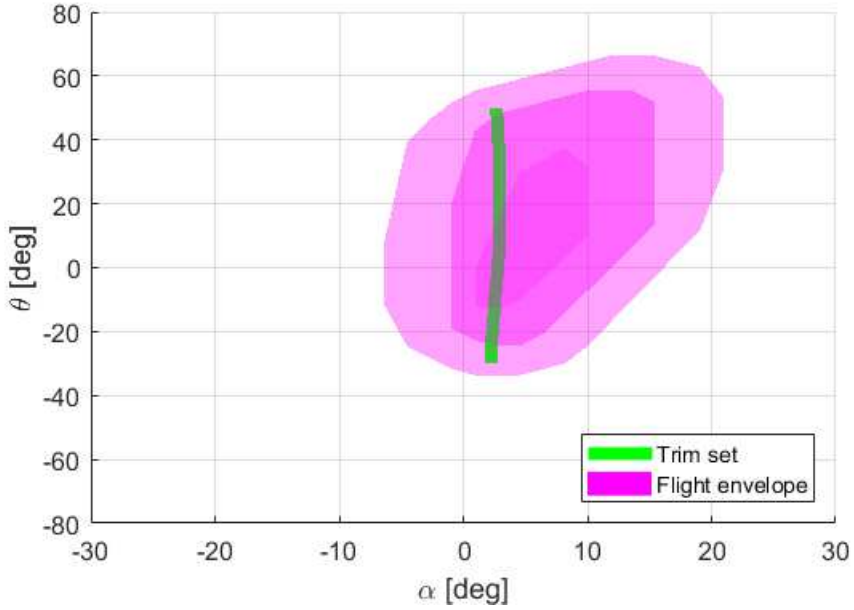

Figure 4-5: Estimated probabilistic safe flight envelope in the longitudinal direction, projected in the θ-α plane.

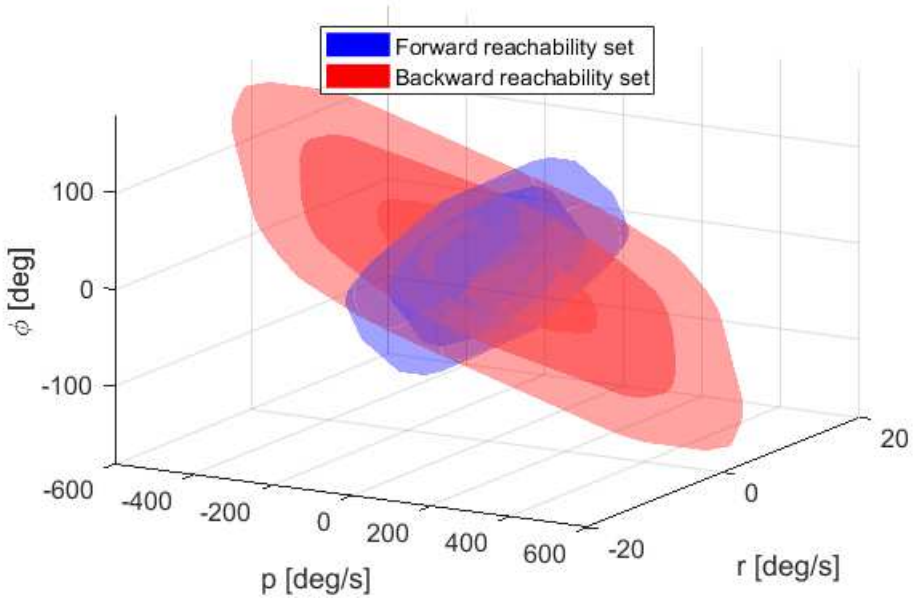

Figure 4-6: Estimated probabilistic forward and backward reachable sets in the lateral direction.

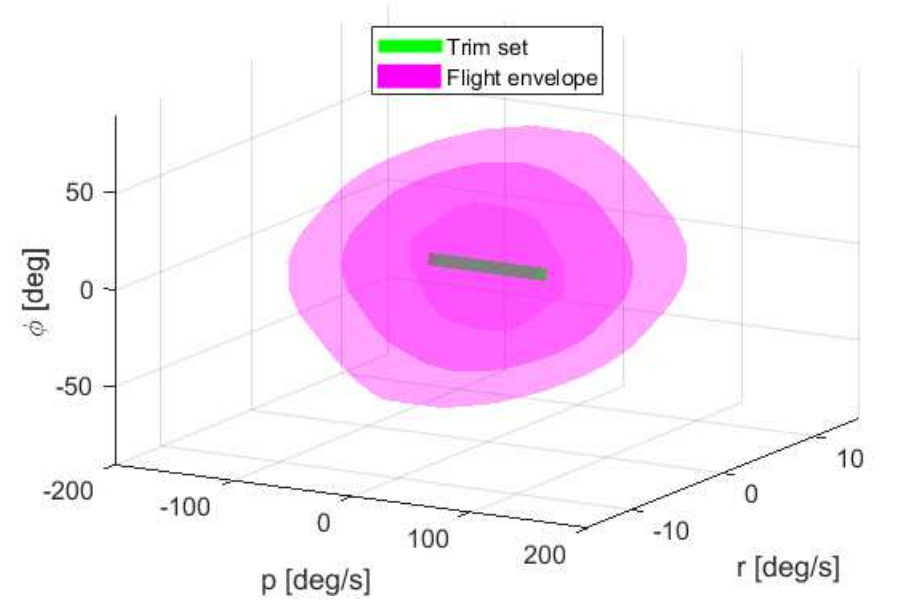

Figure 4-7: Estimated probabilistic safe flight envelope in the lateral direction.

Table 4-2: Summary of parameters in demonstration of envelope-protected nonlinear flight control system.

Parameter	Symbol	Value	Unit
Baseline NDI controller			
Step size of simulation	$\mathrm{d}t$	0.01	s
Rate of control system	f_{ctr}	100	Hz
Selected control effectors	-	All 13	-
Linear controller gain (angle loop)	$K_{p,angle}$	[1.50, 2.40, 1.65]	-
Linear controller gain (rate loop)	$K_{p,rate}$	[5,5,5]	-
Envelope database			
Grid of altitude	h	10,000, 20,000, 30,000	ft
Grid of Mach number	M	0.4, 0.8, 1.2	-
Grid points for other dimensions	n_{grid}	25	-
Selected percentile	-	0.916	-
Example manuever			
Roll angle command	ϕ_c	50	deg
Angle of attack command	α_c	$\pm$ 50	deg
Sideslip angle command	β_c	$\pm$ 10	deg
Time constant of command prefilter	t_{pf}	[10, 2.5, 4]	s

To apply the estimated envelope to envelope protection, the 7-D envelope database was generated, of which comparisons at different attitudes and speeds are illustrated in Figure 4-8 and 4-9 by projecting the envelope onto the α-β plane. It can be seen that the size of the flight envelope changes at different altitudes. Both the size and the shape of the flight envelope differ for different Mach numbers.

With this envelope database, the envelope-protected nonlinear flight control system was tested with a high-angle-of-attack maneuver as illustrated in Figure 4-10. Both the commands of α and β violated the state constraints during the simulation. However, the FEP system successfully detected this and modified the command such that the aircraft response remained within the prescribed flight envelope throughout the simulation. Parameters used in this demonstration of the envelope-protected controller are summarized in Table 4-2.

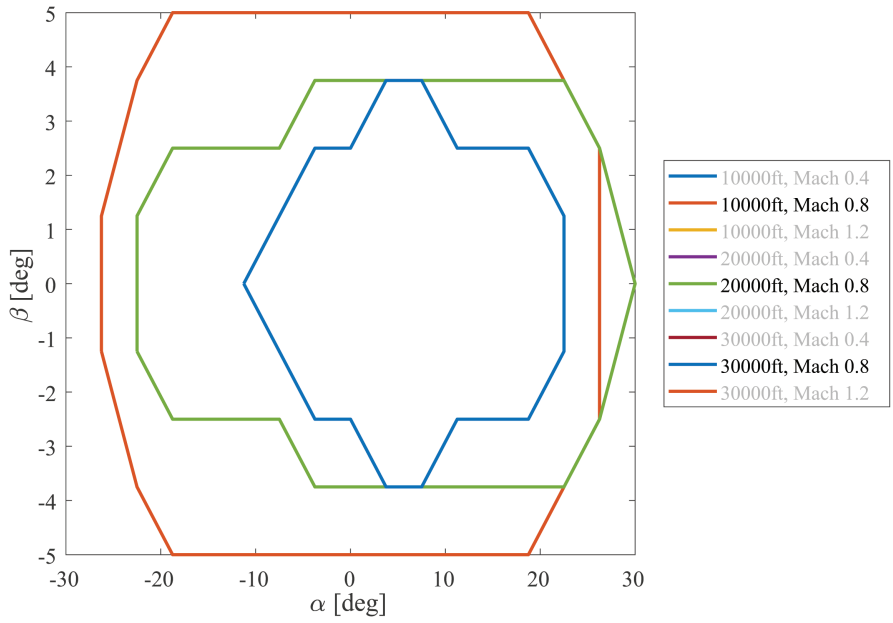

Figure 4-8: Comparison of the α-β envelope for different altitudes at Mach 0.8.

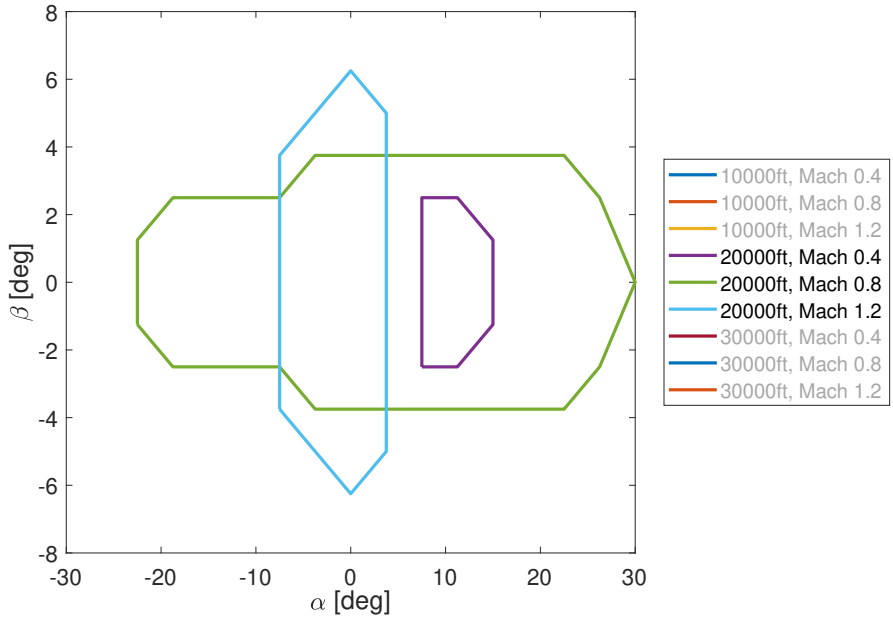

Figure 4-9: Comparison of the α-β envelope for different Mach numbers at FL200.

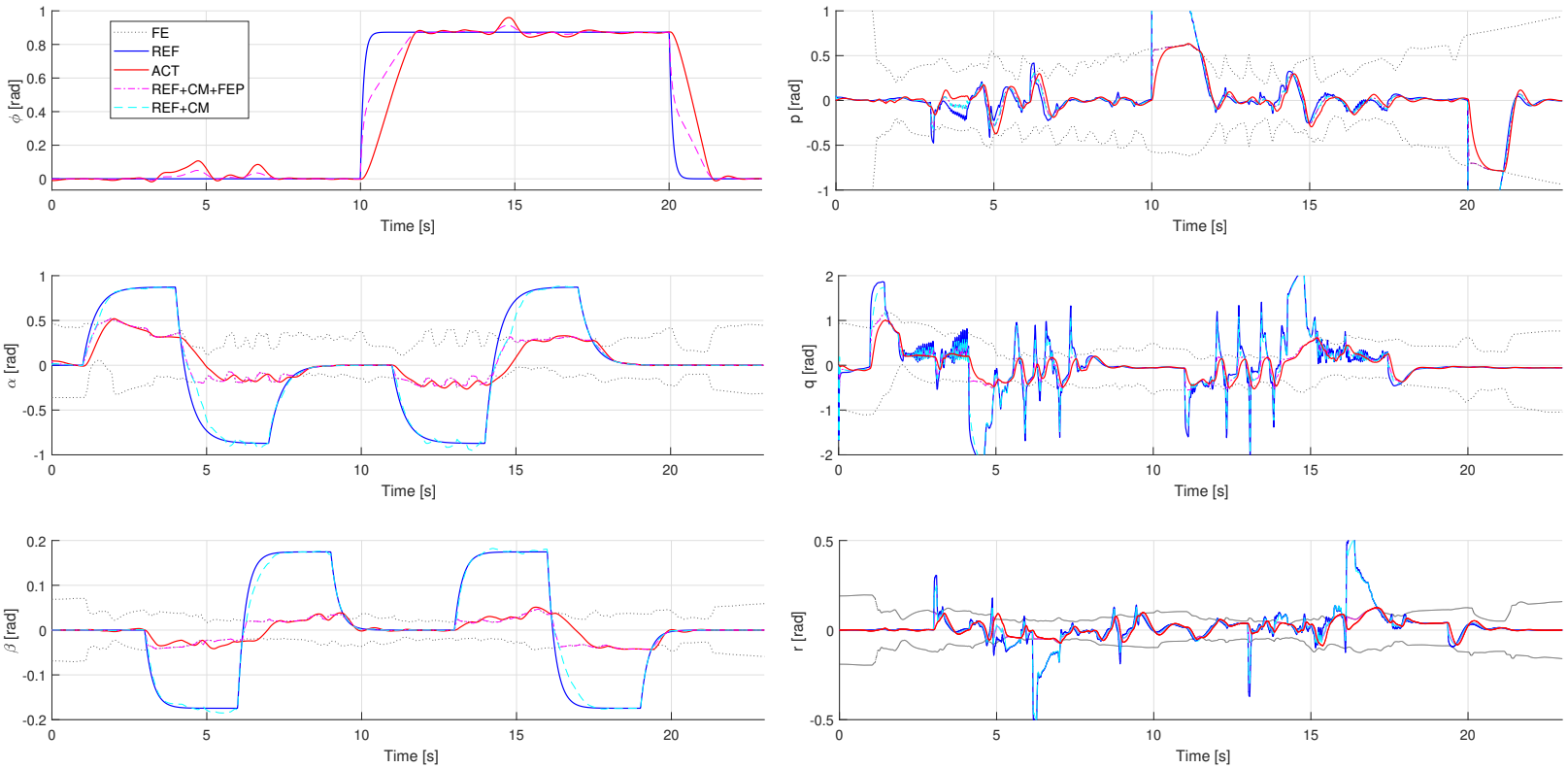

Figure 4-10: Performance of envelope-protected aerodynamic angle control. FE: estimated flight envelope, REF: reference signal, ACT: actual aircraft response, REF+CM: Modified command due to inner-loop envelope protection and/or actuator dynamics, REF+CM+FEP: final command with envelope protection of current states.

Chapter 5

Conclusion

To prevent LOC of the ICE aircraft that was observed in previous research, this project proposes a feasible methodology to estimate the safe flight envelope of the ICE aircraft and automatically protect the aircraft within the estimated envelope with the framework of nonlinear flight control. This methodology applies a novel probabilistic approach to envelope estimation by conducting MC simulations with control inputs that strive for extreme control effectiveness. In this way, the computational complexity issue of conventional envelope estimation methods is tackled for high-dimensional and complex systems. In addition, a unique command modification approach is integrated to an NDI controller to actively constrain the state commands in a multi-loop setup. Early results show that this solution can successfully estimate the flight envelope for any given set of states and effectively protect the aircraft against too aggressive commands.

However, this solution still suffers the following limitations.

- The proposed envelope estimation method is still not efficient enough for realtime applications. Thus, a database approach is used to store the estimated flight envelopes.
- The proposed envelope estimation method cannot be validated by comparison with other methods, as it is not computationally possible for other existing methods to estimate the envelope of the ICE aircraft.
- The methodology can only be validated by simulation since no physical model is available for testing.

Based on the implemented framework, the project will continue to work on validation of the estimated envelopes. Different parameters and flight conditions will be tested for their effects on the flight envelope. Case studies will be conducted to compare the controller performance with and without FEP systems.

Part III

Book of Appendices

Appendix A

Documentation

The whole envelope estimation and protection framework implemented in Matlab / Simulink consists of three parts: trimming, envelope estimation, and envelope protection. The scripts and result files are documented respectively as follows.

A-1 Trimming

`trimICE.m` The main script to generate the trim set of the ICE aircraft. Individual trim points are optimized and then interpolated to form the trim set. The grid points and flight conditions are specified here.

`constraint_ICE.m` Defines the constraints of the optimization problem by running the Simulink model of the ICE aircraft.

`cost_ICE.m` Defines the cost function to be optimized. Objective weighting factor k_{trim} is specified here.

`ICE_v3.slx` The ICE aircraft model with direct control surface deflection commands.

`init_massProperties.m` Initializes the mass properties of the ICE aircraft.

`test_trim.m` Test aircraft responses of generated trimmed flights.

The output trim-set files include the following variables.

`alt_grid, M_grid` The grid of altitudes and Mach numbers where trim points are calculated.

`massConf` Mass configuration setting of the trim set.

`noTV` True if TV is deactivated.

`trimPoint` List of all trim points. Rows correspond to trim point entries. Columns correspond to trimmed states and control surface deflections.

`trimPointInterp` Surface interpolation objects `sfit` of states and control surface deflections to be trimmed.

A-2 Envelope Estimation

`runShooting.m` Generates samples of the probabilistic envelope by MC simulation. Flight conditions are specified here.

`findPdf.m` Constructs kernel density estimators of samples and generates the probabilistic envelope database. Estimated states and their grids are specified here.

`plotTraj.m` Checks trajectories of selected sample points for verification.

`dbGeneration.m` Generates the state-constraint-based envelope database from the kernel density estimator. The threshold is specified here.

`paramDbGeneration.m` Covariance analysis of the results and generation of the parametric probabilistic envelope database.

`findPdf_2d.m, plotting_2d.m` Generates a simplified 2-D envelope database for demonstration. Estimation results at different flight conditions can be compared.

`init_ICESim_shooting.m` The main script to initialize each MC simulation.

`init_initState.m, init_trimPoint.m` Generates a random trimmed flight from the trim set.

`init_loadICEAeroDatabase.m` Loads the aerodynamic database of the ICE aircraft.

`init_massProperties.m` Initializes the mass properties of the ICE aircraft.

`init_modelParameters.m` Initializes other model parameters of the ICE aircraft.

`ICESim_MC_shooting.slx` The ICE aircraft model with extreme control effectiveness control.

`ICESim_MC_shooting_backward.slx` The ICE aircraft model with extreme control effectiveness control and backward dynamics.

The output estimation result files include the following variables.

`T` The time horizon of estimation.

`dt_s` Sampling time of the control inputs.

`massConf` Mass configuration setting of estimation.

`noTV` True if TV is deactivated.

`turb` Turbulence setting of estimation: 0 - none, 1 - light, 2 - moderate, 3 - severe.

`state` List of sample points. Rows correspond to sample points. Columns correspond to recorded states.

`rand_tp` List of random trim points. Rows correspond to sample points. Columns correspond to trimmed states and control surface deflections.

`rand_ctr` List of random control input sampling weightings. Rows correspond to sample points. Columns correspond to weightings in different directions.

`pdf_env` List of simplified 2-D kernel density estimators at different speeds and altitudes.

`pdf_fullEnv` Full 7-D kernel density estimator.

The state-constraint-based envelope database consists of the following variables.

`grid` The grids of all the states in LUTs.

`state_con` Matrix of state constraint LUTs. Rows correspond to protected states. Columns correspond to minimum and maximum constraints. Each element is an LUT of one state constraint value.

The probabilistic envelope database consists of the following variables.

`grid` The grids of all the states in the LUT.

`lut` The LUT of probability density values.

`prob_max` The maximum probability density value.

The parametric probabilistic envelope database consists of the following variables.

`alt_range, v_range` The interpolated ranges of the parametric model.

`fitParam` Parameters of the covariance interpolation. The first two dimensions correspond to elements in the covariance matrix. The third dimension corresponds to parameters in surface interpolation by fourth-order polynomial method `poly44`.

`sigma` List of all calculated covariance matrices. The first two dimensions correspond to the h-V_g grid. The last two dimensions correspond to elements in the covariance matrix.

A-3 Envelope Protection

`init_ICESim_FEP.m` The main initialization script for the NDI controller with FEP. All tunable controller parameters are specified here.

`ICESim_FEP_PCH.slx` The ICE aircraft model with NDI control of aerodynamic angle commands and FEP.

`generateManeuvers.m` Generates sample maneuvers in the form of time series.

`init_ctrParameters.m` Initializes other preset controller parameters.

`init_loadICEAeroDatabase.m` Loads the aerodynamic database of the ICE aircraft.

`init_loadManeuver.m` Loads the selected sample maneuver for simulation.

`init_massProperties.m` Initializes the mass properties of the ICE aircraft.

`init_modelParameters.m` Initializes other model parameters of the ICE aircraft.

`init_trimPoint.m` Initializes the aircraft at a specified trim point.

`plottingCtr.m` Plots controller performances based on logged signals from simulation.

Appendix B

Additional Results

B-1 Trim Sets

In addition to the trim set with nominal flight conditions shown in the paper, the trim sets with other mass configurations and without TV are shown in Figure B-1.

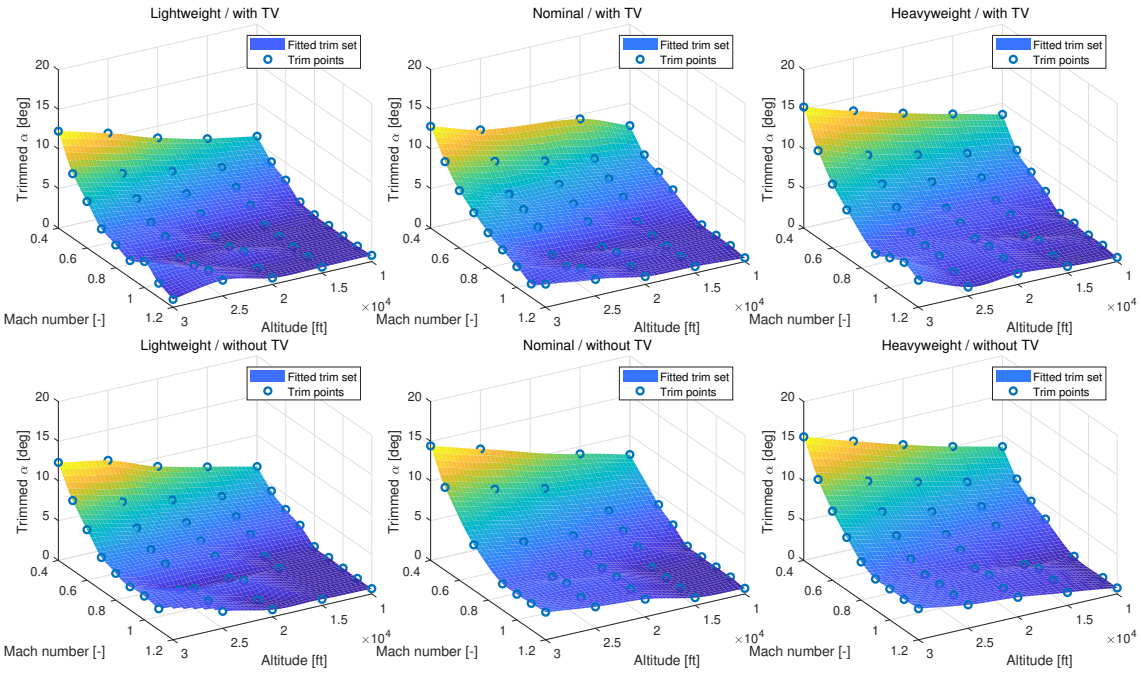

Figure B-1: Trim sets at different flight conditions.

B-2 Characteristic Size and Correlations of the Envelope

The developed non-parametric envelope databases with kernel density estimator consist of 8,621,250 data points. Therefore it is impossible to directly present the results. So the characteristic sizes of each state and the correlations between states are presented at different speeds and altitudes to demonstrate the estimation results. These values are obtained by calculating the covariance matrices of the probabilistic database. The correlation terms between longitudinal and lateral states are zero. The other terms are summarized in Table B-1 to B-9.

Table B-1: Characteristic size of the p-envelope [deg/s].

V_g [ft/s]		400	580	760	940	1120	1300
h [ft]	10,000	76.9	79.2	84.7	89.0	89.8	90.5
	15,000	73.4	76.7	83.9	88.3	88.6	89.8
	20,000	71.0	75.1	82.3	86.3	87.8	87.2
	25,000	69.2	74.1	80.5	86.2	87.3	87.9
	30,000	65.0	71.1	78.6	86.1	86.8	87.9

Table B-2: Characteristic size of the q-envelope [deg/s].

V_g [ft/s]		400	580	760	940	1120	1300
h [ft]	10,000	54.0	55.5	58.7	56.3	48.2	42.4
	15,000	53.7	54.7	57.7	56.8	46.5	41.7
	20,000	49.3	52.7	57.5	54.7	43.7	39.9
	25,000	45.8	51.1	55.2	51.7	42.0	40.0
	30,000	43.1	49.2	52.6	48.6	41.0	38.3

Table B-3: Characteristic size of the r-envelope [deg/s].

V_g [ft/s]		400	580	760	940	1120	1300
h [ft]	10,000	24.4	27.5	33.7	36.8	37.5	38.0
	15,000	23.9	26.8	31.8	35.5	35.8	36.5
	20,000	22.7	25.7	30.6	34.9	35.8	36.3
	25,000	21.9	24.8	28.6	33.9	34.6	34.3
	30,000	21.3	23.5	27.0	31.7	33.6	34.4

B-3 Sample Maneuvers

Two sample maneuvers are used to test the controller in this project. Maneuver A is a high AoA command, whereas Maneuver B is a combined high AoA and high sideslip angle

Table B-4: Characteristic size of the α-envelope [deg].

V_g [ft/s]	400	580	760	940	1120	1300
10,000	21.2	20.7	20.8	19.1	15.5	13.3
15,000	21.6	21.2	20.7	19.3	15.4	13.5
h [ft] 20,000	20.5	21.1	21.0	19.1	15.4	13.8
25,000	19.9	21.2	21.2	18.8	15.2	13.8
30,000	18.9	20.6	20.7	18.2	15.0	13.7

Table B-5: Characteristic size of the β-envelope [deg].

V_g [ft/s]	400	580	760	940	1120	1300
10,000	12.6	14.6	17.8	17.9	16.6	16.7
15,000	12.4	14.3	17.2	17.9	16.4	16.6
h [ft] 20,000	11.9	13.9	16.8	17.6	16.6	16.8
25,000	11.3	13.3	15.7	17.1	16.1	16.0
30,000	10.7	12.3	14.4	15.7	15.2	15.3

Table B-6: Correlation between p- and r-envelope [-].

V_g [ft/s]	400	580	760	940	1120	1300
10,000	0.20	0.21	0.19	0.11	0.11	0.15
15,000	0.17	0.17	0.15	0.11	0.11	0.13
h [ft] 20,000	0.16	0.19	0.18	0.13	0.10	0.09
25,000	0.14	0.16	0.16	0.14	0.10	0.05
30,000	0.11	0.16	0.18	0.15	0.14	0.12

Table B-7: Correlation between p- and β-envelope [-].

V_g [ft/s]	400	580	760	940	1120	1300
10,000	-0.14	-0.17	-0.18	-0.12	-0.13	-0.11
15,000	-0.12	-0.14	-0.14	-0.11	-0.12	-0.13
h [ft] 20,000	-0.10	-0.16	-0.16	-0.14	-0.15	-0.14
25,000	-0.06	-0.11	-0.15	-0.15	-0.16	-0.13
30,000	-0.01	-0.11	-0.16	-0.15	-0.17	-0.16

command. The reference trajectories of the maneuvers are shown in Figure. B-2 and B-3. The prefilter is a low-pass filter with a time constant of 0.4s.

Table B-8: Correlation between r- and β-envelope [-].

V_g [ft/s]		400	580	760	940	1120	1300
h [ft]	10,000	-0.38	-0.49	-0.59	-0.62	-0.66	-0.70
	15,000	-0.36	-0.47	-0.57	-0.62	-0.65	-0.67
	20,000	-0.31	-0.44	-0.56	-0.62	-0.65	-0.68
	25,000	-0.26	-0.40	-0.51	-0.61	-0.63	-0.65
	30,000	-0.22	-0.35	-0.45	-0.53	-0.59	-0.63

Table B-9: Correlation between q- and α-envelope [-].

V_g [ft/s]		400	580	760	940	1120	1300
h [ft]	10,000	0.68	0.65	0.57	0.46	0.30	0.11
	15,000	0.68	0.65	0.57	0.46	0.25	0.08
	20,000	0.64	0.65	0.60	0.46	0.22	0.07
	25,000	0.61	0.65	0.62	0.46	0.20	0.08
	30,000	0.58	0.63	0.61	0.45	0.19	0.06

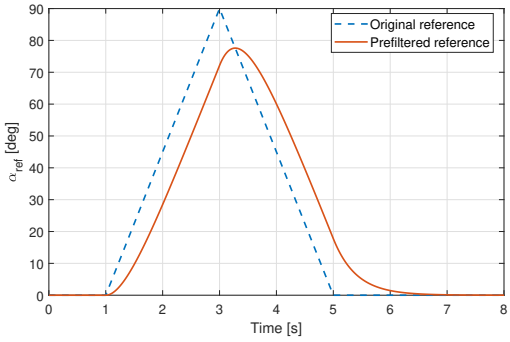

Figure B-2: Reference time trajectory of Maneuver A.

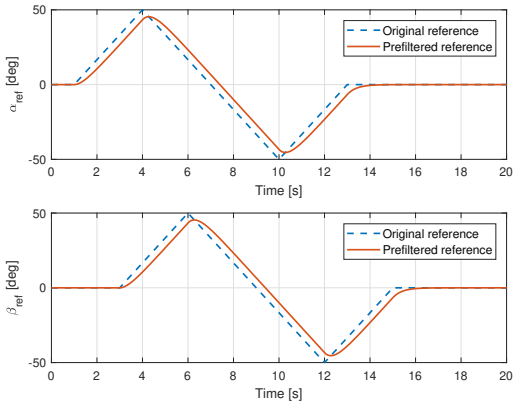

Figure B-3: Reference time trajectory of Maneuver B.

Appendix C

Parametric Envelope Database

One drawback of the non-parametric probabilistic envelope database in the form of LUTs is its large size. The applied database for the ICE aircraft has a size of 62.3 MB. In addition, high-dimensional LUTs can only be interpolated linearly in realtime due to computational limitations. To solve these issues, it is observed that the distribution of the membership values resembles a multivariate Gaussian function for states p, q, r, α, β. Therefore, possibilities were explored to use a Gaussian parametric model to describe the membership value in these five dimensions. Interpolation is still used for the remaining two dimensions h and V_g.

A multivariate Gaussian distribution can be fully parameterized by a mean vector $\boldsymbol{\mu}$ and a covariance matrix $\boldsymbol{\Sigma}$. The mean vector is assumed to be 0 for each state. The covariance matrix is interpolated at the current speed and altitude by a fourth-order polynomial based on the covariance matrices calculated at the h-V_g grid shown in Section B-2. In this way, the envelope metric can be calculated with a semi-parametric model.

The parametrization can significantly reduce the size of the envelope database and obtain similar envelope metric values at normal altitudes and speeds. A comparison of FEP performances is shown in Figure C-1 for the parametric and the non-parametric databases. The Maneuver B is used as the command. The simulations activated both the parametric and the non-parametric models for comparison. The blue lines use compensation terms derived from the non-parametric model for FEP, whereas the red lines use the parametric model. It can be seen that both models can accomplish the task of FEP. However, it should be noted that the parametric model cannot compensate for suboptimal altitudes and speeds of the aircraft since the database is essentially reduced to 5-D with speed and altitude only as parameters.

More sophisticated parametric models can also be explored like spline models. However, this is beyond the scope of the project.

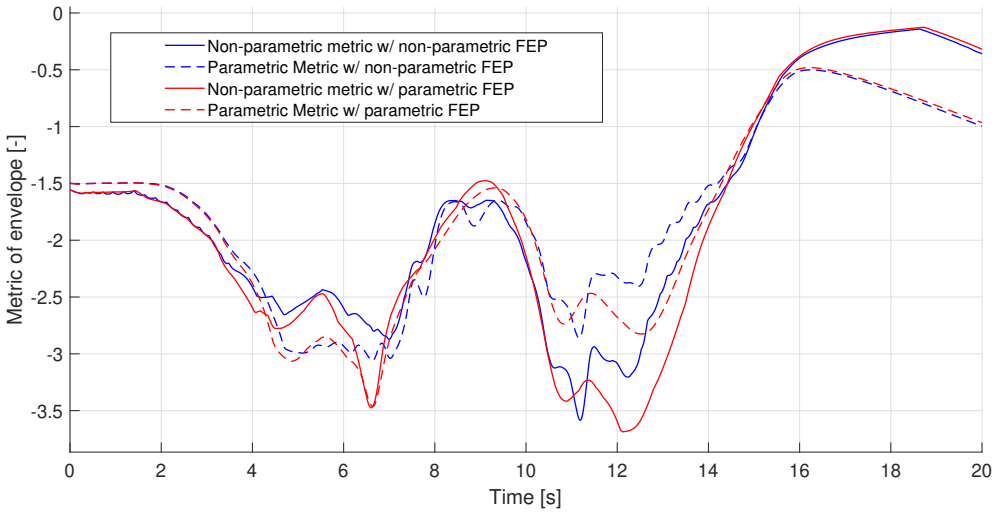

Figure C-1: Comparison of FEP performance for the parametric and non-parametric databases.

Bibliography

Acquatella, P. B., Falkena, W., Kampen, E.-J. van, & Chu, Q. P. (2012). Robust nonlinear spacecraft attitude control using incremental nonlinear dynamic inversion [Conference Proceedings]. In *Aiaa guidance, navigation, and control conference* (p. 1-20).

Acquatella, P. B., Kampen, E. van, & Chu, Q. P. (2013). Incremental backstepping for robust nonlinear flight control [Conference Proceedings]. In *Eurognc 2013, 2nd ceas specialist conference on guidance, navigation and control.*

Ananthkrishnan, N., & Sinha, N. K. (2001). Level flight trim and stability analysis using extended bifurcation and continuation procedure [Journal Article]. *Journal of Guidance Control and Dynamics*, *24*(6), 1225-1228.

Boeing Commercial Airplanes. (2016). *Statistical summary of commercial jet airplane accidents: Worldwide operations 19592015* (Report). Aviation Safety, Boeing Commercial Airplanes. Available from `http://www.boeing.com/news/techissues/pdf/statsum.pdf`

Bokovic, J. D., Redding, J., & Knoebel, N. (2009). An adaptive fault management (afm) system for resilient flight control [Conference Proceedings]. In *Aiaa guidance, navigation, and control conference.*

Bowlus, J., Multhopp, D., & Banda, S. S. (1997). Challenges and opportunities in tailless aircraft stability and control [Conference Proceedings]. In *Guidance, navigation, and control conference* (p. 1713-1718).

Buffington, J. F. (1999). *Modular control law design for the innovative control effectors (ice) tailless fighter aircraft configuration 101-3* (Report). Air Force Research Laboratory - Wright-Patterson Air Force Base.

Buffington, J. M. (1997). Tailless aircraft control allocation [Conference Proceedings]. In *Guidance, navigation, and control conference* (p. 737-747).

Davidson, J. B., Lallman, F. J., & Bundick, W. T. (2001a). Integrated reconfigurable control allocation [Conference Proceedings]. In *Aiaa guidance, navigation, and control conference and exhibit* (p. 1-11).

Davidson, J. B., Lallman, F. J., & Bundick, W. T. (2001b). *Real-time adaptive control allocation applied to a high performance air-*

craft (Report). NASA Langley Research Center. Available from https://ntrs.nasa.gov/archive/nasa/casi.ntrs.nasa.gov/20040086083.pdf

Dong, W., Farrell, J. A., Polycarpou, M. M., Djapic, V., & Sharma, M. (2012). Command filtered adaptive backstepping [Journal Article]. *IEEE Transactions on Control Systems Technology*, *20*(3), 566-580.

Dorsett, K. M. (1997). Directional control for tailless aircraft using all moving wing tips [Conference Proceedings]. In *22nd atmospheric flight mechanics conference* (p. 51). AIAA.

Dorsett, K. M., & Mehl, D. R. (1996). *Innovative control effectors (ice)* (Report). Lockheed Martin Tactical Aircraft Systems. Available from http://www.dtic.mil/dtic/tr/fulltext/u2/b212813.pdf

Efromovich, S. (2010). Orthogonal series density estimation [Journal Article]. *Wiley Interdisciplinary Reviews: Computational Statistics*, *2*(4), 467-476.

Eggermont, P. P. B., & LaRiccia, V. N. (2009). *Maximum penalized likelihood estimation* (Vol. 2) [Book]. New York, NY: Springer.

Enns, D., Bugajski, D., Hendrick, R., & Stein, G. (1994). Dynamic inversion: an evolving methodology for flight control design [Journal Article]. *International Journal of control*, *59*(1), 71-91.

European Aviation Safety Agency. (2011). *Annual safety review* (Report). European Aviation Safety Agency. Available from https://www.easa.europa.eu/system/files/dfu/EASA-Annual-Safety-Review-2011.pdf

Falkena, W., Borst, C., Chu, Q. P., & Mulder, J. A. (2010). Investigation of practical flight envelope protection systems for small aircraft [Journal Article]. *Journal of Guidance Control and Dynamics*, *34*(4), 976.

Farrell, J. A., Polycarpou, M., & Sharma, M. (2004). On-line approximation based control of uncertain nonlinear systems with magnitude, rate and bandwidth constraints on the states and actuators [Conference Proceedings]. In *2003 american control conference* (Vol. 3, p. 2557-2562). IEEE.

Farrell, J. A., Polycarpou, M., Sharma, M., & Dong, W. (2008). Command filtered backstepping [Conference Proceedings]. In *2008 american control conference* (Vol. 54, p. 1391-1395).

Gingras, D. R., Barnhart, B., Ranaudo, R., Ratvasky, T. P., & Morelli, E. (2009). Envelope protection for in-flight ice contamination [Conference Proceedings]. In *47th aiaa aerospace sciences meeting.*

Girard, A. (2005). Reachability of uncertain linear systems using zonotopes [Conference Proceedings]. In *Hybrid systems: Computation and control* (Vol. 5, p. 291-305). Springer.

Goman, M. G., & Demenkov, M. N. (2004). Computation of controllability regions for unstable aircraft dynamics [Journal Article]. *Journal of Guidance Control and Dynamics*, *27*(4), 647-656.

Goman, M. G., Khramtsovsky, A. V., & Kolesnikov, E. N. (2008). Evaluation of aircraft performance and maneuverability by computation of attainable equilibrium sets [Journal Article]. *Journal of guidance, control, and dynamics*, *31*(2), 329.

Guan, Y., Yokoi, K., & Zhang, X. (2008). Numerical methods for reachable space generation of humanoid robots [Journal Article]. *The International Journal of Robotics Research*, *27*(8), 935-950.

Heidenreich, N.-B., Schindler, A., & Sperlich, S. (2010). Bandwidth selection in kernel density estimation: A review [Journal Article]. *SSRN Electronic Journal*.

Helsen, R., Van Kampen, E.-J., Visser, C. C. de, & Chu, Q. P. (2016). Distance-fields-over-grids method for aircraft envelope determination [Journal Article]. *Journal of Guidance, Control, and Dynamics*, *39*(7), 1470-1480.

Holzapfel, F. (2004). *Nichtlineare adaptive regelung eines unbemannten fluggertes*. Thesis.

Hossain, K. N., Sharma, V., Bragg, M. B., & Voulgaris, P. G. (2003). Envelope protection and control adaptation in icing encounters [Conference Proceedings]. In *41st aerospace sciences meeting and exhibit* (Vol. 25).

Johnson, E. N., & Calise, A. J. (2000). Pseudo-control hedging: A new method for adaptive control [Conference Proceedings]. In *Advances in navigation guidance and control technology workshop.*

Johnson, E. N., & Calise, A. J. (2001). Neural network adaptive control of systems with input saturation [Conference Proceedings]. In *2001 american control conference* (Vol. 5, p. 3527-3532). IEEE.

Kampen, E.-J. van, Chu, Q. P., Mulder, J. A., & Emden, M. H. van. (2007). Nonlinear aircraft trim using interval analysis [Conference Proceedings]. In *Aiaa guidance, navigation and control conference and exhibit* (p. 6766).

Kitsios, I., & Lygeros, J. (2005). Launch pad abort flight envelope computation for a personnel launch vehicle using reachability [Conference Proceedings]. In *Aiaa guidance, navigation, and control conference and exhibit.*

Kwatny, H. G., & Allen, R. C. (2012). Safe set maneuverability of impaired aircraft [Conference Proceedings]. In *Aiaa atmospheric flight mechanics conference.*

Kwatny, H. G., Dongmo, J.-E. T., Chang, B.-C., Bajpai, G., Yasar, M., & Belcastro, C. (2012). Nonlinear analysis of aircraft loss of control [Journal Article]. *Journal of Guidance, Control, and Dynamics*, *36*(1), 149-162.

Kwatny, H. G., Donqmo, J.-E. T., Chanq, B.-C., Bajpai, G., Yasar, M., & Belcastro, C. M. (2009). Aircraft accident prevention: Loss-of-control analysis [Conference Proceedings]. In *Aiaa guidance, navigation, and control conference* (p. 10.2514/6.2009-6256).

Lombaerts, T., Looye, G., Chu, Q., & Mulder, J. A. (2010). Pseudo control hedging and its application for safe flight envelope protection [Conference Proceedings]. In *Aiaa guidance, navigation, and control conference.*

Lombaerts, T., Schuet, S., Acosta, D., Kaneshige, J., Shish, K., & Martin, L. (2015). Piloted simulator evaluation of maneuvering envelope information for flight crew awareness [Journal Article]. *AIAA Guidance, Navigation, and Control Conference*.

Lombaerts, T., Schuet, S., Wheeler, K., Acosta, D. M., & Kaneshige, J. (2013). Safe maneuvering envelope estimation based on a physical approach [Conference Proceedings]. In *Aiaa guidance, navigation, and control (gnc) conference* (p. 1-20).

Lu, P., Van Kampen, E.-J., & Chu, Q. P. (2015). Robustness and tuning of incremental backstepping approach [Conference Proceedings]. In *Aiaa guidance, navigation, and control conference* (p. 1762).

Lygeros, J. (2004). On reachability and minimum cost optimal control [Journal Article]. *Automatica*, *40*(6), 917-927.

Mahadevan, S. (1997). Monte carlo simulation [Book Section]. In *Reliability-based mechanical design* (p. 123-146). New York: CRC Press.

Matamoros, I., & Visser, C. C. de. (2018). Incremental nonlinear control allocation for a

tailless aircraft with innovative control effectors [Conference Proceedings]. In *2018 aiaa guidance, navigation, and control conference.*

Menon, P., Kim, J., Sengupta, P., Vaddi, V., Yang, B.-J., & Kwan, J. (2011). Onboard estimation of impaired aircraft performance envelope [Conference Proceedings]. In *Aiaa guidance, navigation, and control conference.*

Mitchell, I. M. (2008). The flexible, extensible and efficient toolbox of level set methods [Journal Article]. *Journal of Scientific Computing*, *35*(2), 300-329.

Nabi, H. N., Lombaerts, T., Zhang, Y., Kampen, E. van, Chu, Q. P., & Visser, C. C. de. (2018). Effects of structural failure on the safe flight envelope of aircraft [Journal Article]. *Journal of Guidance, Control, and Dynamics*, 1-19.

Nieto-Wire, C., & Sobel, K. (2011). Flight control design for a tailless aircraft using eigenstructure assignment [Journal Article]. *International Journal of Aerospace Engineering*, *2011*, 1-13.

Nocedal, J., & Wright, S. J. (2006). Sequential quadratic programming [Book Section]. In *Numerical optimization* (p. 529-562). New York, NY: Springer.

Oort, E. R. van. (2011). *Adaptive backstepping control and safety analysis for modern fighter aircraft.* Thesis.

Oort, E. R. van, Chu, Q. P., & Mulder, J. A. (2011). Maneuver envelope determination through reachability analysis [Book Section]. In *Advances in aerospace guidance, navigation and control* (p. 91-102). Berlin, Heidelberg: Springer.

Peijl, I. V. van der. (2017). *Physical splines for aerodynamic modelling of innovative control effectors.* Thesis.

Peng, L., Wei-wei, Q., & Zhi-qiang, Z. (2009). Nonlinear disturbance observer-based finite-time convergent second order sliding mode control for a tailless aircraft [Conference Proceedings]. In *2009 international conference on mechatronics and automation* (p. 4572-4576). IEEE.

Ranter, H. (2007). *Airliner accident statistics 2006* (Report). Aviation Safety Network.

Roemer, M., Tang, L., Bharadwaj, S., & Belcastro, C. (2008). An integrated aircraft health assessment and fault contingency management system for aircraft [Conference Proceedings]. In *Aiaa guidance, navigation and control conference and exhibit* (p. 6505).

Ruijgrok, G. J. J. (2009). *Elements of airplane performance* [Book]. Delft, the Netherlands: VSSG.

Russell, P., & Pardee, J. (2000). *Final report: Jsat loss of control: Results and analysis* (Report). Federal Aviation Administration: Commercial Airline Safety Team. Available from `http://www.cast-safety.org/pdf/jsat_loss-control.pdf`

Seube, N., Moitie, R., & Leitmann, G. (2002). Viability analysis of an aircraft flight domain for take-off in a windshear [Journal Article]. *Mathematical and computer modelling*, *36*(6), 633-641.

Shtessel, Y., Buffington, J., & Banda, S. (2002). Tailless aircraft flight control using multiple time scale reconfigurable sliding modes [Journal Article]. *IEEE Transactions on Control Systems Technology*, *10*(2), 288-296.

Sieberling, S., Chu, Q. P., & Mulder, J. A. (2010). Robust flight control using incremental nonlinear dynamic inversion and angular acceleration prediction [Journal Article]. *Journal of guidance, control, and dynamics*, *33*(6), 1732-1742.

Silverman, B. W. (1986). *Density estimation for statistics and data analysis* (Vol. 26) [Book]. New York: Routledge.

Simplcio, P., Pavel, M. D., Kampen, E. van, & Chu, Q. P. (2013). An acceleration

measurements-based approach for helicopter nonlinear flight control using incremental nonlinear dynamic inversion [Journal Article]. *Control Engineering Practice*, *21*(8), 1065-1077.

Slotine, J.-J. E., & Li, W. (1991). *Applied nonlinear control* (Vol. 199) [Book]. Englewood Cliff, NJ: Prentice-Hall Inc.

Sonneveldt, L., Chu, Q. P., & Mulder, J. A. (2007). Nonlinear flight control design using constrained adaptive backstepping [Journal Article]. *Journal of Guidance control and Dynamics*, *30*(2), 322-336.

Sonneveldt, L., Van Oort, E. R., Chu, Q. P., & Mulder, J. A. (2009). Nonlinear adaptive trajectory control applied to an f-16 model [Journal Article]. *Journal of Guidance, control, and Dynamics*, *32*(1), 25-39.

Tang, L., Roemer, M., Ge, J., Crassidis, A., Prasad, J. V. R., & Belcastro, C. (2009). Methodologies for adaptive flight envelope estimation and protection [Conference Proceedings]. In *Aiaa guidance, navigation, and control conference* (p. 6260).

Tomlin, C., Lygeros, J., & Sastry, S. (1998). Aerodynamic envelope protection using hybrid control [Conference Proceedings]. In *1998 american control conference* (Vol. 3, p. 1793-1796). IEEE.

Yavrucuk, I., Unnikrishnan, S., & Prasad, J. (2009). Envelope protection for autonomous unmanned aerial vehicles [Journal Article]. *Journal of Guidance, Control, and Dynamics*, *32*(1), 248-261.

Zhang, Y., Visser, C. C. de, & Chu, Q. P. (2016). Online safe flight envelope prediction for damaged aircraft: A database-driven approach [Conference Proceedings]. In *Aiaa modeling and simulation technologies conference* (p. 1189).